OCEAN WAVES

Lecture notes

course presented in 2015 as part of the Master's Programme
'Meteorology, Physical Oceanography and Climate'
Utrecht University, The Netherlands.

H.E. de Swart

General introduction

The phenomena to be studied in this course are wave-like features in the ocean with characteristic timescales of seconds up to several hours and length scales ranging between centimetres and several hundreds of kilometres. Together, they constitute a substantial part of the entire spectrum of sea surface variations (see Figure 1).

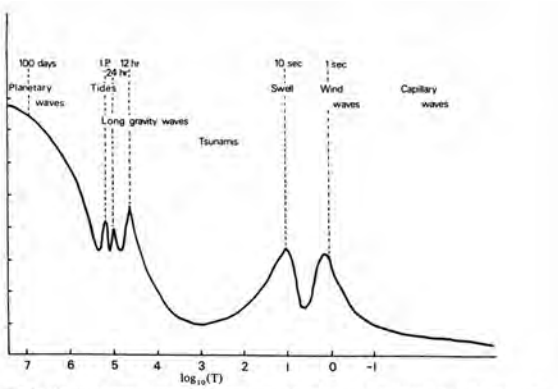

Fig. 2.1. Schematic energy spectrum of oceanic variability, showing the different types of waves occurring in the ocean. I.P. denotes the inertial period and is defined as $\pi/\Omega|\sin\phi|$, where Ω = magnitude of the Earth's rotation vector and ϕ is the geographic latitude (Section 3). In this picture I.P. = 35 hours, corresponding to a latitude of ± 20°. The relative amplitudes of the various parts of the spectrum do not necessarily reflect actual conditions.

Figure 1: Energy density spectrum of sea surface variability, showing the different types of surface waves occurring in the ocean. From *LeBlond and Mysak* [1978].

The aim of the present course is to discuss the current knowledge of the physical characteristics of two classes of ocean surface waves. The first class, considered in part A, comprises short waves. These phenomena have timescales that are much smaller than that of the revolution period of the earth and horizontal length scales that may be of the same order as the water depth. Consequently, their behaviour is hardly influenced by the Coriolis force and they are essentially three-dimensional features. Examples of short waves are wind-generated waves and swell at sea.

The second class, discussed in part B of these notes, comprises long waves in shallow water. Their horizontal length scales are large with respect to the water depth, so that they are quasi two-dimensional phenomena and they can be modelled with shallow water equations. Besides, their behaviour is significantly affected by the Coriolis force. Examples of such waves are tides.

Knowledge about the waves mentioned above is important for understanding the physics of coastal systems, which are discussed in a subsequent course. Only surface waves are considered; internal waves are discussed in the courses 'Dynamical Meteorology' and 'Wave Attractors'. Furthermore, only waves are considered for which it is not essential that the Coriolis parameter varies with latitude. Hence, no Rossby waves will be studied; they are discussed in the courses 'Dynamical Meteorology' and 'Dynamical Oceanography'.

The course consists of 16 oral lectures and 6 tutorials.

H.E. de Swart; August 2015

Contents

Part A

Wind waves

Chapter 1

Short waves: specific topics

Figure 1.1
shows a sketch of the amplitude spectrum of surface waves, including information about the generating and restoring forces.

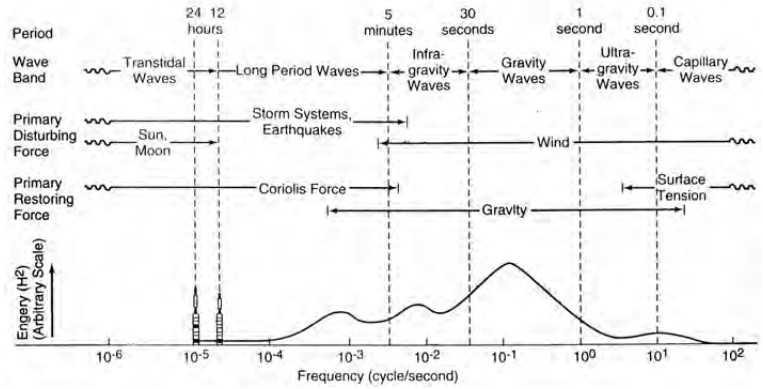

Figure 1.1: Amplitude spectrum of ocean surface waves and wave classification. From *Kinsman* [1965].

In part A of these notes the focus is on

- surface waves: variation of sea surface;
- periods T=O(seconds, minutes);
- wavelengths λ=O(mm, km).

These waves are not significantly affected by the Coriolis force, since $T \ll f^{-1}$, where $f \sim 10^{-4}$ s^{-1} is the Coriolis parameter. Hence short waves.

Restoring forces: the gravitational force or the force due to surface tension. Thus two subclasses: gravity waves and capillary waves.

Topics to be discussed:

I. Which free short waves are possible in an unbounded sea?

Figure 1.2
shows the movement of particles suspended in the water during one wave period in case of both standing and progressive waves.

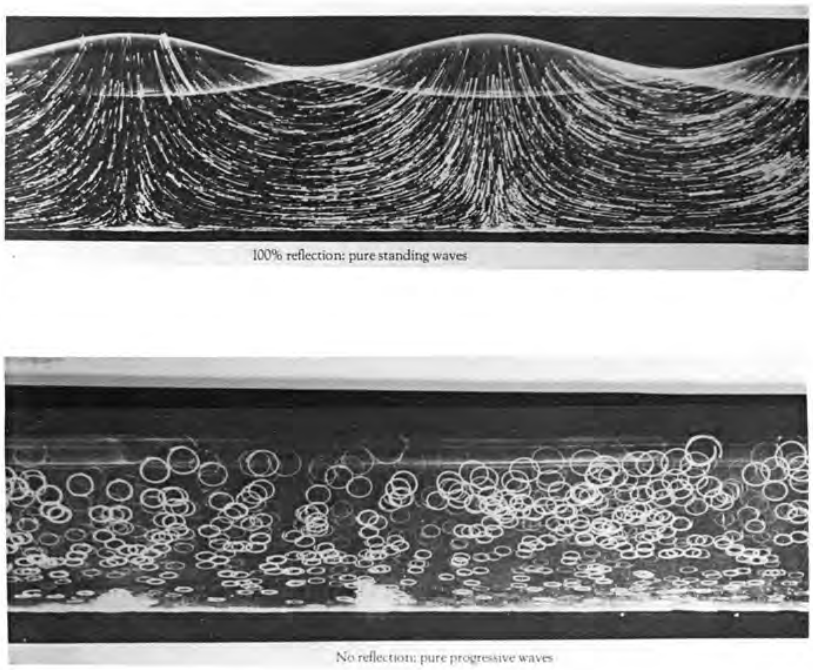

Figure 1.2: Particle orbits in case of pure standing waves (top) and pure progressive waves (bottom). From *Van Dyke* [1982].

As long as the amplitude of the waves is small compared to their wavelength the profile is sinusoidal. In case of progressive waves the particle orbits almost closed: circles nearby the free surface, ellipses at larger depths.

Figure 1.3
shows that with increasing amplitudes (with respect to wavelength) the profile of the wave becomes more peaked: sharper crests, flatter troughs.

Figure 1.4
shows that for even larger steepness 3D waves develop.

If the wave steepness exceeds a critical value (~ 0.4) waves will break and lose energy, see Figure 1.5. At open sea this process is called whitecapping.

Figure 1.3: Waves generated in a laboratory with a moderate steepness ($\sim$ amplitude/wavelength). From *Van Dyke* [1982].

(a) (b)

Figure 1.4: Three-dimensional surface waves observed in the Atlantic Ocean (left) and in the laboratory (right). From *Van Dyke* [1982].

(a) (b)

Figure 1.5: Left: whitecaps; right: wave breaking near the beach.
From *Kinsman* [1965].

II. How are waves generated by wind?

Mechanism: the turbulent wind induces fluctuations in atmospheric pressure, which cause variations if the sea surface. Subsequently, a positive feedback occurs: waves reinforce the atmospheric pressure fluctuations, such that growth of waves occurs. Necessary condition: the wind speed must exceed a critical value (of roughly 0.23 ms^{-1}).

Figure 1.6(a)
just below this value artificially induced disturbances already grow.

Figure 1.6(b)
Above the critical wind speed spontaneous wave growth occurs.

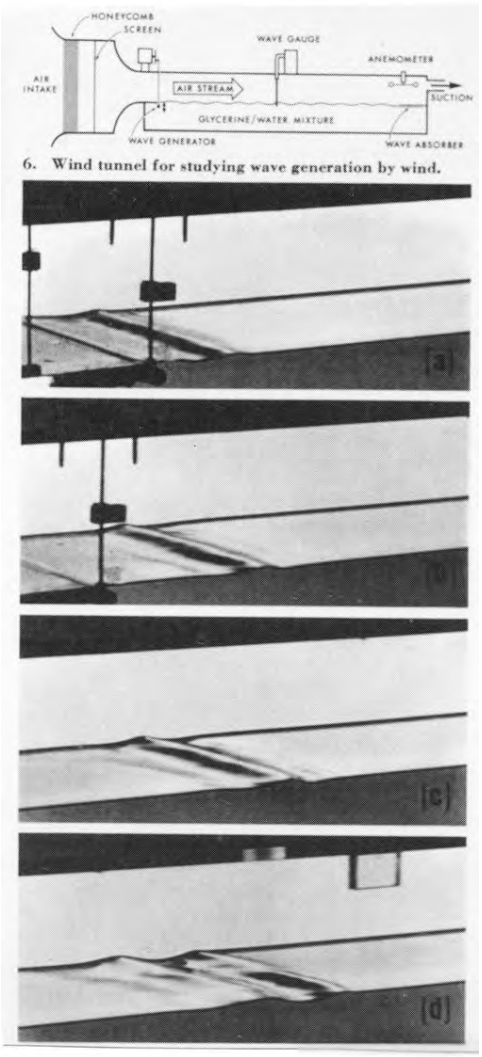

6. **Wind tunnel for studying wave generation by wind.**

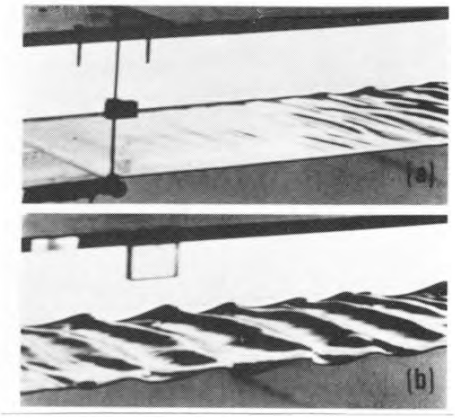

Figure 1.6: Growth of surface waves by wind. Left: behaviour of artifically-induced disturbances just below the critical wind speed of approximately 0.23 ms^{-1}. Right: spontaneous wave growth above the critical wind speed. From *Van Dyke* [1982].

III. How to describe an observed (irregular) wave field?

Figure 1.7(a):
a 2D wave field can be reconstructed with the help of stereo photography. Other possibilities: radar altimeters from satellites.

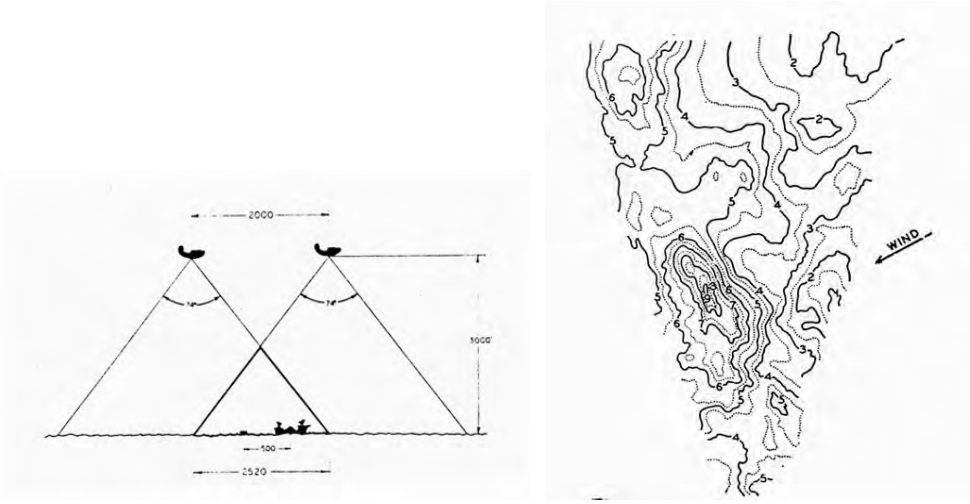

(a) (b)

Figure 1.7: Left: Aircraft flight pattern for the aerial stereo photography of waves. Right: topography of the sea surface derived from stereo photographs of the sea surface. Taken at Jan. 23, 1926 at latitude 59^{o}S, longitude 64^{o}4'W, contours in metres. From *Neumann and Pierson jr.* [1966].

Figure 1.7(b):
result is an irregular structure of sea surface height.
Necessary to describe the wave field by using statistical methods.
Nevertheless, a clear ordening is observed, e.g., wave crests more or less perpendicular to wind direction.

Figure 1.8:
shows variation of sea surface at a fixed time along a transect parallel to the wind direction and an observed time series of sea surface variations at a fixed position. Despite the irregular variations a characteristic wavelength can be identified.

Figure 1.9
shows a characteristic frequency spectrum of wind waves. The concept of wave spectrum was introduced in 1955 by Pierson.

Noticeable: the exponential increase in the low-frequency regime, the peak frequency (spectrum attains a maximum) and the algebraic decay in the high-frequency regime (proportional to σ^{-n} with $n \sim 4 - 5$). Also, note that most (but not all) waves propagate in the direction of the wind.

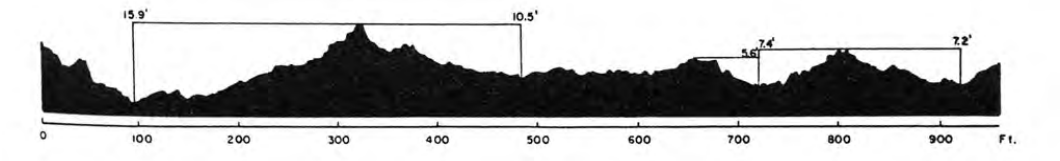

Figure 1.8: Wave profile as a function of distance obtained by stereophotogrammetry. Horizontal and vertical scales are in feet. From *Neumann and Pierson jr.* [1966].

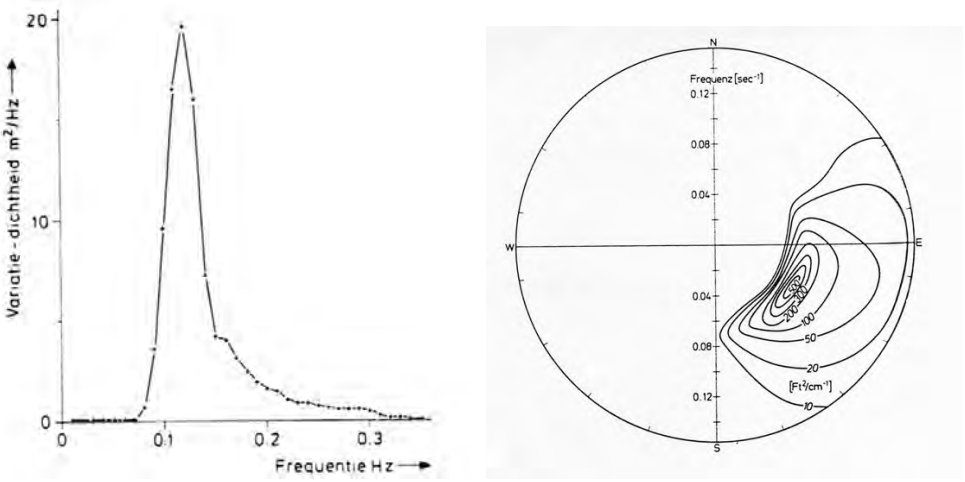

(a) (b)

Figure 1.9: Left: Characteristic shape of the frequency spectrum of wind waves (variance of sea surface elevation per frequency). From *Groen and Dorrestein* [1976]. Right: wave spectrum as a function of frequency and direction of wave propagation. From *Neumann and Pierson jr.* [1966].

IV. How does a wavefield develop in space and time and how is this modelled?

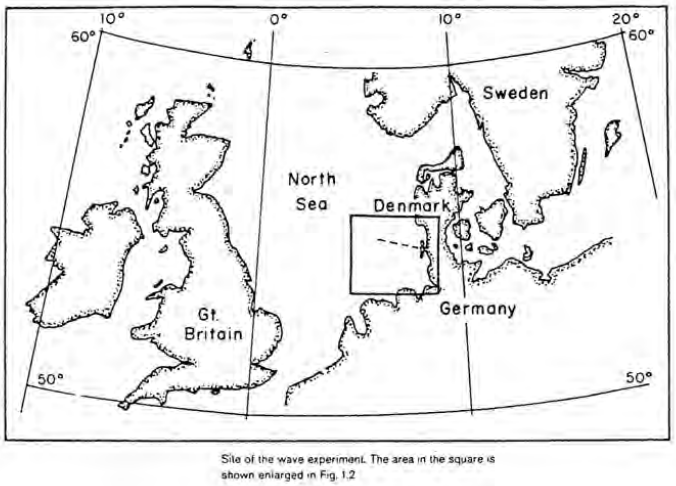

Figure 1.10: JONSWAP (JOint North Sea WAve Project); large measuring campaign in 1973 near the west coast of Denmark. From *Hasselman et al.* [1973].

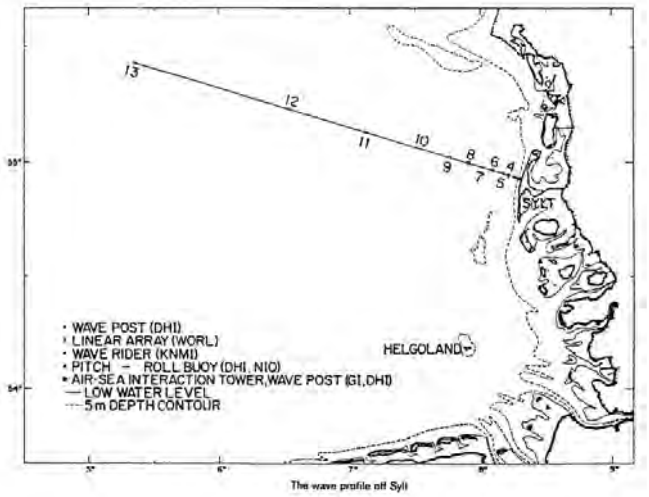

Figure 1.11: Location of observation points during JONSWAP. Data collected with wave buoys during offshore winds. From *Hasselman et al.* [1973].

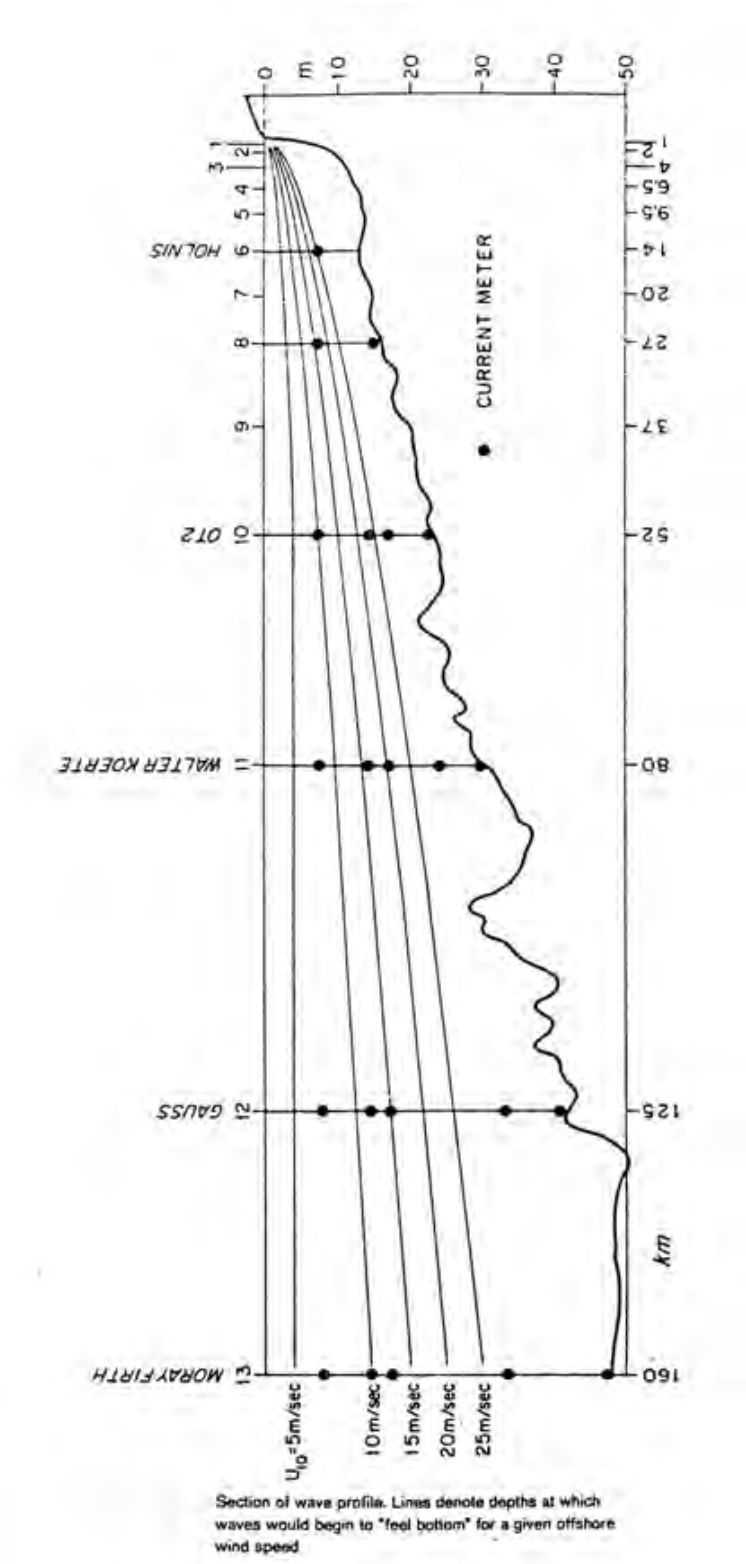

Figure 1.12: Curves indicate, for different offshore windspeeds, at which depth waves feel the presence of the bottom. In most cases: growth of waves in deep water. From *Hasselman et al.* [1973].

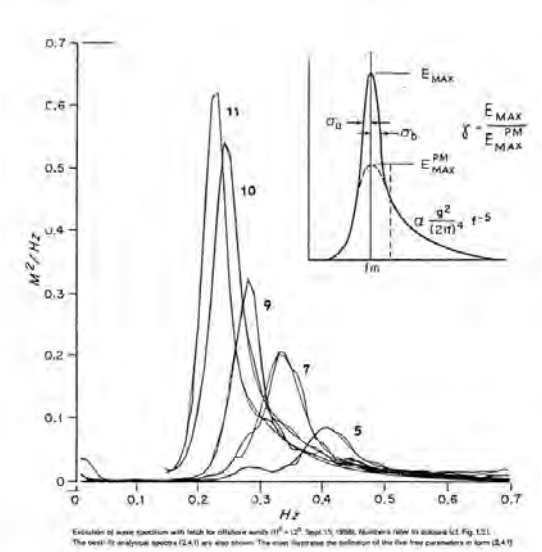

Figure 1.13: Data fitted to a theoretical spectrum, that contains 5 parameters. Remarkable new results: sharp peak in the spectrum and shift of peak frequency towards lower values with increasing fetch (distance to coast). The latter is due to nonlinear interactions between different wave components. From *Hasselman et al.* [1973].

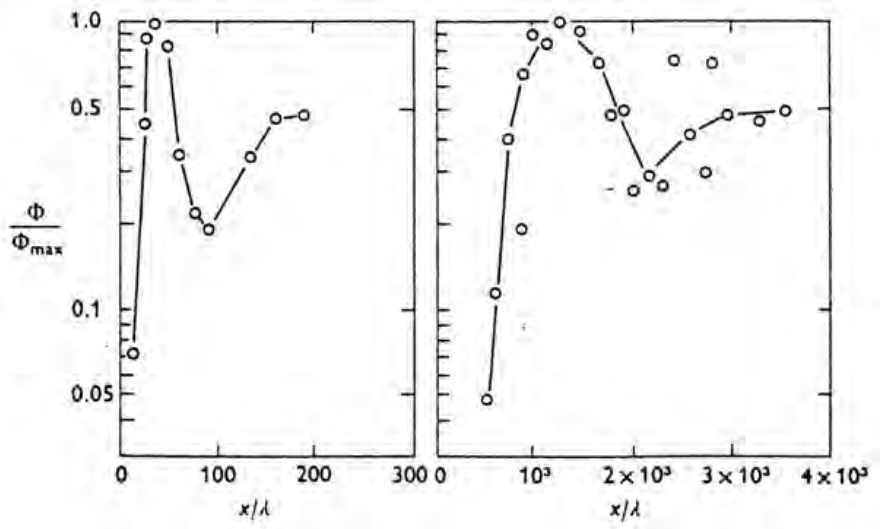

Figure 1.14: Observed growth of energy of the wave component with its phase velocity equal to the wind speed (at 10 m height) as a function of the fetch. In the initial stage linear growth, next exponential increase and finally an equilibrium value is reached. The overshoot is due to nonlinear wave-wave interactions. From *Hasselman et al.* [1973].

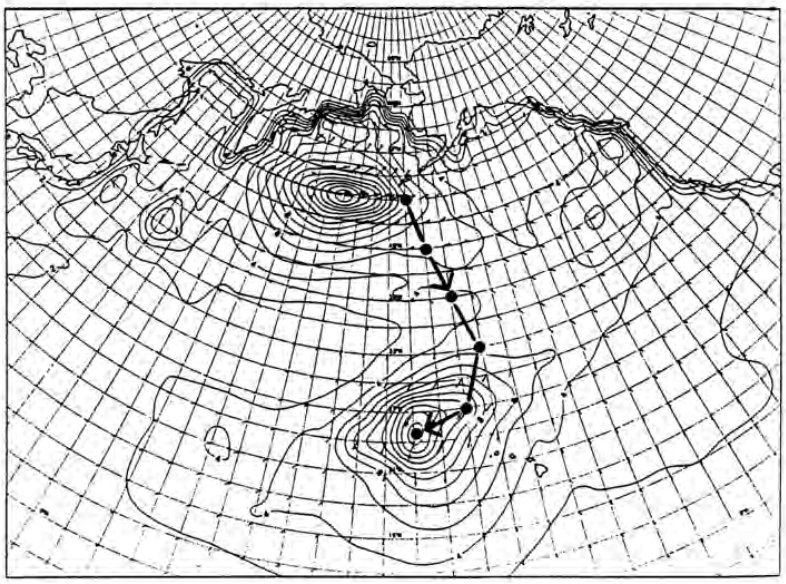

Figure 1.15: Wave field in the North Atlantic Ocean at 12 UTC, 5 November 1988. The dot shows the track of the storm at 12 h intervals. Isolines at 1 m intervals. From *Komen et al.* [1994].

Figure 1.15:
Example of output produced by the WAM-model, a modern wave prediction model. The WAve Modeller group was founded in 1984 by K. Hasselman with the objective to develop a standard wave prediction model. It is a so-called third-generation model: it is based on a spectral description of the wavefield and fully accounts for (nonlinear) wave-wave interactions. Other models: SWAN (described in *Holthuijsen* [2007]) for applications in the nearshore zone. An overview of different wave forecast methods is given in *WMO* [1998].

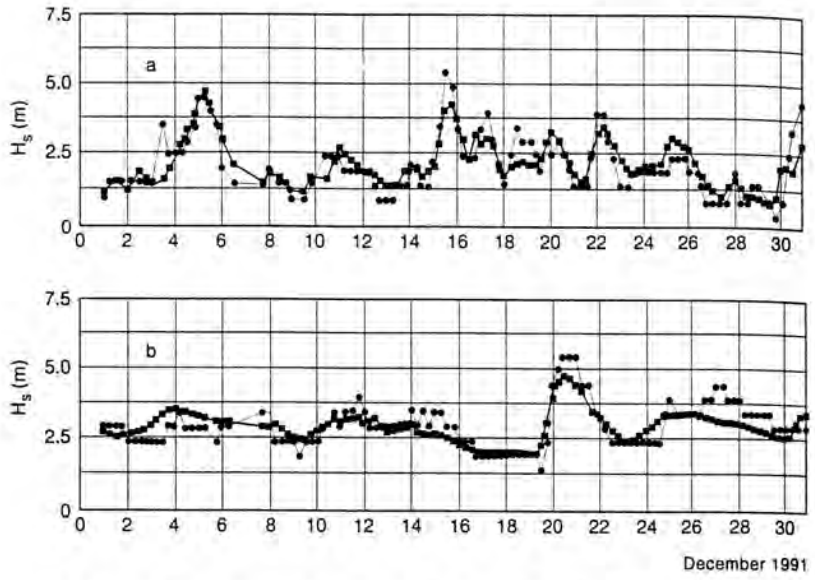

Fig. 4.20. a) Intercomparison between WAM model results (continuous line) and measured data (dotted line). Location: east coast of USA (40.5°N, 69.4°W). Time in days. The model mean wave height is 2.3 m; the observed wave height is 2.2 m. Rms error, bias and SI are 0.53, 0.07 and 0.24 respectively. b) Same as a) at a location close to Hawaii (19.3°N, 160.8°W). Here the model mean wave height was 3.0 m; the observed wave height is 3.1 m. Rms error, bias and SI are 0.46, - 0.05 and 0.15 (after Günther *et al*, 1992).

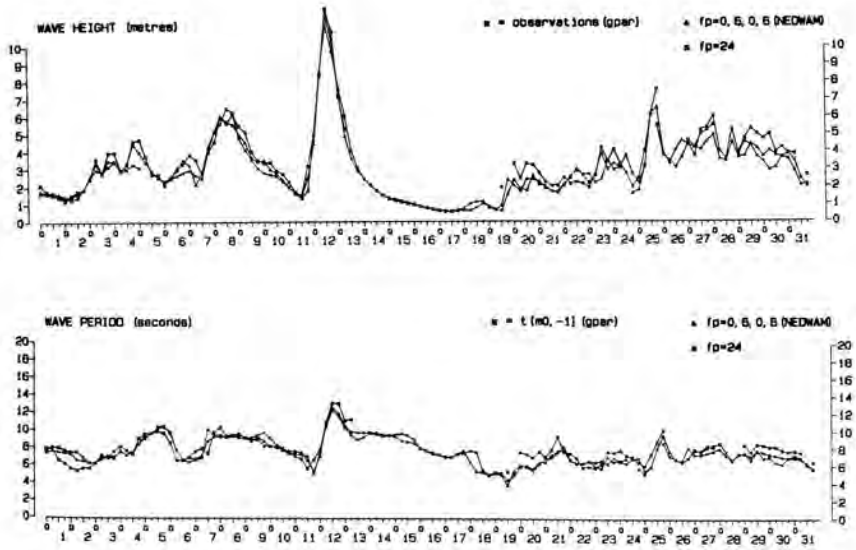

Fig. 4.21. Comparison between analysis (△), 24 h forecast (×) and measured data (□) at station AUK in the North Sea for December 1990.

Figure 1.16: Intercomparison between WAM model results and measured data (dots). From *Komen et al.* [1994]. The model turns out to be quite successful.

Chapter 2

Basic theory

2.1 Equations of motion

The phenomena to be modelled are short waves at the free surface between water and air. Here, short means that characteristic wave periods are small compared to the rotation period of the earth. Furthermore, baroclinic features (variation of internal density surfaces) are not essential.
The most convenient way to filter baroclinic features is to assume that sea water is a homogeneous fluid, i.e., its density

$$\boxed{\rho = \text{constant.}} \tag{2.1}$$

Now a closed set of equations of motion is derived from conservation of mass and of momentum.

Consider a volume element V, enclosed by a surface S with an external normal vector $\vec{n}$. The three-dimensional velocity field of water particles is denoted by $\vec{u}$. Then conservation of mass yields

$$\frac{\partial}{\partial t} \iiint_V \rho \, dV = - \iint_S \rho \, \vec{u} \cdot \vec{n} \, dS.$$

Application of the Gauss theorem to the right-hand side and considering infinitesimally small volume elements finally yields

$$\frac{\partial \rho}{\partial t} + \vec{\nabla} \cdot (\rho \, \vec{u}) \; = \; 0 \qquad\qquad \text{continuity equation.}$$

Momentum balance:

$$\frac{\partial}{\partial t} \iiint_V \rho \, \vec{u} \, dV = - \iint_S (\rho \, \vec{u}) \, \vec{u} \cdot \vec{n} \, dS + \iint_S \underline{\underline{\sigma}} \cdot \vec{n} \, dS + \iiint_V \rho \vec{f} \, dV.$$

Here, $\underline{\underline{\sigma}}$ is the stress tensor; its components σ_{ij} denote the i'th component of the stress acting on a surface elements with a normal in the j'th direction. Furthermore, $\vec{f}$ are volume forces per mass unit.

Again, use the theorem of Gauss and consider infinitesimally small volume elements. After substitution of the continuity equation the result is

$$\rho \left\{ \frac{\partial \vec{u}}{\partial t} + (\vec{u} \cdot \vec{\nabla}) \vec{u}) \right\} = \vec{\nabla} \cdot \underline{\underline{\sigma}} + \rho \vec{f} \qquad \text{momentum equation}\,.$$

Impose the following assumptions:

- homogeneous fluid;
- ideal fluid no frictional effects, so

  $$\underline{\underline{\sigma}} = -p\, \underline{\underline{\delta}}\,,$$

  where p is pressure and $\underline{\underline{\delta}}$ the unity tensor;
- $\vec{f}$ is a potential force per mass unit:

  $$\vec{f} = -\vec{\nabla}\Phi\,.$$

With this the continuity equation and momentum equation reduce to

$$\boxed{\vec{\nabla} \cdot \vec{u} = 0\,,} \tag{2.2}$$

$$\boxed{\frac{\partial u}{\partial t} + (\vec{u} \cdot \vec{\nabla}) \vec{u} = -\frac{1}{\rho}\vec{\nabla} p - \vec{\nabla}\Phi\,.} \tag{2.3}$$

Together with equation (2.1) they form a closed set of equations.

The system is further analysed by deriving the equation for the vorticity

$$\vec{\omega} = \vec{\nabla} \times \vec{u}. \tag{2.4}$$

Application of the curl operator to the rewritten momentum equation

$$\boxed{\frac{\partial \vec{u}}{\partial t} + \vec{\omega} \times \vec{u} = -\nabla \left[\frac{p}{\rho} + \frac{1}{2}\vec{u}^{\,2} + \Phi \right]} \tag{2.5}$$

yields after some manipulations:

$$\boxed{\frac{\partial \vec{\omega}}{\partial t} + (\vec{u} \cdot \vec{\nabla})\, \vec{\omega} = (\vec{\omega} \cdot \vec{\nabla})\, \vec{u}\,.} \tag{2.6}$$

The terms on the right-hand side describe production of vorticity due to stretching and tilting of vortex tubes.

From equation (2.6): if at some time $\vec{\omega} = 0$, then $\vec{\omega} = 0$ for all times. Assume that this is the case, then

$$\boxed{\vec{\omega} \equiv \vec{\nabla} \times \vec{u} = 0, \qquad \text{hence} \qquad \vec{u} = \vec{\nabla}\phi\,.} \tag{2.7}$$

Thus the velocity field is irrotational, the velocity components are computed from the gradient of a velocity potential ϕ, hence potential flow.

Substitute equation (2.7) in continuity equation (2.2) and in the rewritten momentum equation (2.5). This yields

$$\nabla^2\phi = 0\,, \tag{2.8}$$

$$\frac{\partial\phi}{\partial t} + \frac{p}{\rho} + \frac{1}{2}(\vec{\nabla}\phi)^2 + \Phi = 0\,. \tag{2.9}$$

These are the Laplace equation and the Bernouilli equation for the velocity potential and pressure, respectively.

2.2 Boundary conditions

In case of surface waves in a homogeneous sea there are two types of boundaries, as shown in Figure 2.1 below:

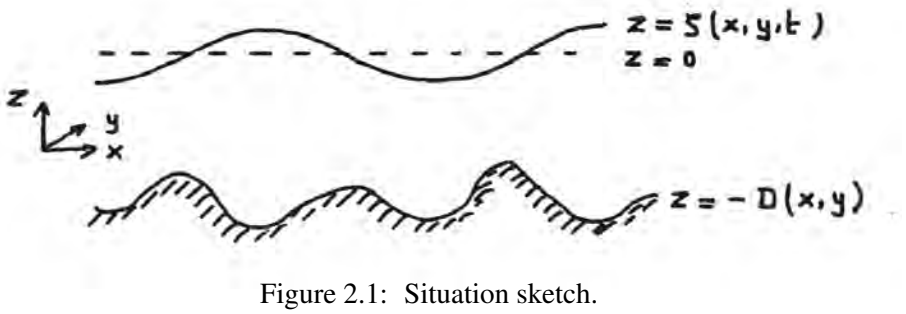

Figure 2.1: Situation sketch.

- the free surface $z = \zeta(x, y, t)$ between water and air;
- the fixed boundary $z = -D(x, y)$ (the bottom).

Here, a Cartesian frame is considered with the z-axis pointing in the vertical direction. The location of the undisturbed water level is $z = 0$. Each boundary can be written as $G(\vec{x}, t) = 0$, where $\vec{x}$ is a position vector with coordinates (x, y, z).

The first condition is that fluid elements at any boundary must stay at this boundary, hence

$$\frac{dG}{dt} \equiv \frac{\partial G}{\partial t} + \vec{u}\cdot\vec{\nabla}G = 0 \qquad \text{at} \quad G(\vec{x}, t) = 0\,. \tag{2.10}$$

This is the so-called kinematic boundary condition.
Hence, for the free surface $G = z - \zeta(x, y, t) = 0$ it follows

$$\frac{\partial\phi}{\partial z} = \frac{\partial\zeta}{\partial t} + \vec{\nabla}_h\phi\cdot\vec{\nabla}_h\zeta \qquad \text{at} \quad z = \zeta(x, y, t)\,, \tag{2.11}$$

where equation (2.7) has been used. Furthermore, $\vec{\nabla}_h$ is the horizontal nabla vector with components $(\partial/\partial x, \partial/\partial y)$.

Likewise for the bottom $G = z + D(x, y) = 0$. From now on a horizontal bottom will be assumed, i.e., $D(x, y) = H =$constant. Then

$$\boxed{\frac{\partial \phi}{\partial z} = 0 \qquad \text{at} \quad z = -H\,.} \tag{2.12}$$

In order to determine the variable location of the free surface an additional boundary condition is needed. The latter follows from the principle that the stresses (i.e., forces per surface area) acting on each element at the free surface must be continuous. If not, a net force would act on a surface element and it would result in an infinite acceleration, because surface elements have no mass.
In this case the fluid is ideal, so there are only stresses that act in the normal direction. The normal stresses acting on a surface element S, enclosed by a curve Γ, are

- water pressure;
- atmospheric pressure;
- a stress that is induced by surface tension.

Surface tension is a consequence of cohesive forces between water molecules. Within the fluid the net effect is zero, but at the free surface a net force is present because there are no water molecules above this surface. Apart from a, dynamically not relevant, constant force downward there is a variable contribution in case of a curved surface, as is sketched in Figure 2.2 below.

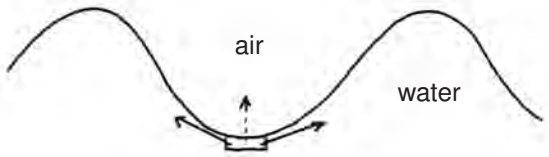

Figure 2.2: In case of positive curvature surface tension induces a net upward-directed force.

Clearly, this restoring mechanism describes wave propagation. Thus, the free surface behaves as a membrane: there is a uniform surface tension τ (~ 0.08 Nm^{-1}).

As seen from Figure 2.3, the net cohesive force acting on a surface element is

$$\vec{F_c} = -\tau \oint_\Gamma \vec{n} \times d\vec{l}$$

where $\vec{n}$: normal vector;
$d\vec{l}$: line element.

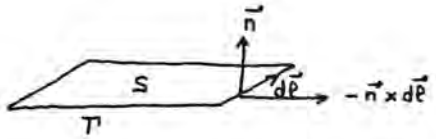

Figure 2.3: Net cohesive force acting at line element $d\vec{l}$. Force is in the direction $\vec{n} \times d\vec{l}$.

Computation of the net work induced by this force in case of a small displacement $\delta\vec{r}$:

$$\vec{F_c} \cdot \delta\vec{r} = -\tau \iint_S (\vec{\nabla} \cdot \vec{n})\, \delta\vec{r} \cdot \vec{n}\, dS\,,$$

where the theorem of Stokes and some vector identities have been used.

The normal $\vec{n}$ at the free surface $G = z - \zeta(x, y, t) = 0$ is given by

$$\boxed{\vec{n} = \frac{\vec{\nabla}\vec{G}}{|\vec{\nabla}\vec{G}|} = \frac{-\vec{\nabla}_h\zeta + \vec{e}_z}{\left[1 + (\vec{\nabla}_h\zeta)^2\right]^{1/2}}\,,} \tag{2.13a}$$

where $\vec{e}_z$ is a unity vector in the vertical direction. Hence, the work done by the cohesive forces is known.

Likewise, the work done by the water pressure force and atmospheric pressure force are

$$\vec{F}_p \cdot \delta\vec{r} = \iint\limits_S p\,\vec{n} \cdot \delta\vec{r}\,dS\,, \qquad \vec{F}_{p0} \cdot \delta\vec{r} = -\iint\limits_S p_0\,\vec{n} \cdot \delta\vec{r}\,dS\,,$$

with p_0 the atmospheric pressure.
Now, the net work done by the three forces must be zero. In that result, consider infinitesimal surface elements and infinitesimal displacements. It then follows the dynamic boundary condition

$$\boxed{\frac{\partial\phi}{\partial t} + \frac{1}{2}(\vec{\nabla}\phi)^2 + g\zeta + \frac{p_0}{\rho} + \frac{\tau}{\rho}\vec{\nabla} \cdot \vec{n} = 0 \quad \text{at} \quad z = \zeta(x, y, t)\,,} \tag{2.13b}$$

where $\vec{n}$ is given in (2.13a). Here, use has been made of the Bernouilli equation (2.9) with $\Phi = \Phi_g = gz$ the gravitational potential.

Summary: the final equations of motion and boundary conditions governing short waves are:

$$\boxed{\begin{array}{lll}
(2.8): & \nabla^2\phi = 0\,, & \\
(2.12): & \frac{\partial\phi}{\partial z} = 0 & \text{at} \quad z = -H, \\
(2.11): & \frac{\partial\phi}{\partial z} = \frac{\partial\zeta}{\partial t} + \vec{\nabla}_h\phi \cdot \vec{\nabla}_h\zeta & \text{at} \quad z = \zeta, \\
(2.13b): & \frac{\partial\phi}{\partial t} + \frac{1}{2}(\vec{\nabla}\phi)^2 + g\,\zeta + \frac{p_0}{\rho} + \frac{\tau}{\rho}\vec{\nabla} \cdot \vec{n} = 0 & \text{at} \quad z = \zeta, \\
(2.13a): & \vec{n} = \frac{\vec{\nabla}\vec{G}}{|\vec{\nabla}\vec{G}|} = \frac{-\vec{\nabla}_h\zeta + \vec{e}_z}{\left[1 + (\vec{\nabla}_h\zeta)^2\right]^{1/2}}, &
\end{array}} \tag{2.14}$$

2.3 Construction of solutions

From system (2.14) it follows: the velocity potential is governed by the Laplace equation and two boundary conditions, a second condition at the free surface surface determines the position of that boundary.

The general procedure is to search for solutions that describe waves propagating in the horizontal plane and that have an unknown vertical structure. Hence

$$\phi(x, y, z, t) = f(z)\,\chi(x, y, t)\,, \tag{2.15a}$$

where $\chi(x, y, t)$ is periodic in x, y, t and an O(1) function.
Substitution in the Laplace equations yields

$$\nabla_h^2 \chi + \kappa^2 \chi \;=\; 0\,, \qquad\qquad \frac{d^2 f}{dz^2} - \kappa^2 f \;=\; 0\,, \tag{2.15b}$$

with $\kappa^2 > 0$ a separation constant; $\kappa = 2\pi/\lambda$ can be interpreted as the wavenumber and λ as the wavelength.

The general solution of the first equation is

$$\chi = \hat{\chi}(t)\;\cos(kx + ly - \varphi(t))\,, \qquad \text{with} \qquad \kappa^2 = k^2 + l^2$$

and φ an as yet arbitrary phase.
The solution of the second equation, which already obeys the bottom boundary condition, is

$$f(z) = \hat{f}\cosh\left[\kappa(z + H)\right]\,,$$

which determines the vertical structure of the velocity potential.

Since the Laplace equation is linear and wavenumbers can be arbitrarily chosen, a general solution can be written as

$$\phi = \iint dkdl\;\hat{A}(k, l, t)\;\cosh\left[\kappa(z + H)\right]\;\sin\left[kx + ly - \varphi(k, l, t)\right]\,, \tag{2.16}$$

i.e., a superposition of travelling waves. The temporal behaviour of amplitudes $\hat{A}$ and phases φ is governed by the two conditions at the free surface.

Chapter 3

Linear analysis: dispersion relation

3.1 Linearisation conditions

If the procedure of constructing solutions, as mentioned in section 2.3 is adopted, the resulting analysis becomes very complicated, because of the following problems:

- the location of the sea surface (free surface) is a priori unknown;
- two of the three boundary conditions are *nonlinear*.

Therefore, no simple solutions of the *full* system (2.14) can be found, only of *subsystems* that can be derived from this system under certain conditions.

In this chapter, a tractable subset of the full equations of motion will be derived. For this purpose, first the following questions are addressed:

- under which condition(s) can the free boundary be replaced by a fixed boundary?
- under which condition(s) can the boundary conditions be linearised?

Ad question 1: from eq. (2.16) it follows that each wave component has a characteristic horizontal length scale κ^{-1}, whilst this is also a characteristic vertical length scale. Furthermore, the wave amplitude a is a typical scale for the elevation of the free surface. Now, suppose that $a \ll \kappa^{-1}$ and $a \ll H$, thus

$$\boxed{\epsilon = a\kappa \ll 1,} \qquad \boxed{\alpha = \frac{a}{H} \ll 1.} \tag{3.1}$$

Then, the velocity potential hardly changes over a vertical distance of order a and the actual depth is almost identical to the undisturbed water depth H. The parameter ϵ is called the wave steepness; apart from a factor of 2π it is the ratio of amplitude and wavelength. Under these conditions the boundary conditions at the free surface $z = \zeta$ can, to a first approximation, be applied at the undisturbed water level $z = 0$ instead. Note that the condition of a small wave steepness implies that $|\vec{\nabla}_h \zeta| \ll 1$, thereby implying that the dominant contribution to the capillary term in the dynamic boundary condition (fourth equation of system (2.14)) is linear, viz. $-(\tau/\rho)\nabla_h^2 \zeta$.

Ad question 2: in order to linearise the boundary conditions it is necessary that

$$\left[\vec{\nabla}\phi\cdot\vec{\nabla}_h\zeta\right] \ll \left[\frac{\partial\phi}{\partial z}\right], \qquad \left[\vec{\nabla}_h\phi\cdot\vec{\nabla}_h\zeta\right] \ll \left[\frac{\partial\zeta}{\partial t}\right],$$
$$\left[(\vec{\nabla}\phi)^2\right] \ll \left[\frac{\partial\phi}{\partial t}\right], \qquad \left[(\vec{\nabla}\phi)^2\right] \ll \max\left(\left[g\zeta\right], \left[-\frac{\tau}{\rho}\nabla_h^2\zeta\right]\right),$$

where $[\cdot]$ denotes the characteristic magnitude of the terms between the brackets. Furthermore, the term $\partial\phi/\partial t$ in the dynamic boundary condition must be of the same order of magnitude as that of the term $g\zeta$ or $(\tau/\rho)\nabla_h^2\zeta$, otherwise there is no force balance at the free surface. This yields a scale for the velocity potential:

$$\boxed{[\phi] \;=\; \frac{g\,a \;+\; (\tau/\rho)\,\kappa^2\,a}{\sigma},} \tag{3.2}$$

where $\sigma = 2\pi/T$ is the (radian) frequency and T the corresponding wave period.

The four linearisation criteria listed above result in the following two conditions:

$$\epsilon \ll 1 \qquad \text{and} \qquad \epsilon \ll F \equiv \frac{\sigma^2}{g\,\kappa + (\tau/\rho)\,\kappa^3} \tag{3.3}$$

Their meaning is that the wave steepness must be small and that the velocity of water particles must be small compared to the phase velocity of the wave. The first condition can be obeyed by considering small enough wave amplitudes. To understand the second condition it is convenient first to *assume* that it is obeyed, next find the solution of the linear system and then re-interpret this condition.

3.2 Solution of the linear system

Now assume that the conditions (3.1) and (3.3) are obeyed. The equations of motion and boundary conditions then, *to a first approximation*, become

$$\boxed{\begin{array}{lll} \nabla^2\phi = 0 & & \\ \dfrac{\partial\phi}{\partial z} \;=\; 0 & \text{at} \quad z = -H, & \\ \dfrac{\partial\phi}{\partial z} \;=\; \dfrac{\partial\zeta}{\partial t} & \text{at} \quad z = 0, & \\ \dfrac{\partial\phi}{\partial t} \;+\; g\,\zeta \;-\; \dfrac{\tau}{\rho}\,\nabla_h^2\zeta \;=\; 0 & \text{at} \quad z = 0. & \end{array}} \tag{3.4}$$

Here, free waves are considered, hence the atmospheric pressure p_0 has been assumed constant and has been subsequently transformed away (by choosing a new reference level of the velocity potential).

The structure of the velocity potential that satisfies both the Laplace equation and bottom boundary condition has already been given in eq. (2.16) as a superposition

of waves. In this case system (3.4) is linear, so a plane harmonic wave, described by a velocity potential

$$\phi = \hat{A}\,\cosh[\kappa(z+H)]\,\sin(\kappa x - \sigma t)\,,$$

with a *constant* amplitude $\hat{A}$, will be a solution. Note that the wavevector points in the same direction as the x-axis, an assumption that has no dynamical consequences. The corresponding variations of the free surface are

$$\zeta = a\cos(\kappa x - \sigma t)\,. \tag{3.5}$$

Substitution of the expressions for the velocity potential and the free surface in the boundary conditions of system (3.4) that apply at $z = 0$ yields two equations. In matrix form they can be written as

$$\begin{pmatrix} \kappa\sinh(\kappa H) & -\sigma \\ -\sigma\cosh(\kappa H) & g + (\tau/\rho)\kappa^2 \end{pmatrix} \cdot \begin{pmatrix} \hat{A} \\ a \end{pmatrix} \;=\; 0.$$

Non-trivial solutions exist only if the determinant of the coefficient matrix vanishes. This condition yields

$$\boxed{\sigma^2 = \left(g\kappa \;+\; \frac{\tau}{\rho}\kappa^3\right)\,\tanh(\kappa H),} \tag{3.6}$$

the dispersion relation for linear free capillary gravity waves.

The velocity potential thus becomes

$$\boxed{\phi = \frac{\sigma}{\kappa}\,a\,\frac{\cosh[\kappa(z+H)]}{\sinh(\kappa H)}\,\sin(\kappa x - \sigma t).} \tag{3.7}$$

The solution of the linear system (3.4) is now given by equations (3.5), (3.6) and (3.7).

Finally, reconsider the second condition in eq. (3.3), which was necessary to linearise the boundary conditions at the free surface. Using dispersion relation (3.6) it follows that this condition can also be written as

$$\epsilon \ll \tanh\beta \qquad \text{with} \qquad \boxed{\beta = \kappa H \sim \frac{\text{water depth}}{\text{wavelength}}\,.} \tag{3.8}$$

With respect to the condition of a small wave steepness this only implies an additional constraints if $\beta \ll 1$, i.e., in shallow water. It then follows that $\alpha \ll 1$, where parameter α was defined in eq. (3.1).

So the final conclusion: the use of the linear system (3.4) is allowed *to a first approximation* if the wave amplitude is small with respect to *both* the wavelength and the undisturbed water depth. Thus, strictly speaking, linear waves are valid only in the *limit* $\epsilon \to 0$ and $\alpha \to 0$. In other words, linear waves have infinitesimal amplitudes. Finite-amplitude waves will be discussed in the last section of the next chapter.

Chapter 4

Further analysis of linear free waves

4.1 Deep and shallow water

In this chapter additional information about linear free capillary gravity waves is obtained. First, consider the case

$$\kappa H \gg 1 \quad : \quad \tanh(\kappa H) \sim 1\,, \qquad \sinh(\kappa H) \sim \cosh(\kappa H) \sim \frac{1}{2}\, e^{\kappa H}\,.$$

This is the deep water limit : the wavelength is much smaller than the water depth and the waves do not experience the presence of the bottom. In this case the solutions (3.6)-(3.7) become

$$\boxed{\begin{aligned} \kappa H \gg 1: \qquad & \sigma^2 \;\to\; g\kappa \,+\, \frac{\tau}{\rho}\kappa^3\,, \\ & \phi \;\;\to\; \frac{\sigma}{\kappa}\, a\, e^{\kappa z}\, \sin(\kappa x - \sigma t)\,. \end{aligned}} \tag{4.1}$$

The counter case is the shallow water limit:

$$\kappa H \ll 1 \; : \quad \tanh(\kappa H) \sim \sinh(\kappa H) \sim \kappa H\,, \quad \cosh(\kappa H) \sim 1 + \frac{1}{2}(\kappa H)^2\,,$$

with corresponding solutions

$$\boxed{\begin{aligned} \kappa H \ll 1: \qquad & \sigma^2 \;\to\; gH\,\kappa^2 \,+\, \frac{\tau}{\rho}\,\kappa^4 H\,, \\ & \phi \;\;\to\; \frac{\sigma}{\kappa}\, a\, \left[\frac{1 + \frac{1}{2}\kappa^2 (z+H)^2}{\kappa H}\right] \sin(\kappa x - \sigma t)\,. \end{aligned}} \tag{4.2}$$

4.2 Phase velocity

In this section the so-called phase (or phase function) is investigated, which is defined as

$$\vartheta = \kappa x \,-\, \sigma t\,. \tag{4.3}$$

A wave crest is a phase plane ϑ =constant. An observer moving with the velocity of a phase plane will always see the same phase, i.e.,

$$\left(\frac{d\vartheta}{dt}\right)_{\theta=\text{constant}} \equiv \frac{\partial\vartheta}{\partial t} + c\,\frac{\partial\vartheta}{\partial x} = 0\,.$$

The use of definition (4.3) yields

$$\boxed{c = \frac{\sigma}{\kappa}\,.} \tag{4.4}$$

This is the phase velocity. Application of the dispersion relation (3.6) yields

$$\boxed{c^2 = \left[\frac{g}{\kappa} + \frac{\tau}{\rho}\,\kappa\right]\,\tanh(\kappa H).} \tag{4.5}$$

with the deep and shallow water limits

$$\kappa H \gg 1: \qquad c^2 \;\rightarrow\; \frac{g}{\kappa} + \frac{\tau}{\rho}\,\kappa\,, \tag{4.6a}$$

$$\kappa H \ll 1: \qquad c^2 \;\rightarrow\; gH + \frac{\tau}{\rho}\,\kappa^2 H\,. \tag{4.6b}$$

The two values for c correspond to waves travelling in the positive and negative x-direction. The phase velocity consists of a contribution due to gravity effects, for which $|c|$ decreases with increasing κ, and a capillary contribution for which $|c|$ increases with increasing κ. The behaviour of $c(\kappa)$ is shown in Figure 4.1.

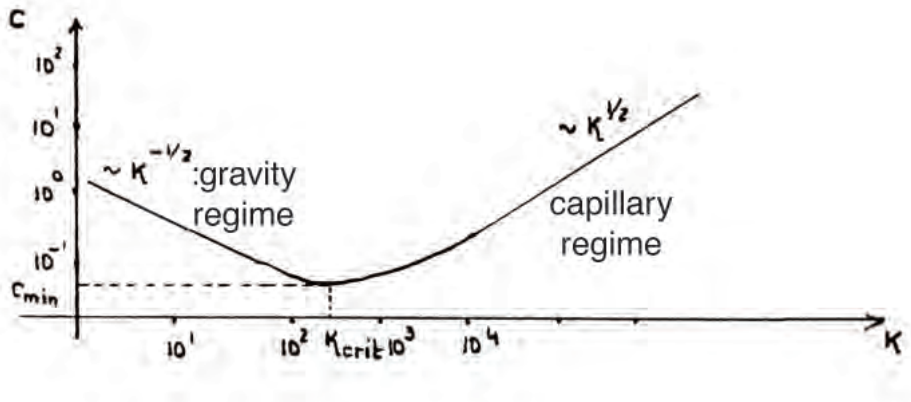

Figure 4.1: Phase velocity c of free linear capillary-gravity waves as a function of wavenumber κ.

For wavenumber $\kappa = \kappa_{\text{crit}}$ the phase velocity attains a minimum. The wavenumber and minimum velocity can be computed from

$$\frac{d}{d\kappa}c^2 = 0 \qquad \text{for} \qquad \kappa = \kappa_{\text{crit}}\,.$$

Elaboration in case of the deep water limit yields

$$\kappa_{\text{crit}} = \sqrt{\frac{\rho\, g}{\tau}} \simeq 3.5 \times 10^2 \text{ m}^{-1} \qquad \text{and} \qquad c_{\text{min}} \simeq 23 \times 10^{-2} \text{ ms}^{-1}$$

for $\rho = 10^3$ kgm^{-3}, $\tau = 0.08$ Nm^{-1} and $g = 9.81$ ms^{-2}.

Thus, for

$$\begin{aligned} B \equiv \frac{\tau\kappa^2}{\rho\, g} \ll 1 \quad &: \quad \text{gravity waves,} \\ B \gg 1 \quad &: \quad \text{capillary waves.} \end{aligned}$$

Parameter B is the Bond number or Weber number.

4.3 Pressure and velocity field

The pressure field is found by substitution of the dispersion relation (3.6) and expression (3.7) for the velocity potential in linearised version of the Bernouilli equation (2.9), i.e.

$$p = -\rho \left\{ \frac{\partial \phi}{\partial t} + gz \right\} .$$

The result is

$$\boxed{p \;=\; -\rho g z \;+\; \rho g a \,(1+B)\, \frac{\cosh[\kappa(z+H)]}{\cosh(\kappa H)}\, \cos(\kappa x - \sigma t)\,.} \tag{4.7}$$

The contributions on the right-hand side describe the hydrostatic pressure and the pressure induced by variations of the free surface, respectively. This result is often used in practice to convert registrations of pressure sensors to sea level variations. Note that the wave-induced pressure decreases with depth and that this decrease is larger for larger wavenumbers. So, if a sensor with a finite resolution is located at a certain depth, it will not detect waves with too small wavelengths.

The deep- and shallow water limits for the pressure are

$$\boxed{\begin{aligned} &\kappa H \gg 1: \quad p \;\rightarrow\; -\rho g z \;+\; \rho g a\,(1+B)\, e^{\kappa z}\, \cos(\kappa x - \sigma t)\,, && \text{(4.8a)} \\ &\kappa H \ll 1: \quad p \;\rightarrow\; -\rho g z \;+\; \rho g a\,(1+B) \qquad \cos(\kappa x - \sigma t)\,. && \text{(4.8b)} \end{aligned}}$$

In shallow water the wave-induced pressure is independent of depth, hence in that case the vertical momentum equation reduces to hydrostatic balance.

As shown by (2.7), the velocity field is governed by the gradient of the velocity potential, given by expression (3.7). The results are

$$
\begin{aligned}
u \equiv \frac{\partial \phi}{\partial x} &= \sigma a \frac{\cosh[\kappa(z+H)]}{\sinh(\kappa H)} \cos(\kappa x - \sigma t)\,, \\
v \equiv \frac{\partial \phi}{\partial y} &= 0\,, \\
w \equiv \frac{\partial \phi}{\partial z} &= \sigma a \frac{\sinh[\kappa(z+H)]}{\sinh(\kappa H)} \sin(\kappa x - \sigma t)\,,
\end{aligned}
\tag{4.9}
$$

with the deep- and shallow water limits

$$
\begin{aligned}
\kappa H \gg 1: \qquad u &\rightarrow \sigma a\, e^{\kappa z} \cos(\kappa x - \sigma t)\,, \\
w &\rightarrow \sigma a\, e^{\kappa z} \sin(\kappa x - \sigma t)\,,
\end{aligned}
\tag{4.10a}
$$

$$
\begin{aligned}
\kappa H \ll 1: \qquad u &\rightarrow \frac{\sigma a}{\kappa H} \cos(\kappa x - \sigma t)\,, \\
w &\rightarrow \sigma a \left(1 + \frac{z}{H}\right) \sin(\kappa x - \sigma t)\,.
\end{aligned}
\tag{4.10b}
$$

Note that the amplitude of the vertical velocity field is always smaller than (or at most equal to) that of the horizontal velocity field. The amplitudes are equal in the deep water limit. Furthermore, in the shallow water limit the horizontal velocity field is independent of depth, whereas the vertical velocity component decreases linearly from its maximum value at the free surface to zero at the bottom.

From the expressions for the velocity field the orbits of individual water particles in the x, z-plane can be computed. By definition,

$$
\frac{dx}{dt} = u\,, \qquad\qquad \frac{dz}{dt} = w\,,
$$

so

$$
x(t) = x_0 + \int_0^t u(x, z, t')\, dt'\,, \qquad z(t) = z_0 + \int_0^t w(x, z, t')\, dt'\,, \tag{4.11}
$$

where x_0, z_0 is the initial position of a particle. An exact computation of the orbits is complicated, because both the velocity components u and w explicitly depend on x and z. It is however possible to find approximate expressions for the particle orbits in case of linear waves, by using the fact that their amplitudes are small (with respect to both their wavelength and depth). By means of Taylor expansions it follows that

$$
\begin{aligned}
u(x, z, t) &= u(x_0, z_0, t) \left[1 + \mathcal{O}(\kappa H, \frac{a}{H}\right]\,, \\
w(x, z, t) &= w(x_0, z_0, t) \left[1 + \mathcal{O}(\kappa H, \frac{a}{H}\right]\,.
\end{aligned}
$$

To lowest order it follows for the particle orbits

$$
\begin{aligned}
x &= \tilde{x}_0 - a \frac{\cosh[\kappa(z_0+H)]}{\sinh(\kappa H)} \sin(\kappa x_0 - \sigma t)\,, \\
z &= \tilde{z}_0 + a \frac{\sinh[\kappa(z_0+H)]}{\sinh(\kappa H)} \cos(\kappa x_0 - \sigma t)\,,
\end{aligned}
\tag{4.12}
$$

where

$$\tilde{x}_0 = x_0 + \frac{a\cosh[\kappa(z_0+H)]}{\sinh(\kappa H)}\sin(\kappa x_0)\,,$$
$$\tilde{z}_0 = z_0 - \frac{a\sinh[\kappa(z_0+H)]}{\sinh(\kappa H)}\cos(\kappa x_0)\,.$$

These expressions describe an ellipse in the x,z-plane, of which the length of the major and minor axes depend on depth. The deep- and shallow water limits are

$$\kappa H \gg 1: \quad \begin{aligned} x-\tilde{x}_0 &= -a\,e^{\kappa z_0}\sin(\kappa x_0-\sigma t)\,, \\ z-\tilde{z}_0 &= a\,e^{\kappa z_0}\cos(\kappa x_0-\sigma t)\,, \end{aligned} \tag{4.13a}$$

$$\kappa H \ll 1: \quad \begin{aligned} x-\tilde{x}_0 &= \frac{-a}{\kappa H}\sin(\kappa x_0-\sigma t)\,, \\ z-\tilde{z}_0 &= a\left(1+\frac{z_0}{H}\right)\cos(\kappa x_0-\sigma t)\,, \end{aligned} \tag{4.13b}$$

In deep water the ellipse reduces to a circle, whereas in shallow water the particles move almost exclusively in the horizontal plane. Some particle orbits for different cases are sketched in Figure 4.2.

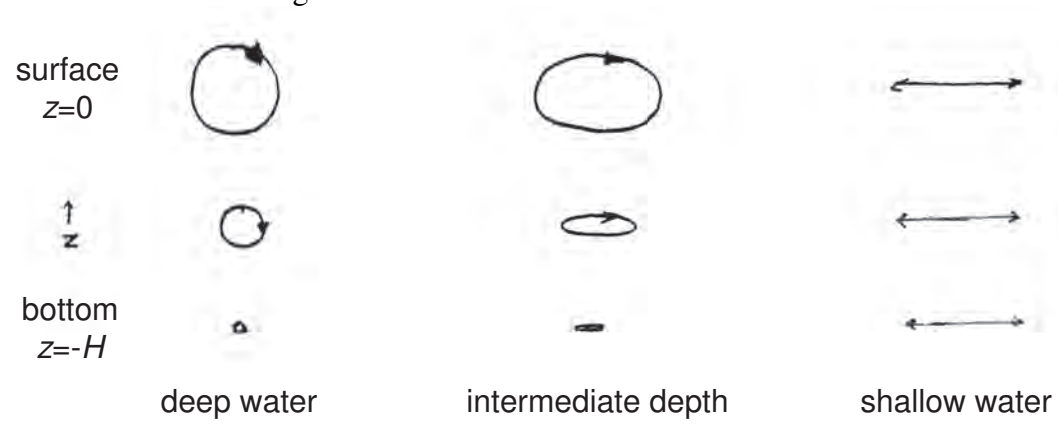

Figure 4.2: Particle orbits at different depths in case of deep water (left), intermediate depth (middle) and shallow water (right).

4.4 Group velocity and energy balance

Next we consider the group velocity. Three different interpretations will be discussed, which all require the introduction of the concept of a wave group. The simplest way to understand its meaning is to realise that solution (3.5)–(3.7) is only one specific solution of the linear system (3.4). A more general solution is found by superposition of waves with different wavenumbers, amplitudes, and directions of propagation. A simple example is the case of two waves moving in the same direction, but having slightly different wavenumbers and frequencies:

$$\zeta_1 = a\,\cos(\kappa x-\sigma t) \qquad , \qquad \zeta_2 = a\,\cos[(\kappa+\Delta\kappa)x-(\sigma+\Delta\sigma)t].$$

Superposition yields

$$\zeta = 2a\,\cos\left\{\frac{1}{2}\left[(2\kappa+\Delta\kappa)\,x-(2\sigma+\Delta\sigma)\,t\right]\right\}\,\cos\left[\frac{1}{2}\left(\Delta\kappa\,x-\Delta\sigma\,t\right)\right]$$
$$\simeq 2a\,\cos\left[\frac{1}{2}\left(\Delta\kappa\,x-\Delta\sigma\,t\right)\right]\,\cos(\kappa x-\sigma t)\,.$$

This describes a sinusoidal wave with a slowly varying amplitude, as can be seen in Figure 4.3. The envelope wave has wavenumber $\frac{1}{2}\Delta\kappa$, frequency $\frac{1}{2}\Delta\sigma$ and propa-

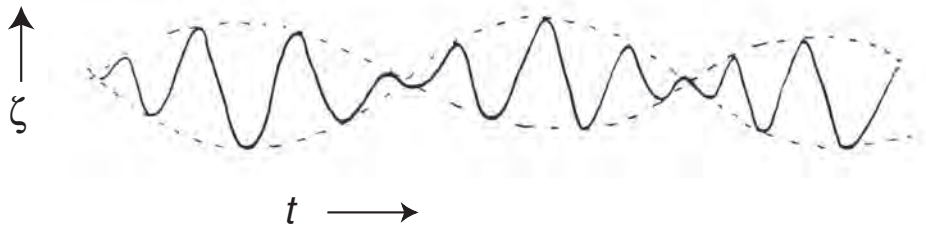

Figure 4.3: A modulated wave.

gates with velocity $\Delta\sigma/\Delta\kappa$. In the limit $\Delta\sigma\to 0, \Delta\kappa\to 0$ this becomes the group velocity

$$\boxed{c_g\;=\;\frac{\partial\sigma}{\partial\kappa}\,.} \tag{4.14}$$

So the envelope of a wave group travels with the group velocity.

A second interpretation of the group velocity is that it is the propagation velocity of the local wavenumber. For this, consider definition (4.3) of the wave phase and assume that both the wavenumber and frequency are *slowly varying* functions of space and time:

$$\vartheta = \kappa(x,t)\,x\;-\;\sigma(x,t)\,t\,.$$

The latter means that κ and σ vary on a spatial (temporal) scale that is large compared to the local wavelength (period) of the wave. Thus, locally

$$\kappa=\frac{\partial\vartheta}{\partial x}\,,\qquad\qquad \sigma=-\frac{\partial\vartheta}{\partial t}\,,$$

from which it follows that

$$\boxed{\frac{\partial\kappa}{\partial t}\;+\;\frac{\partial\sigma}{\partial x}\;=\;0\,.} \tag{4.15}$$

This is the law of conservation of wave crests. Its interpretation is that the change in the number of wave crests in a certain domain is determined by the difference between incoming and outgoing waves through the boundaries.
Using the dispersion relation allows equation (4.15) to be rewritten as

$$\frac{\partial\kappa}{\partial t}\;+\;c_g\,\frac{\partial\kappa}{\partial x}\;=\;0\,. \tag{4.16}$$

Hence, an observer moving with the group velocity will always see the same wavenumber and frequency, but individual wavecrests move because the phase velocity generally differs from the group velocity. This follows from elaboration of the definitions (4.4) and (4.14), which yields

$$\boxed{c_g \,=\, c \,+\, \kappa\,\frac{\partial c}{\partial \kappa}} \tag{4.17}$$

Using the dispersion relation (3.6) yields for the group velocity of free linear capillary-gravity waves:

$$\boxed{c_g \,=\, c\,\left\{\frac{1}{2} \,+\, \frac{\kappa H}{\sinh(2\kappa H)} \,+\, \frac{\tau\kappa^2}{\rho\, g + \tau\kappa^2}\right\}\,.} \tag{4.18}$$

Now consider the dispersion properties of these waves. A wave is called dispersionless if the phase velocity equals the group velocity. For many waves, the phase velocity decreases with increasing wavenumber (long waves travel faster than short waves); this is called normal dispersion. Investigation of the different limits of the group velocity yields the results summarised in the table below.

	gravity waves	capillary waves
deep water	$c_g = \frac{1}{2}c$ normal dispersion	$c_g = \frac{3}{2}c$ anormal dispersion
shallow water	$c_g = c$ no dispersion	$c_g = 2\,c$ anormal dispersion

The third interpretation of the group velocity is that it is the propagation velocity of the energy. To understand this, return to the equations of motion (2.2) and (2.5) and use that the vorticity $\vec{\omega} = 0$ (irrotational flow). The energy balance is derived by multiplication of the momentum equations with $\vec{u}$ and subsequent substitution of the continuity equation. The result is

$$\frac{\partial}{\partial t}\left(\frac{1}{2}\rho|\vec{u}|^2\right) \,+\, \vec{\nabla}\cdot\left[\left(p + \rho g\, z + \frac{1}{2}\rho|\vec{u}|^{\,2}\right)\vec{u}\right] \,=\, 0\,.$$

The first term describes the local change of the kinetic energy per volume unit, the second term is the divergence of the energy flux vector (related to work per unit area done by the wave-induced pressure force and advection of kinetic energy).
Next, consider the energy balance of a column of seawater with unit surface by integration of this expression over the entire depth (from bottom to free surface). Using the kinematic and dynamic boundary conditions, given in equation (2.14), it follows in case of free waves:

$$\frac{\partial E}{\partial t} \,+\, \vec{\nabla}_h \cdot \vec{F} \,=\, 0\,, \tag{4.19a}$$

with

$$E = \int_{-H}^{\zeta} \frac{1}{2}\rho\,|\vec{u}|^2 dz \quad + \frac{1}{2}\rho g\zeta^2 \;+\; \tau\left[1+|\vec{\nabla}_h\zeta|^2\right]^{1/2} - \;\tau$$

$$(1) \qquad\qquad (2) \qquad\qquad (3)$$

and

$$\vec{\mathcal{F}} \;=\; \int_{-H}^{\zeta} (p + \frac{1}{2}\rho|\vec{u}|^2 + \rho g z)\,\vec{u}_h\,dz \;+\; \tau\,\vec{n}\,\frac{\partial\zeta}{\partial t}\,. \tag{4.19b}$$

Here, $\vec{u}_h$ is the horizontal velocity field and $\vec{n}$ is the normal vector at the free surface; the latter is defined in (2.14). Furthermore, E is the instantaneous energy density, i.e., the total energy per surface unit. It consists of a kinetic energy density (1), the potential energy density (2) due to gravity and the potential energy density (3) due to surface tension. Finally, $\vec{\mathcal{F}}$ is the energy density flux.

Consider again weakly modulated linear waves of the type (3.5), where both the wave amplitude, wavenumber and frequency are slowly varying functions of space and time. Since the focus is on linear waves, it is only necessary to compute the lowest-order contributions, i.e., up to O(a^2). Use the expressions for the pressure field (4.7) and velocity field (4.9) to calculate the energy density and the energy density flux vector (in this case $\vec{\mathcal{F}} = (\mathcal{F}_{\S}, \prime)$). Finally, average these results over the phase of the wave, such that quantities are obtained that only vary slowly in space and time. The final results are

$$<E> \;\equiv\; \frac{1}{2\pi}\int_0^{2\pi} E\,d\vartheta = \frac{1}{2}\,(\rho g \;+\; \tau\kappa^2)\,a^2\,, \tag{4.20a}$$

$$<\mathcal{F}_x> \;=\; \frac{1}{2}\,\frac{\sigma}{\kappa}\,a^2\left\{(\rho g + \tau\kappa^2)\left[\frac{1}{2} + \frac{\kappa H}{\sinh(2\kappa H)}\right] + \tau\kappa^2\right\}. \tag{4.20b}$$

The corresponding energy balance is

$$\boxed{\frac{\partial}{\partial t}<E> \;+\frac{\partial}{\partial x}<\mathcal{F}_x> = \;0\,,} \tag{4.21a}$$

with, by definition,

$$<\mathcal{F}_x> = \;c_E\;<E> \tag{4.21b}$$

and c_E is the propagation velocity of the energy density.
Substitution of expressions (4.20a) and (4.20b) in (4.21b) shows, after comparison with (4.18), that

$$\boxed{c_E \;=\; c_g\,.} \tag{4.22}$$

4.5 Waves and currents

So far, linear free capillary gravity waves have been considered in the absence of any background current. In many cases, such currents are present and they influence the wave dynamics in two ways: they cause a Doppler shift of the frequency (hence, the dispersion relation is modified) and they affect the energy balance of the waves.

In case of a background current $\vec{U}$, the modified dispersion relation is

$$\boxed{\sigma_i^2 \equiv (\sigma - \vec{U}\cdot\vec{\kappa})^2 \quad = \quad g\,\kappa\,(1+B)\,\tanh(\kappa H)\,.} \tag{4.23}$$

Here, σ is called the absolute frequency (as experienced by an inertial observer) and σ_i the intrinsic wave frequency, as experienced by an observer who moves with the current.

To compute the energy balance of gravity waves is quite a difficult task, full derivations are given in *Crapper* [1984] and *Mei* [1989]. In fact the energy of waves is no longer conserved, because transfer of energy between waves and currents is possible. The most compact way to express the final result is that, in case of currents, another wave quantity is conserved, viz. the wave action $\mathcal{A}$. The conservation law for the wave action reads

$$\boxed{\frac{\partial}{\partial t}\mathcal{A} + \vec{\nabla}_h\cdot\left[(\vec{U} + \vec{c}_{g,i})\,\mathcal{A}\right] = 0\,, \qquad \mathcal{A} = \frac{<E>}{\sigma_i}\,,} \tag{4.24}$$

with $\vec{c}_{g,i}$ the intrinsic group velocity. It is interesting to note that this equation is not only valid for linear waves, but even for nonlinear waves. The latter fact follows from the analysis of a variational formulation for water waves, as is for example discussed in the book of *Whitham* [1974].

Finally, it is remarked that currents not only affect waves, but waves also affect (and even force) currents. The latter is due to two facts: waves transfer net mass and waves transfer net momentum. The fact that waves transfer net mass follows from computing the over the wave period averaged vertically integrated mass flux:

$$M = < \int_{-H}^{\zeta} \rho\,u\,dz = \frac{<E>}{c} \tag{4.25}$$

The latter result is obtained by substitution of the velocity field (4.9) and making a Taylor expansion of the integral. This implies two things. First, orbits of water particles are not exactly closed: particles experience a small net displacement in the direction of wave propagation. This is known as the Stokes drift and it can be computed by returning to equation (4.11) and including higher-order correction terms. The derivation is not discussed here,details are given in *Kinsman* [1965]. A sketch of the particle orbits and net Lagrangain current (i.e., the net displacement of particles per wave period) is given in Figure 4.4.
The second consequence of the net transfer of mass by waves is that close to the coast (an almost inpermeable boundary) this mass flux is compensated by a (seaward-directed) return flow: the undertow.

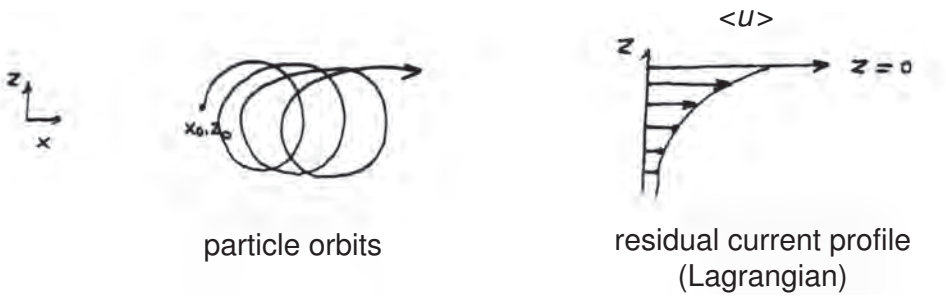

Figure 4.4: Stokes drift. Left: particle orbit in a few wave periods. Right: Lagrangian residual current profile.

As already mentioned, waves also cause a net transfer of momentum. In fact, this is equivalent to stating that waves induce net stresses, similar as turbulent eddies. The computation of these so-called radiation stresses S_{ij} (net transfer by waves of j-momentum in the ith direction) will be discussed in the course 'Physics of coastal systems'. Here, it suffices to state that these stresses depend on the wave properties, like amplitude, wavenumber and wave direction. Hence, if these stresses vary in space then net forces occur that drive net currents. Well-known examples of such currents are longshore currents in the nearshore zone.

4.6 A few remarks about nonlinear waves

As mentioned in the beginning of chapter 3, the problems in constructing solutions of the full equations of motion (2.14) are that

- two conditions are specified at the free surface, of which the position is part of the final solution;
- the conditions at the free surface are nonlinear.

The solutions considered so far are strictly valid in case of infinitesimal amplitudes only, i.e., the wave steepness $\epsilon = a\kappa \to 0$ and parameter $\alpha = (a/H) \to 0$. It is however possible to construct more general solutionsof system (2.14) which have small, but finite amplitudes. In other words, they are valid for $\epsilon \ll 1$ and $\alpha \ll 1$. The results are so-called weakly nonlinear waves. Here, only a few general remarks are made and no details are discussed. There is a vast amount of literature on this topic, for example the books of *Whitham* [1974]; *Mei* [1989]; *Debnath* [1994]; *Dingemans* [1997] and scientific journals like Journal of Fluid Mechanics.

Weakly nonlinear solutions are obtained by application of perturbation methods, which assume that approximate solutions of the equations of motion can be found as series expansions in the small parameters ϵ and α. For example, in the deep water limit (when ϵ is the only relevant parameter):

$$\begin{aligned} \phi &= \phi_0 + \epsilon\phi_1 + \epsilon^2\phi_2 + \ldots, \\ \zeta &= \zeta_0 + \epsilon\zeta_1 + \epsilon^2\zeta_2 + \ldots. \end{aligned}$$

Here, the solutions ϕ_0, ζ_0 represent the linear wave solution and variables like ϕ_1, ζ_1, ϕ_2 and ζ_2 represent higher-order, *nonlinear* corrections to the linear solution.

Furthermore, by using Taylor expansions, the boundary conditions at the free surface can be transformed to conditions at the *fixed* surface $z = 0$. For example, the kinematic boundary condition at the free surface (third equation in system (2.14)) can be written as

$$\frac{\partial \phi}{\partial z} + \zeta \frac{\partial^2 \phi}{\partial z^2} + \ldots = \frac{\partial \zeta}{\partial t} + \vec{\nabla}_h \phi \cdot \vec{\nabla}_h \zeta + \zeta \vec{\nabla}_h \frac{\partial \phi}{\partial z} \cdot \vec{\nabla}_h \zeta + \ldots \quad \text{at} \quad z = 0\,.$$

The procedure is now to substitute the perturbation series in the rewritten equations of motion (conditions at $z = \zeta$ converted to conditions at $z = 0$) and collect terms with equal powers in the small parameter. This yields at each order a system of equations that can be successively solved, since the solutions at the previous order are known.

This method was first successfully used by Stokes in 1834; he constructed a free periodic gravity wave (no surface tension) in deep water with a small, but finite amplitude (wave steepness $\epsilon \ll 1$). His results were the following:

- the profile of the waves becomes asymmetrical: the crests are sharper and the troughs are flatter (see Figure 4.5).

Figure 4.5: Profiles of a linear wave and of a Stokes wave, i.e., the sea surface elevation at a function of coordinate x at a fixed time. The waves travel from left to right.

- Nonlinear terms modify the dispersion relation; it reads

$$\sigma = \sqrt{g\kappa}\left(1 + \frac{1}{2}\epsilon^2 + \ldots\right)\,.$$

  The new term (proportional to ϵ^2) describes amplitude dispersion: large waves travel faster than small waves.

- The results of Stokes and others indicate that, by increasing the number of terms in the perturbation series, the crests become more sharp and ultimately tend to peak. Stokes demonstrated that, *if* the waves peak, then the peak angle is 120^o, as illustrated in Figure 4.6.

Figure 4.6: A Stokes wave with a peak angle of 120^o.

All these findings are consistent with laboratory and field observations, as can be concluded from inspection of e.g. Figure 1.3 in chapter 1.

The Stokes expansion can also be applied in case the water depth is finite (i.e., parameter $\beta = \kappa H$ has a finite value). As shown in *Whitham* [1974] the condition under which the result is valid is that the wave steepness is small ($\epsilon \ll 1$) and that

$$\epsilon \ll 1\,, \qquad\qquad U_r = \frac{\epsilon}{\beta^3} \ll 1\,. \tag{4.26}$$

Parameter U_r is called the Ursell parameter and it measures the relative influence of amplitude dispersion with respect to linear wave dispersion. In case that the conditions (4.26) apply the new dispersion relation becomes

$$\frac{\sigma^2}{g\kappa} = \tanh\beta \left\{ 1 + \epsilon^2 \left[\frac{9\tanh^4\beta - 10\tanh^2\beta + 9}{8\tanh^4\beta} \right] + \mathcal{O}\left(\epsilon^4\right) \right\}\,. \tag{4.27}$$

The calculations are much more extensive than in case of the deep water limit, whereas no new physical insights are obtained.

Regarding the convergence of the Stokes expansion, it turns out to be possible to prove convergence of the series, although no explicit expressions for the radius of convergence are known. However, the value is probably very small. A more serious problem is that deep water Stokes waves are unstable: they lose energy due to interaction with waves with a slightly different wavelength. The underlying mechanism is called side-band instability and was first decsribed in 1967 by Benjamin and Feir. Their results show that Stokes waves are only stable in case that $\beta < 1.36$. The limitation of the Stokes wave expansion is that it is a priori assumed that the solution is periodic with wavenumber κ. Consequently, only modulations in time are allowed, thereby resulting in a modified dispersion relation. A more general case involves modulations both in space and time. This means that, to lowest order, a wave is described as

$$\zeta = \frac{1}{2} A\, e^{i(\kappa x - \sigma t)} + c.c.\,,$$

with c.c. denoting a complex conjugation, where the complex amplitude A is a function of slow space and time variables. By exploiting this method the final result is the so-called nonlinear Schrödinger equation, which contains the Stokes wave as a specific solution. Those who are interested in this (popular) topic are referred to the book of *Mei* [1989] and journals like Physica D.

It is also possible to apply a Stokes expansion for the case of pure capillary waves. This even results in exact solutions (albeit of a subset of the full system of equations), which are called Crapper waves. In contrast with gravity waves their profiles are characterised by flat troughs and sharp crests (see also Figure 4.7).
Finally, it is remarked that finite-amplitude waves can also be constructed in case of shallow water. In practice, this is only done for gravity waves as capillary waves never occur in shallow water. Rather than wave steepness ϵ, parameter $\alpha = a/H$ is the relevant parameter measuring the relative influence of nonlinear terms with

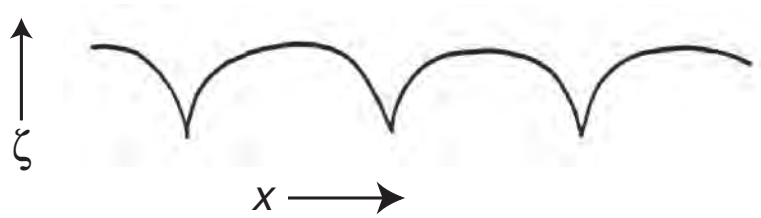

Figure 4.7: Profile of the Crapper wave, a finite-amplitude capillary wave.

respect to linear terms. Different results are obtained, depending on the value of parameter U_r, which can also be written as $U_r = \alpha/\beta^2$. The results are

- if $U_r \ll 1$:
  a classical Stokes wave solution can be constructed;

- if $U_r \gg 1$:
  system (2.14) reduces to the nonlinear shallow water equations. This system describes waves that ultimately break, as shown in Figure 4.8;

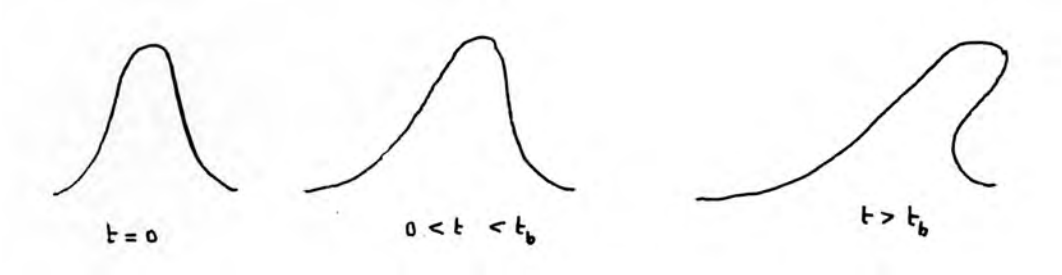

Figure 4.8: Profile of a gravity wave at different times computed from solving the nonlinear shallow water equations. After some time this wave breaks.

- if $U_r \sim 1$:
  system (2.14) can be approximated by the so-called Boussinesq equations, or (in case that waves travel in one direction only) the Korteweg-de Vries equation. These systems allow for *exact* analytical solutions that describe solitary waves and periodic waves (cnoidal waves). The profiles of these waves are sketched in Figure 4.9. The physical reason that these shape-preserving solutions exist is that amplitude dispersion (causing the steepening of spatial gradients) is balanced by linear wave dispersion (that tends to smooth spatial gradients).
  All these solutions have the characteristic property that their phase velocity increases with increasing amplitude. Another interesting property is that solitary waves are quite robust: they survive after mutual interactions.

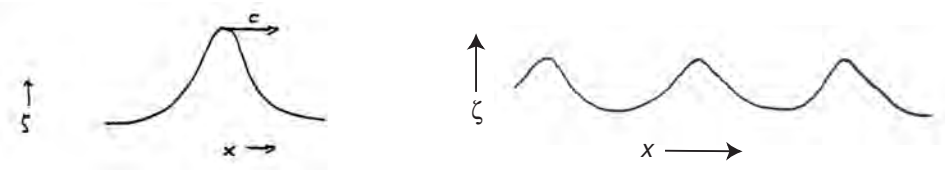

(a) (b)

Figure 4.9: Wave profiles described by the Boussinesq and Korteweg-de Vries equation. Left: a solitary wave, right: a cnoidal wave. Remark: these are solutions of *fully nonlinear* equations, but it should be realised that these equations are derived from a more general system of equations by assuming that the wave amplitude is small.

Chapter 5

Generation of short waves by wind

5.1 Introductory remarks

Investigation of the physical mechanisms that cause the growth of waves at the sea surface is still an actual topic of research. Basic theories are available, but there still are discrepancies between observations and model predictions. It took a relatively long time before quantitative hypotheses for growth of waves by wind were developed. Indeed, the theory of linear and nonlinear water waves was already developed in the 19th century, in particular by Airy, Stokes and Rayleigh, but it was not clear how this knowledge could be used to describe wave evolution at sea. This is partly due to lack of a theoretical concept to describe irregular waves (for this, see chapter 6 hereafter), but also lack of good data was a problem.

In 1925 H. Jeffreys presented the first (semi-empirical) theory of growth by waves, which was based on the sheltering hypothesis. This theory was applied for almost 50 years, for instance it was part of the so-called Sverdrup-Munk theory, which was developed in relation to the landing operations at D-day in World War II. Basically, this theory survived for such a long time because of lack of a better alternative.

The idea underlying the sheltering hypothesis is that if a wind blows over a wavy sea, it causes an underpressure at the lee side of the wave and an overpressure at the stoss side, as shown in Figure 5.1.

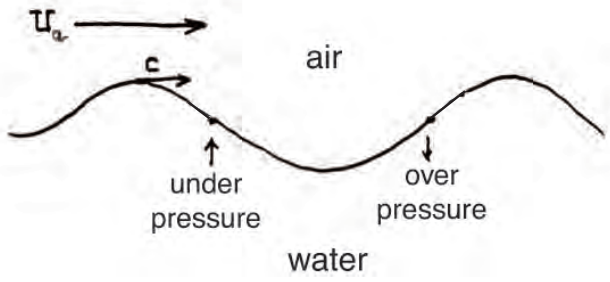

Figure 5.1: A wind blowing over a wavy surface causes over and underpressure. The vertical arrows indicate the direction of the vertical velocity of the wave.

Since these atmospheric pressure fluctuations are in phase with the vertical velocity of the wave, an energy transfer from atmosphere to waves takes place and the waves thereby grow. The empirical part of the theory concerns the relationship between the pressure fluctuation and the free surface. Jeffreys modelled this, using dimensional analysis, as

$$p_0{}' = s\,\rho_a\,(U_a - c)^2\,\frac{\partial \zeta}{\partial x}\,,$$

with s a dimensionless sheltering coefficient, ρ_a the density of air, U_a the wind speed and c the phase velocity of the wave.

Jeffreys considered both the production of wave energy (by wind) and dissipation of energy by viscous terms. He stated that growth of waves would only occur in case that the production term exceeds the dissipation term. From this he derived an expression that relates the minimum wind speed U_{min} (below which waves will not grow) to the sheltering coefficient. Based on observations $U_{\text{min}} = 1.1\ \text{m}\,\text{s}^{-1}$ was taken, thereby yielding $s \simeq 0.27$.

The drawbacks of the sheltering hypothesis are that measured pressure fluctuations in the laboratory turned out to be much smaller than predicted by the theory. Also, waves can grow even in the case that their phase velocity is smaller than the wind speed. Finally, the sheltering mechanism only acts if waves are already present at the sea surface.

In 1957 two important new theorical concepts related to growth of waves by wind were presented, which were both based on fundamental physical laws. They were the resonance mechanism, developed by Phillips, and the shear instability mechanism developed by Miles. The Phillips mechanism assumes that turbulent eddies, with many different length scales, are present in the atmospheric boundary layer. They are advected by the mean wind, which has a logarithmic profile (see Figure 5.2).

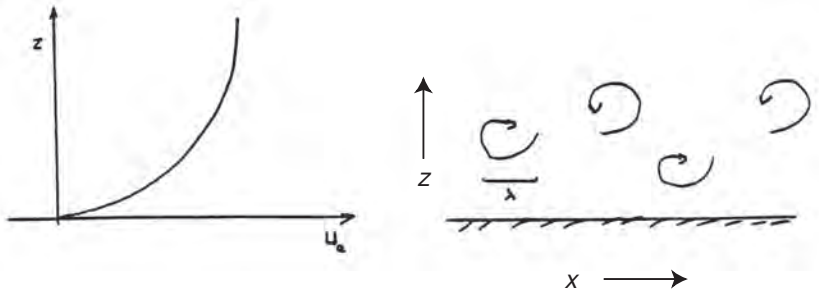

Figure 5.2: Mean wind profile in the atmospheric boundary layer and the presence of turbulent eddies.

These eddies induce pressure fluctuations at the sea surface. If the number of eddies per time unit, σ_1, that pass a fixed observation point equals the frequency σ of a free wave, then resonant growth of this wave will occur. Now, $\sigma_1 = \vec{U}_a \cdot \vec{\kappa}$, where $\vec{U}_a$ is the velocity by which the turbulent eddy is advected and $\vec{\kappa}$ the wavevector of the eddy. For frequency σ the dispersion relation (3.6) can be used. The resonance

condition thus reads:

$$\sigma_1 = \sigma\,, \qquad \text{or} \qquad \left[\frac{g}{\kappa} + \frac{\tau}{\rho}\,\kappa\right]^{1/2} = U_A\,\cos\alpha \tag{5.1}$$

where in the last step the definition of the phase speed is used; α is the angle between wavevector and windvector. Equation (5.1) is transcedental because the advection speed depends on the wavenumber: it is the wind speed at a height κ^{-1} above the undisturbed sea level. Figure 5.3 shows the graphical solution of equation (5.1) in case that $\alpha = 0$ (waves propagate in the direction of the wind).

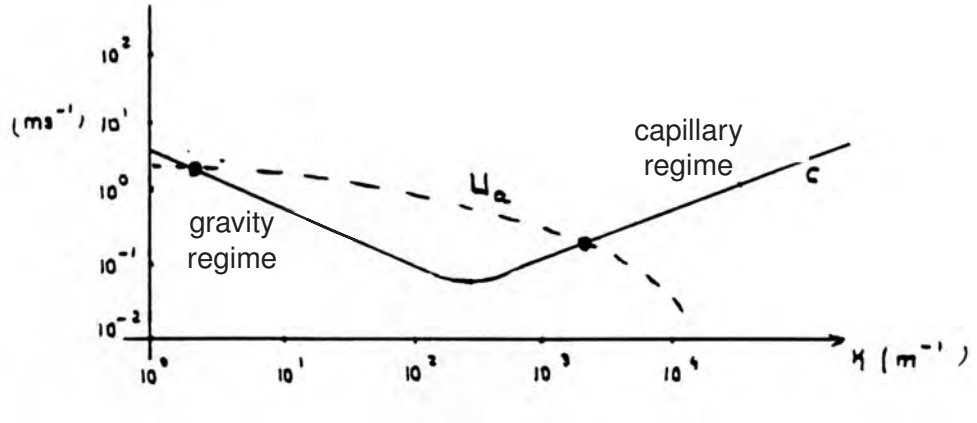

Figure 5.3: Graphical solution of the transcedental equation (5.1).

The intersection of the two curves $c(\kappa)$ and $U_a(\kappa)\cos\alpha$ yields two resonant wavenumbers, one in the gravity wave regime and one in the capillary wave regime. If angle α is nonzero, then the resonant wavenumbers move closer to eachother. They even disappear if $\alpha = \alpha_c$, where

$$\alpha_c \simeq \arccos\left(\frac{c_{\min}}{U_a}\right) = \arccos\left(\left[\frac{4\,g\,\tau}{\rho\,U_a^4}\right]^{1/4}\right)\,. \tag{5.2}$$

Using a statistical description of sea waves, *Phillips* [1977] also demonstrated that the growth of energy of the wave field is linear in time: $< E(t) > \sim t$.

The strong points of the Phillips resonance mechanism are:

- it is based on fundamental physics (no empirical knowledge);
- waves can grow from an initially smooth surface (no a priori presence of waves required);
- it predicts that no growth of waves occurs if $U_a < c_{\min}$, in other words, a minimum wind speed is required before waves grow, which is consistent with observations. See e.g. Figure 1.14 in chapter 1;
- linear growth of wave energy is indeed observed during the first stage of wave growth from a smooth sea surface, when amplitudes are still very small.

However, the Phillips mechanism also has an important drawback, viz. it ignores the feedback of the waves to the windfield. This is the reason that the theory can only be used at the earliest stage of wave growth and it is not much used anymore. A better description of wave growth is obtained by using the shear instability mechanism, that will be discussed in the next sections.

5.2 Shear instability mechanism; basic equations

This theory is based on the hypothesis that sea waves arise as a free instability of the coupled sea-atmosphere system. In fact, the waves grow by extracting energy from the mean wind field, that is an exact solution of the system in case of a smooth water surface. Miles originally developed his theory in 1957 for inviscid air and water; here the more general case will be explored.

In Figure 5.4 a sketch is presented of the density distribution and mean velocity profile near the sea surface.

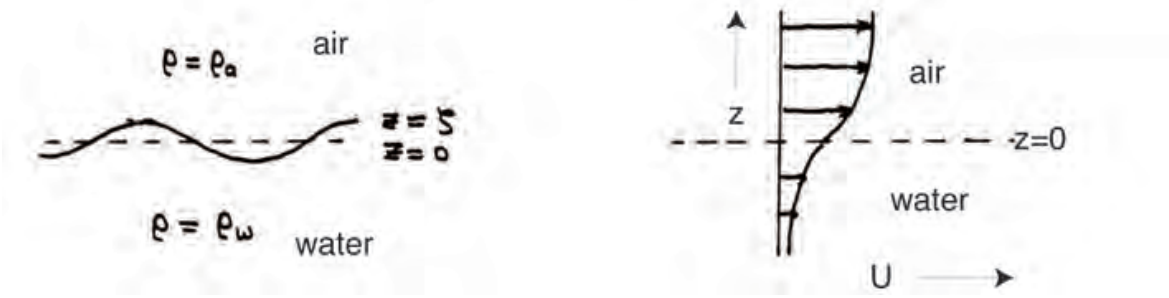

Figure 5.4: Density distribution and velocity profiles near the sea surface.

In principle, the densities ρ_a, ρ_w (of air and water, respectively) may depend on the vertical coordinate z (see chapter II.2 in the book of *Komen et al.* [1994]). Here, for simplicity, these densities are assumed to be constant. Consequently, thermodynamic effects need not to be taken into account. The equations of motion then become

$$\begin{aligned} &\rho \left\{ \frac{\partial \vec{u}}{\partial t} + \vec{\nabla} \cdot (\vec{u}\vec{u}) \right\} = -\vec{\nabla} p - \rho \vec{g} + \rho \nu \nabla^2 \vec{u} + \frac{\partial}{\partial z} \vec{\tau}\,, \\ &\vec{\nabla} \cdot \vec{u} = 0\,, \end{aligned} \tag{5.3}$$

with $\vec{u}$ the 3D-velocity field, ν the kinematic viscosity coefficient ($= \nu_a \sim 1.5 \times 10^{-5}$ m^{2}s^{-1} for air and $\nu_w \sim 1 \times 10^{-6}$ m^{2}s^{-1} for water) and $\vec{\tau}$ is a vector with components $(\tau_{xz}, \tau_{yz}, \tau_{zz})$ that are shear stresses. The latter describe the transport of momentum in the vertical direction due to turbulent eddies. The sea is assumed to be unbounded in the vertical (deep water limit) and Coriolis effects are neglected.

The boundary conditions become, in case of an inviscid fluid:

$$\begin{aligned} &w \to 0 \qquad && \text{for } \; z \to \pm\infty\,, && \\ &w = \frac{d\zeta}{dt} \qquad && \text{at } \; z = \zeta, && \lim_{z\uparrow\zeta} p = \lim_{z\downarrow\zeta} \left(p + \tau \vec{\nabla} \cdot \vec{n} \right)\,, \end{aligned} \tag{5.4}$$

with τ the surface tension, see section 2.2. For a viscous fluid the pressure p must be replaced by the normal component of the tension acting at the free surface and besides, the tangential component of the tension must be continuous at $z = \zeta$.

In the absence of variations of the free surface, system (5.3)-(5.4) has an equilibrium solution which is uniform in the horizontal direction. In order to describe it, it is

convenient to introduce the horizontal velocity field $\vec{u}_h$ and a two-dimensional vector $\vec{\tau}_h$ with components (τ_{xz}, τ_{yz}). Then, the equilibrium solution is characterised by $\vec{u}_h = \vec{U}(z), w = 0, p = P(z)$, where

$$\frac{d}{dz}\left[\nu\frac{d\vec{U}}{dz} + \frac{\vec{\tau}_h}{\rho}\right] = 0, \qquad \frac{dP}{dz} = -\rho\, g\,. \tag{5.5}$$

with corresponding dynamic boundary conditions at the free surface. So, this flow has a constant tangential shear stress and is in hydrostatic balance.

In inviscid theory (i.e., $\nu = 0, \vec{\tau} = 0$) any velocity profile $\vec{U}$ is an equilibrium solution. In viscous theory, the velocity is determined by the parameterization of the turbulent shear stresses. In many cases the so-called K-theory is used to express the shear stresses in terms of the velocity field:

$$\vec{\tau}_h = \rho K(z)\frac{\partial}{\partial z}\vec{u}_h\,, \tag{5.6}$$

with $K(z)$ a turbulent viscosity coefficient. In the atmospheric boundary layer the latter is determined by two parameters: the shear stress $|\vec{\tau}_h|(z = 0)$ at the undisturbed free surface and the distance z to the undisturbed water surface. The only combination that yields the correct dimension for the turbulent viscosity coefficient is

$$K_a(z) = k\, u_*\, z, \qquad \rho_a\, u_*^2 = |\vec{\tau}_h(z = 0)|\,, \tag{5.7}$$

with $k \sim 0.41$ being von Karman's constant and u_* the friction velocity.

Integration of the momentum equation in (5.5), and use of equations (5.6) and (5.7), yields a logarithmic wind profile in the atmospheric boundary layer:

$$\boxed{|\vec{U_a}| = |\vec{U}|\,(z = 0) + \frac{u_*}{k}\ln\left(1 + \frac{z}{z_0}\right)\,,} \tag{5.8}$$

with $z_0 = \nu_a/(ku_*)$ the so-called roughness length: $z_0 \sim 10^{-5}$ m in case of a smooth sea surface.

Miles assumed the velocity at the sea surface $\vec{U}(z = 0) = 0$ to vanish; consequently, there is no current in the sea. However, in case of a viscous fluid the shear stress acting at the free surface generates currents in the water. The velocity profile in the sea is often chosen such that current decrease exponentially with depth:

$$\boxed{|\vec{U_w}| = |\vec{U}(z = 0)|\, e^{\lambda z}} \qquad \lambda = \frac{\rho_a\, u_*^2}{\rho_w \nu_w |\vec{U}(z = 0)|}\,, \tag{5.9}$$

where parameter λ is chosen such that the tangential shear stress is continuous at the sea surface ($\lambda^{-1} \sim 10^{-2}$ m). Note that (5.9) is a solution of equations (5.5) and (5.6) if $(K_w + \nu_w) = \nu_w e^{-\lambda z}$, i.e., the turbulent viscosity coefficient *increases* exponentially with depth.

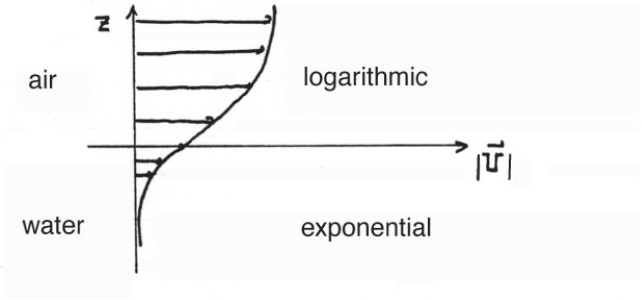

Figure 5.5: Velocity profile of the basic state in the Miles model. In the atmospheric boundary layer the profile is logarithmic, in the sea it is exponential.

The final velocity profile of the equilibrium state (also called: basic state) is sketched in Figure 5.5.
This is an example of a shear current, which agrees well with observations. But note that, in principle, the theory allows for any basic velocity profile as long as a suitable corresponding turbulent viscosity coefficient is chosen.

The solution discussed above will change in case that waves are present at the sea surface. To analyse this case, assume plane harmonic waves propagating in the x-direction (hence, no wave-induced velocity in the y-direction). Also, assume the direction of wave propagation to coincide with the wind direction. Next, write the velocity, pressure and free surface as a superposition of their basic state values and wave-induced fluctuations:

$$\begin{aligned} u &= U(z,t) + u'(x,z,t)\,, & p &= P(z,t) + p'(x,z,t)\,, \\ w &= \qquad\quad w'(x,z,t)\,, & \zeta &= \qquad\quad \zeta'(x,t)\,. \end{aligned} \tag{5.10}$$

Note that now the basic state variables are also assumed to be depend on time. The reason is that, due to wave-current interactions, these variables will change in time. These variations however are *slow*: they occur on a timescale that is large compared to the period of the waves.

Substitution in the equations of motion (5.3) and subsequent *linearisation* of the equations (this is allowed if the fluctuations have small amplitudes in the sense that $u' \ll U$) yields

$$\begin{aligned} &\frac{\partial U}{\partial t} + \frac{\partial u'}{\partial t} + U\frac{\partial u'}{\partial x} + w'\frac{\partial U}{\partial z} = -\frac{1}{\rho}\frac{\partial p'}{\partial x} + \nu\left[\frac{\partial^2 u'}{\partial x^2} + \frac{\partial^2 u'}{\partial z^2}\right] + \frac{1}{\rho}\frac{\partial \tau_{xz}{}'}{\partial z}\,, \\ &\qquad \frac{\partial w'}{\partial t} + U\frac{\partial w'}{\partial x} \qquad\qquad = -\frac{1}{\rho}\frac{\partial p'}{\partial z} + \nu\left[\frac{\partial^2 w'}{\partial x^2} + \frac{\partial^2 w'}{\partial z^2}\right]\,, \\ &\frac{\partial u'}{\partial x} + \frac{\partial w'}{\partial z} = 0\,. \end{aligned} \tag{5.11}$$

The conditions at the free surface $z = \zeta$ can be transformed to conditions at the undisturbed surface $z = 0$ (with the use of Taylor expansions, see remarks at the

end of chapter 4). Development yields

$$
\begin{aligned}
& w' = \frac{\partial \zeta'}{\partial t} + U\,\frac{\partial \zeta'}{\partial x} && \text{at} \quad z = 0\,, \\
& w' \to 0 && \text{for} \quad z \to \pm\infty\,, \\
& \lim_{z\uparrow 0}\,(\,p' \,-\, \rho_w g \zeta'\,) \,=\, \lim_{z\downarrow 0}\left(p' - \rho_a g \zeta' - \tau \frac{\partial^2 \zeta'}{\partial x^2}\right)\,, \\
& \lim_{z\uparrow 0}\left(\rho\nu\frac{\partial u'}{\partial z} + \tau_{xz}'\right) = \lim_{z\downarrow 0}\left(\rho\nu\frac{\partial u'}{\partial z} + \tau_{xz}{}'\right)\,.
\end{aligned}
\tag{5.12}
$$

At this point the (fargoing!) assumption is made that $\tau_{xz}{}' = 0$, i.e., the *turbulent* structure of the wind field in the atmospheric boundary layer and current field in the surface layer of the sea is not influenced by waves. At this moment, modification of this assumption is an active topic of research, see also the final remarks at the end of this chapter. From hereon, there are two possible ways to analyse system (5.11). They are discussed in the subsequent two sections.

5.3 Stability theory: method of Miles

Miles analysed system (5.11) with $\tau_{xz}{}' = 0$ on the *short* timescale of the waves. This implies that the term $(\partial U/\partial t)$ can be neglected and the focus is on the growth of (the amplitude) of the waves. Now, the continuity equation allows the introduction of a stream function ψ', such that

$$
u' = \frac{\partial \psi'}{\partial z}, \qquad\qquad w' = -\frac{\partial \psi'}{\partial x}\,. \tag{5.13}
$$

An equation for ψ' is derived by elimination of the pressure from the momentum equations. The result is the vorticity equation

$$
\frac{\partial}{\partial t}\nabla^2\psi' + U\frac{\partial}{\partial x}\nabla^2\psi' - \frac{\partial \psi'}{\partial x}\frac{d^2U}{dz^2} \;=\; \nu\nabla^4\psi'\,. \tag{5.14}
$$

Here,

$$
\nabla^2\psi' \;=\; \frac{\partial^2\psi'}{\partial x^2} + \frac{\partial^2\psi'}{\partial z^2} \;\equiv\; \frac{\partial u'}{\partial z} - \frac{\partial w'}{\partial x}
$$

is the y-component of the vorticity vector. The second term in (5.14) describes the advection of perturbed vorticity by the basic state current; the third term is the advection of background vorticity by the wave-induced velocity field. Finally, the term on the right-hand side describes dissipation of vorticity.

Equation (5.14) allows for solutions of the following form:

$$
\psi' = \Re\left[\hat{\psi}(z)\; e^{i\kappa(x-ct)}\right] \equiv \Re\left[\hat{\psi}(z)\; e^{i\kappa(x-c_r t)}\; e^{\kappa c_i t}\right]\,, \tag{5.15}
$$

where $\Re$ denotes the real part and it has been assumed that $c = c_r + ic_i$. They represent plane harmonic waves with wavenumber κ that propagate with velocity c_r along the x-axis with an as yet unknown vertical structure. Their amplitude behaves exponentially in time, where κc_i is the growthrate, which is to be determined. Note that the waves *grow* if $c_i > 0$. Substitution of (5.15) in the vorticity equation (5.14) yields

$$\boxed{(U-c)\left(\frac{d^2}{dz^2}-\kappa^2\right)\hat{\psi}-\frac{d^2U}{dz^2}\,\hat{\psi}=-\frac{i\nu}{\kappa}\left(\frac{d^2}{dz^2}-\kappa^2\right)^2\hat{\psi}\,.} \tag{5.16}$$

This is the Orr-Sommerfeld equation, which is also obtained in case of many other hydrodynamic stability models. Together with the boundary conditions, it defines an eigenvalue problem where c are the (complex) eigenvalues. The problem is to obtain solutions of (5.16), because in general $U(z)$ is a complicated function of vertical coordinate z. Often, they are obtained by numerical methods. In some cases asymptotic and even exact solutions can be constructed, see remarks in e.g. the book of *Komen et al.* [1994].

From hereon, a brief summary is given of the original work of Miles.

- He used inviscid theory, i.e. $\nu = 0$.
  Consequently, (5.16) reduces to the Rayleigh equation.
- He assumed that in equilibrium (no waves) there is no current below the sea surface. This implies that solutions of the Rayleigh equation for $z < 0$ become simple exponential functions.
- He assumed a logarithmic wind profile, given by (5.8), in the atmospheric boundary layer.

Remark: Miles realised that both the shear and curvature of the wind profile were important for excitation of wind waves. By that time it was known that in case that U_a=constant the Rayleigh equation describes the Kelvin-Helmholtz instability mechanism. This, however, does not give a satisfactory explanation for the generation of waves by wind, since it predicts that instabilities only occur if wavenumber $\kappa > g\rho_w/(\rho_a U_a^2)$. For realistic parameter values this means that only ultrashort waves (wavelengths of the order of millimetres and smaller) can grow.

Miles used known, but rather advanced, mathematical methods to find approximate solutions (for $\varepsilon \equiv (\rho_a/\rho_w) \ll 1$) of the Rayleigh equation and the corresponding eigenvalues c. His classical expression for the growth rate $\gamma_a \equiv \kappa c_i$ reads

$$\boxed{\frac{\gamma_a}{\varepsilon\sigma} = -\frac{\pi}{2\kappa}\,|\chi_c|^2\,\frac{\left(\frac{\partial^2 U_a}{\partial z^2}\right)_{z=z_c}}{\left(\frac{\partial U_a}{\partial z}\right)_{z=z_c}}\,,} \tag{5.17}$$

where σ is the frequency of the wave and $\chi_c = \hat{w}_a/(\sigma a)$ is the dimensional amplitude of the wave-induced velocity field at the critical level $z = z_c$, where the wind speed U_a equals the phase speed $c = \sigma/\kappa$ of the wave. In Figure 5.6 the growth rate is plotted as a function of the ratio of friction velocity and phase velocity.

The result of Miles demonstrates that

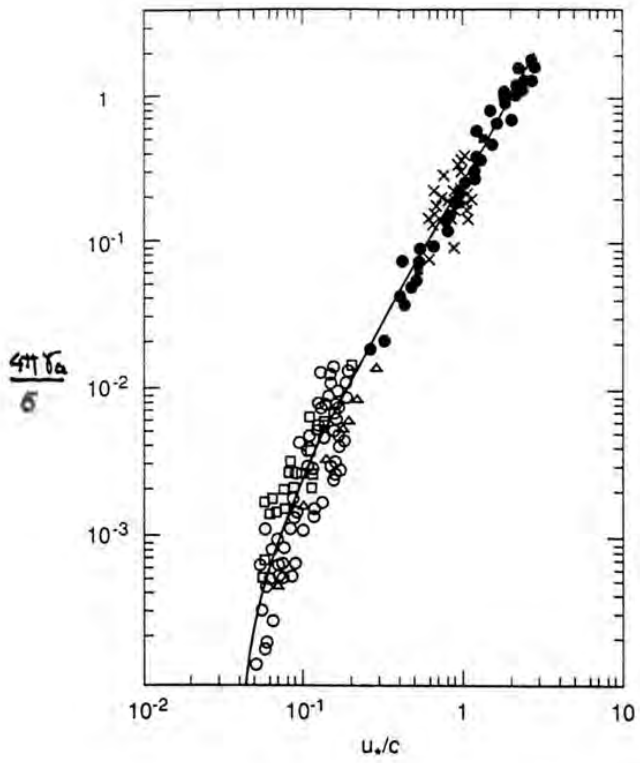

Figure 5.6: Dimensionless growth rate of wind waves as a function of u_*/c, where u_* and c are the friction velocity and phase speed, respectively. The solid curve is the result by Miles, the symbols are data. Adopted from *Komen et al.* [1994].

- wave-like perturbations at the sea surface grow and gain their energy from the mean wind in the atmospheric boundary layer;
- effective coupling between waves and wind only occurs at the critical level $z = z_c$;
- both shear and curvature of the wind profile are necessary for growth of waves.

Figure 5.6 shows that the computed growth rates agree rather well with observations. This is the reason that the result of Miles, albeit often in a modified form, is still used in many wave prediction models.

Important limitations of the Miles model concern the facts that viscous effects are neglected, the effect of waves on the turbulent structure of the atmospheric boundary layer is ignored and nonlinear effects are not considered (hence the waves must have small amplitudes). Besides, perturbations of the sea surface (albeit that their amplitudes may be very small) must be present before the mechanism acts and also the (thermodynamic) stability of the atmospheric boundary layer influences the growth mechanism. Finally, note that (5.17) predicts growth of waves for all wavenumbers and windspeeds, whereas observations indicate that there is a minimum wind speed before growth of waves occurs. Some of these aspects will be revisited in the final section of this chapter.

5.4 Lighthill interpretation of the Miles mechanism

The way in which Miles derived his result was correct, but rather mathematical; therefore, it was difficult to understand the underlying physical mechanism. In 1962, Lighthill presented a very elegant interpretation of the shear instability mechanism. His starting point were equations (5.3)-(5.4) and solutions of the form (5.10), resulting in the full equations for the perturbations, i.e., the nonlinear version of system (5.11). But, contrary to what Miles did, Lighthill considered the latter equations on a long timescale (long compared to the typical wave period) and averaged the equations over a wavelength. After averaging over the wavelength of the pertubations (denoted by an overbar) he obtained the following horizontal momentum balance:

$$\boxed{\frac{\partial U_a}{\partial t} + \frac{\partial}{\partial z}\overline{{u_a}' {w_a}'} = 0\,.} \tag{5.18}$$

This equation shows that the change of the wind speed is due to the divergence of the wave-induced shear stress $-\overline{{u_a}'{w_a}'}$. It can also be recasted as

$$\frac{\partial U_a}{\partial t} = -\overline{{\omega_y}' {w_a}'} \qquad \text{with} \qquad {\omega_y}' = \frac{\partial {u_a}'}{\partial z} - \frac{\partial {w_a}'}{\partial x}\,, \tag{5.19}$$

where use has been made of the continuity equation for the wave-induced fluctuations and the definition of the averaging operator. Note that ${\omega_y}'$ is the y-component of the vorticity vector of the fluctuations. Thus, changes in the mean wind profile are caused by vertical transport of this vorticity component by the waves.

This forcing term at the right-hand side of (5.19) can be fully expressed in terms of the vertical velocity field. For this, consider an air parcel that, due to the wave-induced vertical velocity, is displaced from vertical level $z_a - {h_a}'$ to level z_a. Since the parcel takes its background vorticity $\partial U_a/\partial z$ with it, it induces at level z_a a perturbation in the vorticity:

$${\omega_y}' = -\left.\frac{\partial U_a}{\partial z}\right|_{z=z_a} + \left.\frac{\partial U_a}{\partial z}\right|_{z=z_a-{h_a}'} \simeq \quad -{h_a}'\left.\frac{\partial^2 U_a}{\partial z^2}\right|_{z=z_a}\,, \tag{5.20}$$

where in the last step a Taylor approximation has been used. Finally, the displacement ${h_a}'$ follows from integration of the vertical velocity field.

Thus, after substitution of (5.20) in momentum equation (5.19), the final results are

$$\frac{\partial U_a}{\partial t} = \overline{{h_a}' {w_a}'}\,\frac{\partial^2 U_a}{\partial z^2} \qquad \text{and} \qquad {h_a}' = \int_0^t {w_a}' dt'\,. \tag{5.21}$$

The first equation is a diffusion equation with $\overline{{h_a}'{w_a}'}$ a diffusion coefficient that provides for the coupling between wave field and wind field. To find an explicit expression for this diffusion coefficient the structure of the wave-induced vertical velocity is analysed. It can be written as

$${w_a}' = \hat{w}_a(z)\cos[\kappa(x-ct)]\,, \tag{5.22}$$

with $\hat{w}_a(z)$ a height-dependent amplitude. For the computation of the vertical displacement $h_a^{'}$of an air parcel, it is important to realize that this parcel is also advected in the horizontal plane (by both the mean wind and the wave-induced horizontal velocity). It is therefore convenient to apply the coordinate transformation

$$\xi \;=\; x \;-\; U_a(z)\,t$$

where ξ is a coordinate in a frame moving with the local mean wind speed. In Figure 5.7 the situation in this co-moving frame is sketched. In this new coordinate

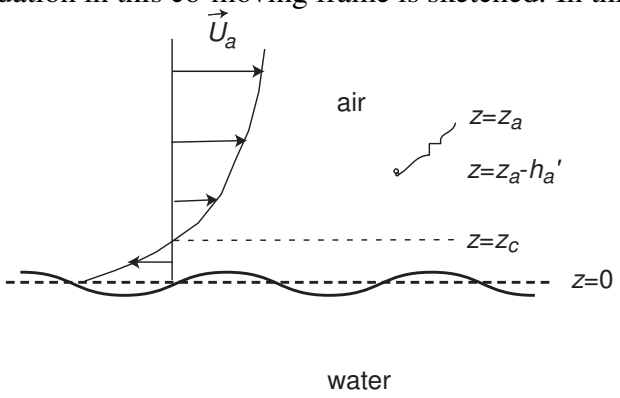

Figure 5.7: Situation sketch in a frame that moves with the wind speed at the critical level $z = z_c$, which is equivalent to the phase velocity of the wave.

system the vertical velocity reads

$$w_a{}' = \hat{w}_a(z)\cos[\kappa\xi + \kappa(U_a - c)t\,] \;\simeq\; \hat{w}_a(z)\cos[\kappa(U_a - c)t\,] \tag{5.23}$$

in case of small-amplitude waves (with corresponding small displacements). Combination of (5.19) and (5.23) yields

$$h_a{}'\,w_a{}' \;=\; \frac{\hat{w}_a(z)^2\,\sin[2\tilde{\sigma}(z)t\,]}{2\,\tilde{\sigma}(z)}, \qquad\qquad \tilde{\sigma}(z) = \kappa(U_a - c)\,. \tag{5.24}$$

To obtain an expression for the wave-induced dispersion coefficient, this result must be averaged over the time that air parcels need to move one wavelength in the horizontal plane. As long as the wind speed differs from the phase speed this time $\tilde{T} = w\pi/(\tilde{\sigma}(z))$ is finite and it follows from (5.24) that

$$\overline{h_a{}'\,w_a{}'} = 0 \qquad \text{if} \qquad \tilde{\sigma}(z) \neq 0\,.$$

However, at the critical level $z = z_c$, where the wind speed equals the phase speed, this time becomes infinite. From (5.24) it then follows

$$\lim_{t\to\infty} h_a{}'\,w_a{}' = \hat{w}_a(z)^2 \lim_{t\to\infty} \frac{\sin[2\tilde{\sigma}(z)t]}{2\tilde{\sigma}(z)} = \pi\,\hat{w}_a(z)^2\,\delta\,[2\tilde{\sigma}(z)]\,,$$

where a definition of the Dirac delta function δ has been applied. This result shows that there is only coupling between wave field and wind field at the critical level.

The final result for the wave dispersion coefficient can be written in a more convenient form by application of the identity

$$\delta\left[f(x)\right] \;=\; |\frac{df}{dx}|^{-1}\,\delta(x-x_0) \qquad \text{with} \qquad f(x_0)=0\,.$$

This yields

$$\boxed{\overline{h_a^{\,\prime}\,w_a^{\,\prime}} \;=\; \frac{\pi\,\hat{w}_a(z)^{\,2}}{2\kappa\,\frac{\partial U_a}{\partial z}}\;\delta(z-z_c)\,.} \tag{5.25}$$

It is now possible to calculate the energy transferred from the mean wind field to the wave field. The vertically integrated energy equation for the atmospheric boundary layer is found by multiplication of (5.21) by $\rho_a U_a$. Thus,

$$\begin{aligned}\frac{\partial}{\partial t}\int_0^\infty \frac{1}{2}\rho_a U_a^2 dz \;&=\; \rho_a\int_0^\infty U_a\,\overline{h_a{}'\,w_a{}'}\;\frac{\partial^2 U_a}{\partial z^2}\,dz \\ &=\; \frac{\pi\rho_a\hat{w}_a(z_c)^2}{2\kappa}\;U_a(z_c)\;\frac{\frac{\partial^2 U_a}{\partial z^2}\Big|_{z=z_c}}{\frac{\partial U_a}{\partial z}\Big|_{z=z_c}} \;<\; 0\,.\end{aligned}$$

The decrease in energy density of the wind field is transferred to that of the wave field, hence

$$\frac{\partial}{\partial t}<E>=\frac{1}{2}(\rho g+\tau\kappa^2)\,\frac{\partial}{\partial t}a^2 = -\frac{\pi\rho_a\hat{w}_a(z_c)^2}{2\kappa}\;U_a(z_c)\;\frac{\frac{\partial^2 U_a}{\partial z^2}\Big|_{z=z_c}}{\frac{\partial U_a}{\partial z}\Big|_{z=z_c}}\,.$$

where the definition (4.20a) of the wave energy density has been used. Note at this point the equivalence between this result of Lighthill and the result (5.17) of Miles.

The amplitude of the wave-induced vertical velocity at the critical level will be proportional to wave amplitude a, hence it follows that

$$\frac{\partial}{\partial t}\,a^2 \;\sim\; a^2\,,$$

in other words, the energy density of the waves grows *exponentially* in time. In fact, the constant of proportionality in the expression above is precisely $2\gamma_a$, where the growth rate γ_a is given in (5.17).

5.5 Final remarks

The results of the theories developed by Phillips and Miles can be summarised as follows. Starting from a perfectly smooth surface the Phillips resonance mechanism causes initial growth of waves. At this stage the energy density grows linearly in time. Once the waves are present, feedbacks between the waves and the wind become important. This is accounted for by the shear instability mechanism of

Miles, with the result that the energy density grows exponentially in time. After a certain time, waves have become so large that nonlinear interactions between different wave components become important. Waves ultimately break (whitecapping at open sea, breaking by decrease in water depth near the shore), which cause dissipation of wave energy. A typical development of energy density of a wave with a fixed frequency is sketched in Figure 5.8 (see also figure 1.14 in chapter 1).

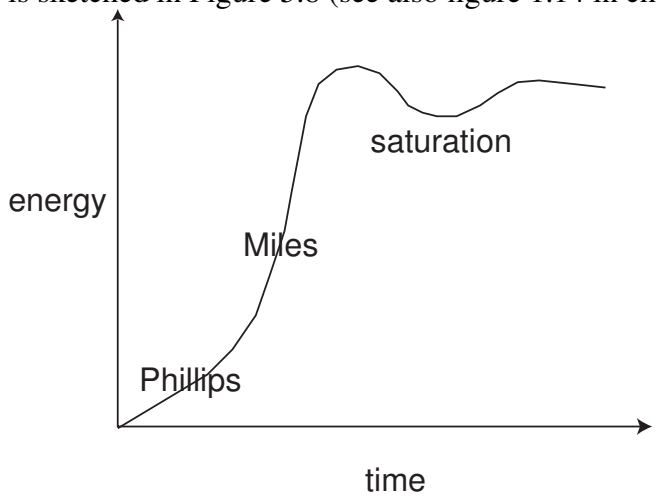

Figure 5.8: Typical evolution in time of the energy density of a wave with a fixed frequency due to wind (solid curve) and nonlinear effects (dashed curve).

The inviscid theory of Miles yields a good description of the growth of waves with relatively long wavelengths (such that $u_*/c < 10$), albeit that the actual growth rate is often underestimated (by a factor of $\sim$ 2). On the other hand, observations are difficult to analyse and interpret, see the discussion in the book of *Komen et al.* [1994].

The major criticism to the Miles theory concerns the fact that, for maintaining the logarithmic wind profile in the atmosphere, turbulent fluctuations are necessary whereas their role in the actual growth process is neglected. This is active point of research, e.g. at the KNMI in de Bilt (in relation to wave prediction models). A few results:

- Accounting for molecular viscous terms and surface tension in the shear instability model leads to growth of capillary gravity waves. The growth rate is computed from the Orr-Sommerfeld equation (5.16), instead of from the Rayleigh equation. Important contributions were given by (again!) Miles, Valenzuela and K. van Gastel. Also, a minimum wind speed occurs ($u_{*,\min} \sim 0.05$ ms^{-1}) below which waves do not grow (see Figure 5.9).

- Modelling of coupling wavefield-turbulence: in the first instance with numerical models (Chalikov & Makin, Gent & Taylor), using higher-order closure schemes (hence no K-theory).
- First semi-analytical results by Duin & Janssen (1992). Satisfactory results for short waves, but not for long waves (damping rather than growth).

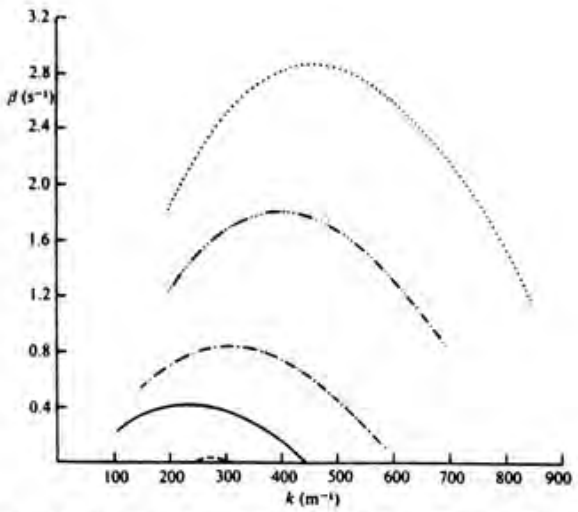

FIG. 2. Growth rate as a function of wavenumber for various wind speeds: ..... $u_* = 0.248$ m s^{-1}, $U_a = 0.102$ m s^{-1}; —·—·—, 0.214, 0.098; —·—, 0.170, 0.096; ——, 0.136, 0.075; - - -, 0.050, 0.025.

Figure 5.9: Growth rate of wind-generated capillary-gravity waves versus wavenumber for different wind speeds. Results obtained by K. van Gastel (1987). Full reference to this work is given in *Komen et al.* [1994].

Probable reason: K-theory is not correct for long waves, because turbulence has insufficient time to adapt to changing wave conditions. The condition under which K-theory can be applied is

$$\frac{z_c}{u_*} \ll T \qquad \text{or} \qquad \frac{c}{u_*} \leq 20\,.$$

The first expression states that the eddy turn-over time must be much smaller than the wave period T. Theories for growth of low-frequency gravity waves, including the coupling between waves and turbulent eddies, have been developed by Belcher & Hunt (J. Fluid Mech. 1993), Mastenbroek & Makin, etc.

- Another topic of research concerns the influence of the thermodynamic stability of the atmospheric boundary layer on the growth of waves.
- In recent studies also the role of slow variations in the wind speed (wave gustiness) on the growth of waves is investigated.

Chapter 6

Statistical description: wave spectra

6.1 Probability concepts

Up to now mainly simple waves have been analysed which are described by deterministic equations of motion. However, in nature the sea surface elevation is composed of a large number of different wave components, each having a different wavelength, frequency, amplitude and direction of propagation. The resulting behaviour of the sea surface is very complex, because all wave components are randomly forced (because the wind in the atmospheric boundary layer is turbulent) and waves have mutual nonlinear interactions. Describing all details of the wavefield is a formidable, if not impossible, task. Fortunately, for many practical purposes it is sufficient to know the behaviour of *mean* quantities (e.g., mean and standard deviation of sea surface elevations). This requires a statistical description of the wavefield.

The first important concept in statistical theory is that of statistical variables. They are quantities of which the detailed behaviour in space and time is not known; rather that behaviour can only be described in terms of probability that variables attain a certain value. The behaviour of a statistical variable is called a stochastic process. In this chapter the statistical quantity that will be considered is the variation of the sea surface.

The second concept is that of an ensemble. The latter is a collection of realizations of a statistical variable under identical macroscopic conditions, but different microscopic conditions. To illustrate their meaning, imagine an experiment in a laboratory which contains N identical wavetanks. Over each of them air is blown with the same mean speed, but the turbulent structure of the windfield will differ for each tank. In this example, macroscopic variables are e.g. the length of the tank, the density of the water, the mean windspeed, etc.. The turbulent fluctuations in the windfield are microscopic variables of which the detailed behaviour in space and time is not known. However, it is assumed that they are characterized by *statistical variables* (such as intensity) that are macroscopic variables. In this way, an N-partite wave ensemble is constructed.

From now on, the statistical variable that will be considered is the elevation of the

sea surface, $\zeta(\vec{x},t)$, with $\vec{x}$ a vector in the horizontal plane. In an N-partite wave ensemble this quantify has the realizations

$$\left\{\zeta^{(n)}(\vec{x},t);\ n=1,2,\ldots,N\right\}\ , \tag{6.1}$$

which can attain numerical values Z.

Next, the concept of ensemble average is introduced. For the moment, only functions $F[\zeta(\vec{x},t)] \equiv F(\zeta)$ are considered. By definition the ensemble average of such a function is

$$<F(\zeta)>=\ \lim_{N\to\infty}\frac{1}{N}\sum_{n=1}^{N}F\left[\zeta^{(n)}(\vec{x},t)\right]\ . \tag{6.2}$$

In words: it is the mean of all possible wave realizations. Note that the average is a function of space and time.

Now, an important choice for the function F is discussed. First, apply a partitioning of the range of numerical values into intervals with width ΔZ, each bounded by the values Z_i and Z_{i+1} $(i=1,2,\ldots)$. Next, define the function

$$\Delta\mu(\zeta;Z_i)\ =\ \begin{cases}1 & \text{if } Z_i\le\zeta<Z_i+\Delta Z\,,\\ 0 & \text{in other cases}\,.\end{cases} \tag{6.3}$$

Then, according to (6.2), the ensemble average $<\Delta\mu(\zeta,Z_i)>$ is the fraction of all realizations $\zeta^{(n)}(\vec{x},t)$ that attain numerical values in the interval $[Z_i,Z_{i+1})$. Hence,

$$<\Delta\mu(\zeta,Z_i)>=\ P(Z_i\le\zeta<Z_i+\Delta Z)\,, \tag{6.4}$$

where $P(Z_i\le\zeta<Z_i+\Delta Z)$ is the probability that a measurement of the sea level at location $\vec{x}$ and time t has a value in the interval $[Z_i,Z_{i+1})$. From probability theory it follows that

$$\lim_{\Delta Z\to 0}P(Z_i\le\zeta<Z_i+\Delta Z)\ =\ p(Z_i)\,dZ\,. \tag{6.5}$$

Here, $p(Z)$ is the probability density over all numerical values Z of the statistical variable $\zeta(\vec{x},t)$. This function has the properties

$$p(Z)\ge 0\,,\qquad\qquad \int_{-\infty}^{\infty}p\,(Z)\,dZ=1\,. \tag{6.6}$$

With the use of (6.3)-(6.6) an alternative formulaton of the ensemble average, in terms of the probability density, can be given. For this, it is used that, by definition, in the limit $\Delta Z\to 0$

$$F(\zeta^{(n)})\ =\ \int_{-\infty}^{\infty}F(Z)\,d\mu(\zeta^{(n)};Z)\,,$$

so that

$$<F(\zeta)>=\ \int_{-\infty}^{\infty}F(Z)\,p\,(Z)\,dZ\,. \tag{6.7}$$

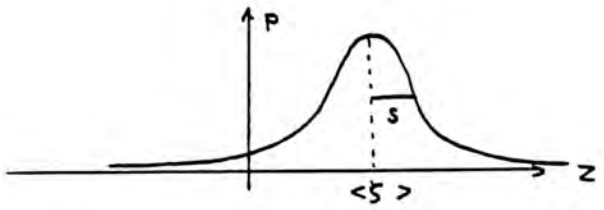

Figure 6.1: Sketch of the probability density function.

So the ensemble average also follows from an integration over all values of the function $F(Z)$, weighted by the probability density function $p(Z)$. The characteristic shape of $p(Z)$ is sketched in Figure 6.1.
It closely resembles a Gaussian distribution, which is fully characterized by the mean and the standard deviation. This result is not a coincidence: it is due to the fact that the sea surface is comprised by a large number of different wave components. Since nonlinear terms in the equations of motion are small (albeit significant) with respect to linear terms, these wave components are to a good approximation statistically independent. Then, the law of the large numbers, a well-known theorem in statistical physics, implies that the resulting probability distribution is Gaussian. This is explained in detail in e.g. *Kinsman* [1965].

Ensemble averages that are often used in practice are

$$<\zeta^m>: \qquad \text{the } m\text{'th-order moments}\,, \tag{6.8}$$

with in particular: $m = 1$: the mean sea level and $m = 2$: the intensity of the sea surface elevations. Furthermore,

$$s^2 = <\zeta^2> - <\zeta>^2 \tag{6.9}$$

is the variance and s the standard deviation of $\zeta(\vec{x}, t)$. The variance is proportional to the total energy density $<E>$ of the wavefield. This can be understood from the fact that in chapter 4 it was shown that, in case that the mean sea level $<\zeta>= 0$, the energy density is given by $<E>= \rho g\ <\zeta^2>$, see expression (4.20a).

The concept of ensemble average can also be applied to functions which depend on multiple (e.g., two) variables. Consider

$$F\left[\zeta(\vec{x}_1, t_1), \zeta(\vec{x}_2, t_2)\right] \equiv F(\zeta_1, \zeta_2)\,, \tag{6.10}$$

where $\zeta(\vec{x}_1, t_1)$ and $\zeta(\vec{x}_2, t_2)$ are the sea surface elevation at two different locations and two different times, respectively. In this case the ensemble average is

$$\begin{aligned} <F(\zeta_1, \zeta_2)> &= \lim_{N\to\infty} \frac{1}{N} \sum_{n=1}^{N} F\left(\zeta_1^{(n)}, \zeta_2^{(n)}\right) \\ &= \iint F(Z_1, Z_2)\, p\left(Z_1, Z_2\right) dZ_1 dZ_2\,. \end{aligned} \tag{6.11}$$

Here, $p(Z_1, Z_2)\, dZ_1 dZ_2$ is the probability that the variable $\zeta(\vec{x}_1, t_1)$ attains a numerical value in the interval $[Z_1, Z_1 + \Delta Z)$, whilst $\zeta(\vec{x}_2, t_2)$ attains a numerical value in

the interval $[Z_2, Z_2 + \Delta Z)$. The joint probability density function $p(Z_1, Z_2)$ obeys

$$p\,(Z_1, Z_2) \geq 0\,, \qquad \iint p\,(Z_1, Z_2)\,dZ_1 dZ_2 \;=\; 1\,. \tag{6.12}$$

Its characteristic shape is sketched in Figure 6.2.

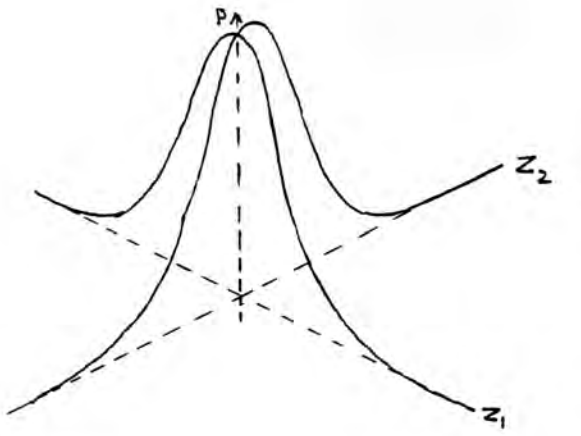

Figure 6.2: Sketch of probability density function $p\,(Z_1, Z_2)$.

Note that it closely resembles the product of two Gaussian functions. This is again an indication that the sea surface is built up by wave components which are (almost) statistically independent.

An important example of a two-point ensemble average is the covariance function

$$\begin{aligned} H(\vec{x}, \vec{r}; t, \tau) = &<[\zeta(\vec{x}, t) - <\zeta>(\vec{x}, t)] \times \\ &[\zeta(\vec{x} + \vec{r}, t + \tau) - <\zeta>(\vec{x} + \vec{r}, t + \tau)]> \;. \end{aligned} \tag{6.13}$$

It yields information about the statistical dependence between the sea level fluctuations (with respect to the local mean sea level) at location $\vec{x}$ and time t and the sea level fluctautions at a distance $\vec{r}$ from this location and with a timeshift τ. In particular, $H(\vec{x}, \vec{r}; t, 0)$ is the correlation function, $H(\vec{x}, 0; t, \tau)$ is the autocorrelation function and $H(\vec{x}, 0; t, 0)$ is the variance s^2 defined in (6.9).

The concepts introduced so far are too abstract for practical applications. The main reason is that nature does not provide a wave ensemble: only one realization of the sea surface is observed. And even if this problem could be overcome, a further complication would be that ensemble averages generally depend on both space and time. This implies that knowledge of macroscopic variables at a certain location and time yields no information about these variables at other locations and times. So computing ensemble averages would be an enormous task.

In order to overcome these problems two assumptions are made. The first is that sea surface variations are either statistically stationary or statistically homogeneous. This means that (ensemble) averages do not depend on either time or space. In case of a statistically stationary wavefield it is useful to introduce the concept of time

average, which is formally defined as

$$\overline{F\left[\zeta\right]} \;=\; \lim_{T\to\infty} \frac{1}{2T} \int_{t-T}^{t+T} F\left[\zeta(t')\right]\, dt' \,. \tag{6.14}$$

Because of statistical stationarity this quantity is independent of the choice of time t. Likewise, in case of statistically homogeneous processes the concept of space average is introduced.

It should be realised that in general the time average defined in (6.14) will differ from the ensemble average (6.2). Thus, to avoid the use of ensemble averages a second assumption must be made, i.e., that $\zeta(t)$ is an ergodic process. This is a special statistically stationary (or homogeneous) stochastic process for which ensemble averages are identical to time (or space) averages. Hence, in the example given above

$$\overline{F\left(\zeta\right)} \;=<F\left(\zeta\right)>\;. \tag{6.15}$$

In geophysics, the ergodic hypothesis is often *a priori* adopted in order to avoid the often unmanageable concept of ensemble average. For ergodic homogeneous processes the left-hand side of (6.14) should be interpreted as a space average. The development is slightly more elaborated because the average involves an integration over two spatial coordinates, rather than one time coordinate.

6.2 Statistical quantities from wave records

In case of stationary ergodic processes quantities like the mean wave height can in principle be computed from a given time series of sea surface elevations. Of course, there are still problems to overcome, because time series are not infinitely long and have a finite resolution. To retrieve meaningful information from such time series is a topic on its own and a detailed discussion is beyond the scope of this chapter. Here, only the following remarks are made. A typical wave record will show a sequence of zero-down and zero-up crossings of the sea surface (see Figure 6.3).

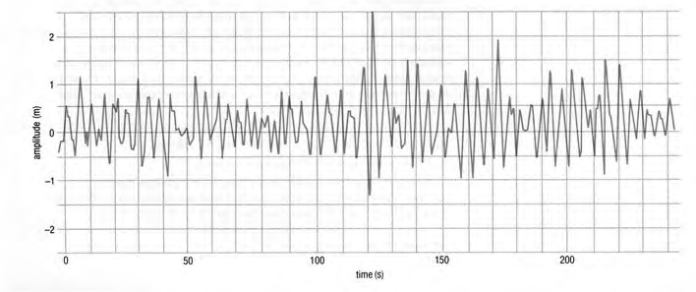

Figure 6.3: Observed wave record.

From this, a mean wave period can be computed by dividing the record length by the number of downcrossings (or upcrossings). Concerning the record length, this quantity should not be too long, because the sea state will not be stationary on the long term (due to changing wind and swell conditions, etc). Thus, sea surface

variations are only *approximately* stationary: their averages are still slowly varying functions of time (i.e., they vary on a timescale that is much longer than the mean wave period). On the other hand the record length should not be too short, otherwise no meaningsful averages can be computed. In practice, wave records having roughly 200 down-crossings yield useful information. This means that most wave records have a length of 15-30 minutes. Concerning the resolution of the records (the time interval Δt between successive data points), it should be realised that the highest frequency that is identified in a record is the Nyquist frequency $f_N = 2\Delta t$. So if one wishes to be able to identify waves with periods that are 10 times smaller than the mean wave period, each mean wave period should be sampled at least 20 times.

In this way it is also possible to compute the autocorrelation function; this will be discussed later on. Other important quantities that are extracted from wave records are:

- the average wave height;
- the probability distribution of the height of wave crests;
- the significant wave height H_s: the average height of the 1/3 highest waves;
- the significant wave period: the average period of the 1/3 highest waves.

The probability distribution $\tilde{p}(H)$ of the height H of wave crests is relevant for characterising the properties of the random wavefield. Thus $\tilde{p}(H)\Delta H$ is the probability that the height of a wave crest (with respect to mean sea level) is in the interval $[H, H + \Delta H)$. Note that here the concept of wave height (rather than wave amplitude) is used. The significant wave height is defined as

$$H_s = \frac{\int_r^\infty H\,\tilde{p}\,(H)\,dH}{\int_r^\infty \tilde{p}\,(H)\,dH} \qquad \text{with} \qquad \int_r^\infty \tilde{p}\,(H)\,dH = \frac{1}{3}\,. \tag{6.16}$$

Both observations and theoretical concepts (which were developed by Longuet Higgins) indicate that often $\tilde{p}(H)$ can be approximated by a Rayleigh distribution

$$\tilde{p}\,(H) \;=\; \frac{H}{4s^2}\,\exp\left(\frac{-H^2}{8s^2}\right)\,, \tag{6.17}$$

with $s^2 = H_{rms}^2/8$ the variance of the wavefield and H_{rms} the root-mean square wave height. In that case the significant wave height can be computed analytically from by combination of equations (6.16) and (6.17). It follows

$$\int_r^\infty \tilde{p}\,(H)\,dH = \exp\left(\frac{-r^2}{H_{rms}^2}\right)\,, \quad \text{yielding} \quad H_s = 4\,s\,. \tag{6.18}$$

Note that both the significant wave height and sigificant wave period can be (and often are) estimated by means of direct visual observations (no wave record needed). Consequently, if the Rayleigh distribution is accepted, the expression above immediately yields the variance of the wavefield.

6.3 Wave spectra: basic aspects

In the remaining part of this chapter it is assumed that sea surface elevations are both statistically stationary and homogeneous. To analyse such processes it is convenient to use Fourier theory. In particular, it is interesting to investigate how different Fourier wave components contribute to the variance (proportional to the energy density) of the wavefield. The procedure is to substitute the Fourier-transformed quantities

$$\begin{aligned} \zeta(\vec{x},t) &= \iiint \hat{\zeta}(\vec{\kappa}'',\sigma'')\, e^{-i(\vec{\kappa}''\cdot\vec{x}-\sigma''t)}\, d\vec{\kappa}''\, d\sigma'' \,, \\ \zeta(\vec{x}+\vec{r},t+\tau) &= \iiint \hat{\zeta}^*(\vec{\kappa},\sigma)\, e^{i(\vec{\kappa}\cdot\vec{r}-\sigma\tau)}\, e^{i(\vec{\kappa}\cdot\vec{x}-\sigma t)}\, d\vec{\kappa}\, d\sigma \,, \end{aligned} \tag{6.19}$$

in expression (6.13) for the covariance function. Here, the asterix * denotes a complex conjugation. After some algebra this yields

$$\boxed{H(\vec{x},\vec{r};t,\tau) = \iiint F(\vec{\kappa},\sigma;\vec{x},t)\, e^{i(\vec{\kappa}\cdot\vec{r}-\sigma\tau)}\, d\vec{\kappa}\, d\sigma \,.} \tag{6.20}$$

Thus, the covariance function is the Fourier transform of a function $F(\vec{\kappa},\sigma;\vec{x},t)$, which is defined as

$$F(\vec{\kappa},\sigma;\vec{x},t) = \iiint \chi(\vec{\kappa},\sigma;\vec{\kappa}',\sigma') < e^{i(\vec{\kappa}'\cdot\vec{x}-\sigma' t)} > \, d\vec{\kappa}'\, d\sigma' \,, \tag{6.21a}$$

$$\chi(\vec{\kappa},\sigma;\vec{\kappa}',\sigma') = \hat{\zeta}^*(\vec{\kappa},\sigma)\, \hat{\zeta}(\vec{\kappa}-\vec{\kappa}',\sigma-\sigma') \,. \tag{6.21b}$$

The function $F(\vec{\kappa},\sigma;\vec{x},t)$ is called the wave vector-frequency spectrum. Its physical interpretation follows from noting that

$$s^2 \;=\; H(\vec{r}=0,\tau=0) \;=\; \iiint F(\vec{\kappa},\sigma)\, d\vec{\kappa}\, d\sigma \tag{6.22}$$

so $F(\vec{\kappa},\sigma)\Delta\vec{\kappa}\,\Delta\sigma$ is the contribution to the total variance s^2 of the wavefield of Fourier components with wave vectors in the interval $[\vec{\kappa},\vec{\kappa}+\Delta\vec{\kappa})$ and wave frequencies in the range $[\sigma,\sigma+\Delta\sigma)$. In other words, $F(\vec{\kappa},\sigma)$ is the wave variance per wave vector and per frequency (unit m^4 s).

Expression (6.21) is quite complicated to evaluate, but an alternative expression for the full spectrum is obtained by taking the inverse Fourier transform of (6.20), yielding

$$F(\vec{\kappa},\sigma;\vec{x},t) = \frac{1}{(2\pi)^3} \iiint H(\vec{x},\vec{r};t,\tau)\, e^{-i(\vec{\kappa}\cdot\vec{r}-\sigma\tau)}\, d\vec{r}\, d\tau \,. \tag{6.23}$$

In principle, the covariance function can be calculated from observed time series of the sea surface at many different locations. If the process is both stationary and homogeneous the mean sea level is set to $<\zeta>=0$. In that case the results are

$$
\begin{aligned}
H(\vec{r},\tau) &= <\zeta(\vec{x},t)\zeta(\vec{x}+\vec{r},t+\tau)>, \\
H(\vec{r},\tau) &= \iiint F(\vec{\kappa},\sigma)\, e^{i(\vec{\kappa}\cdot\vec{r}-\sigma\tau)}\, d\vec{\kappa}\, d\sigma\,, \\
F(\vec{\kappa},\sigma) &= \frac{1}{(2\pi)^3} \iiint H(\vec{r};\tau)\, e^{-i(\vec{\kappa}\cdot\vec{r}-\sigma\tau)}\, d\vec{r}\, d\tau\,.
\end{aligned}
\tag{6.24}
$$

In this result the covariance function and the spectrum may be considered as slowly varying functions of space and time (see the remarks in the previous section).

In many practical cases not sufficient data is available to compute the full wave vector–frequency spectrum, but still *reduced spectra* can be calculated. In case that data are available at a specific time in a spatial domain (e.g., from stereophotography) it is possible to compute the wave vector spectrum, defined as

$$
F(\vec{\kappa}) = \int F(\vec{\kappa},\sigma)\, d\sigma\,. \tag{6.25}
$$

Here, the notation is adopted that the type of the spectrum is determined by the dependent variables.
From equation (6.24) it follows

$$
H(\vec{r},0) = \iint F(\vec{\kappa})\, e^{i\vec{\kappa}\cdot\vec{r}}\, d\vec{\kappa}\,, \quad \text{so} \quad F(\vec{\kappa}) = \frac{1}{(2\pi)^2} \iint H(\vec{r},0)\, e^{-i\vec{\kappa}\cdot\vec{r}}\, d\vec{r}\,. \tag{6.26}
$$

This shows that the wave vector spectrum is the Fourier transform of the correlation function. Likewise, in case that timeseries at a specific location are available, it is possible to compute the frequency spectrum, defined as

$$
F(\sigma) \;=\; \int F(\vec{\kappa},\sigma)\, d\vec{\kappa} \;=\; \frac{1}{2\pi} \int_{-\infty}^{\infty} H(0,\tau)\, e^{i\sigma\tau}\, d\tau\,, \tag{6.27}
$$

where in the last step (6.24) has been used. The frequency spectrum (unit $\mathrm{m}^2\mathrm{s}$) is the Fourier transform of the autocorrelation function and it describes the variance per frequency, such that the intergral of the spectrum yields the total variance. A characteristic shape of the frequency spectrum of wind waves was already shown in Figure 1.9(a) in the introductory chapter.

If the wavefield is considered as approximately linear, which is often a valid assumption, then a relation can be derived between the frequency spectrum and the wavenumber spectrum $F(\kappa)$, where $\kappa = |\vec{\kappa}|$. This follows from application of the linear dispersion relation. In that case the full wave vector-frequency spectrum given in (6.27) reduces to

$$
F(\vec{\kappa},\sigma) \;=\; F(\vec{\kappa})\; \delta(\sigma - \sigma\,') \qquad \text{with} \qquad \sigma\,' \;=\; \sigma\,'(\kappa)\,,
$$

i.e., it only is nonzero for frequencies that satisfy the dispersion relation. Next, introduce polar coordinates κ and θ, it thus follows that

$$
F(\sigma) \;=\; \int_0^{2\pi} \int_0^{\infty} \kappa F(\kappa,\theta)\, \delta(\sigma - \sigma\,')\, d\kappa\, d\theta\,.
$$

Finally, use that $d\sigma' = c_g d\kappa$, with c_g the group velocity, such that the integration over κ is replaced by an integration over frequency σ'. The result is

$$F(\sigma) \;=\; \frac{\kappa(\sigma)}{c_g(\sigma)} \int_0^{2\pi} F(\kappa,\theta)\, d\theta \;=\; \frac{\kappa(\sigma)}{c_g(\sigma)}\, F(\kappa)\,. \tag{6.28}$$

It should be realised that this result is not exact, because nonlinear interactions between different wave component can only be ignored to first order in the wave steepness.

6.4 Wave spectra; practical aspects

In section 6.3 it was already explained that frequency spectra can be computed as a Fourier transformation of a measured autocorrelation function. A typical result is shown in Figure 6.4. The autocorrelation function shows a damped oscillation, where the e-folding time of the damping is a measure of the correlation time (or memory timescale) of the wavefield. The period of the oscillation is a measure of the dominant wave period and its inverse is in fact the peak frequency in the spectrum (right subplot).

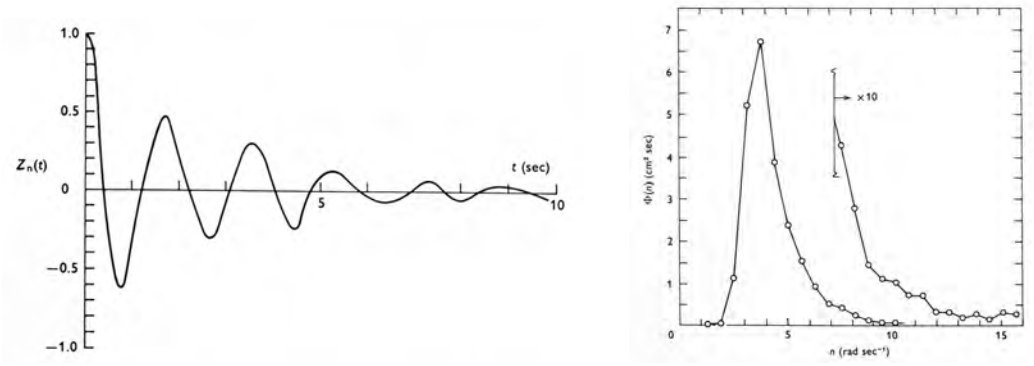

(a) (b)

Figure 6.4: Left: measured autocorrelation function from a wave record. Right: corresponding frequency spectrum. From *Phillips* [1977].

In practice, often an alternative method is used to compute the spectrum, which uses (6.21). In case of a single wave record, only the frequency spectrum can be computed. In that case the relevant expressions to be considered are

$$\hat{\zeta}(\sigma) = \frac{1}{2\pi} \int \zeta(t)\, e^{-i\sigma t}\, dt\,,$$

as is obtained from inverting the reduced version of expression (6.19), and

$$F(\sigma) \;=\; \int \hat{\zeta}^*(\sigma)\, \hat{\zeta}(\sigma - \sigma')\; <e^{-i\sigma' t}>\; d\sigma'\,.$$

Note that $\hat{\zeta}(\sigma)$ has the unit ms. Now, a wave record is a discrete time series having a sampling time Δt and a finite length $N\,\Delta t$, where N is the number of points. By discretization of the expressions given above it follows

$$a_m \;\equiv\; \hat{\zeta}(m\Delta\sigma)\,\Delta\sigma \;=\; \sum_{n=0}^{N-1} \zeta(n\Delta t)\; e^{-2\pi i m n/N}$$

and

$$F(m\Delta\sigma) \;=\; \frac{|a_m|^2}{\Delta\sigma} \qquad m = -\frac{N}{2}, \ldots, 0, \ldots, \frac{N}{2}\,.$$

In other words, apply a Fourier transformation to the time series, then the value of $F(\sigma_m)$ at the frequency $\sigma_m = m\Delta\sigma$ is the squared absolute value of the complex amplitude a_m, sampled at frequency σ_m, divided by the frequency band $\Delta\sigma = 2\pi/(N\Delta t)$.

In processing data of wind waves in deep water, measured frequency spectra are often fitted to a function of the form

$$F(\sigma) \;=\; \alpha\, F_1(\sigma)\; F_2(\sigma)\; F_3(\sigma)\,, \tag{6.29a}$$

with

$$F_1 \;=\; \sigma^{-m}\,, \quad F_2 \;=\; \exp\left[\frac{-m}{n}\left(\frac{\sigma}{\sigma_p}\right)^{-n}\right]\,, \quad F_3 = \gamma^{\exp\left[\frac{-(\sigma-\sigma_p)^2}{2\hat{s}^2\sigma_p^2}\right]}\,, \tag{6.29b}$$

where

$$\hat{s} = \begin{cases} s_A & \text{if} \quad \sigma \le \sigma_p \\ s_B & \text{if} \quad \sigma > \sigma_p \end{cases}\,. \tag{6.29c}$$

The fitting parameters are $\alpha, m, n, \sigma_p, \gamma, s_A$ and s_B. The behaviour of the functions F_1, F_2 and F_3 is sketched in Figure 6.5. Since the spectrum attains a maximum at frequency σ_p, the latter is called the peak frequency.

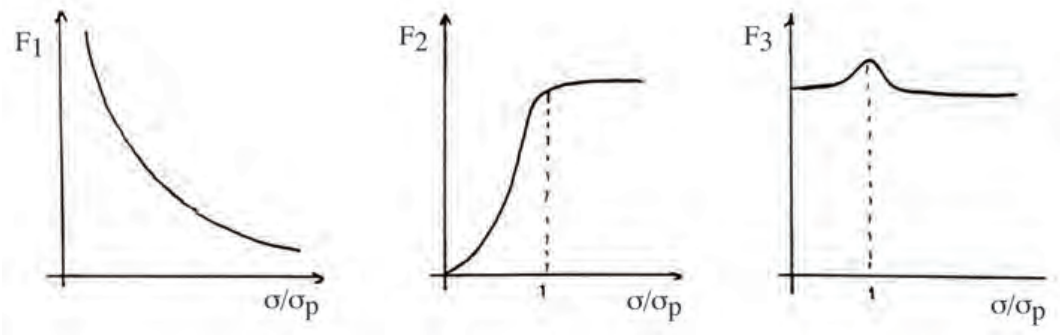

Figure 6.5: Behaviour of building blocks of a generic wave frequency spectrum.

The figure shows that the function F_1 (and thereby parameter m) governs the high-frequency part of the spectrum, whilst function F_2 governs the low-frequency part.

Function F_3 is called the peak enhancement function, which was introduced after the JONSWAP measuring campaign in 1973, which was already discussed in chapter 1. Before 1973 it was common to work with the Pierson-Moskowitz spectrum, hereafter abbreviated as PM-spectrum, given by

$$F_{PM} \;=\; \alpha g^2 \sigma^{-5} \exp\left[\frac{-5}{4}\left(\frac{\sigma}{\sigma_p}\right)^{-4}\right], \tag{6.30}$$

which implies that $m = 5, n = 4$ and $\gamma = 1$ (no peak enhancement). The fitting parameters left are α and the peak frequency. For fully developed wind waves in deep water $\alpha = 8.1 \times 10^{-3}$ and $\sigma_p \sim 0.77 g/U$, where U is the wind speed at 10 m above the sea surface.

The results of the JONSWAP campaign clearly indicated that this spectrum underestimated the energy density contained in the frequencies close to the peak frequency. This resulted in the introduction of the peak enhancement function. From that moment on it is common to work with the JONSWAP spectrum, defined as

$$F_J \;=\; F_{PM}\; F_3\,(\sigma)\,. \tag{6.31}$$

Based on the JONSWAP data the three shape parameters in the peak enhancement function turned out to have the values $\gamma \sim 3.3$, $s_A = 0.07$ and $s_B = 0.09$.

In shallower water, i.e. in the coastal area, wave data are often fitted to a spectrum that is of the type

$$F_{sw}(\sigma) \;=\; F_J(\sigma)\, F_{\text{corr}}(\sigma)\,,$$

where F_{corr} is a known subspectrum that corrects for the waves being in water of intermediate to small depth. A well-known example of such a spectrum is the TMA-spectrum, for details see *Khandekar* [1989]; *Lavrenov* [2003].

The algebraic shape of the high-frequency range of the deep-water wave spectrum can be understood from the fact that most of the waves in this regime gain energy from the wind but at the same time lose energy due to whitecapping. This is due to the fact that vertical accelerations of water particles are larger than acceleration due to gravity, g. Based on dimension analysis, it may be expected that in equilibrium the spectrum in this regime will depend on two parameters: σ and g. Thus, the general shape of the spectrum will be $F(\sigma) \sim g^\mu \sigma^\nu$, with parameters μ and ν to be determined. Now, the dimension of the frequency spectrum is (length)$^2\times$ time, which implies that $\mu = 2$ and $\nu = -5$. This is precisely the form of the function F_1 in (6.29b).

6.5 Wave prediction

6.5.1 Empirical methods

Prediction of wave characteristics, such as significant wave height, wave period and dominant direction of propagation, is important for ship routing, offshore industry,

etc.. The first method was developed by Sverdrup & Munk. Although published in 1947, the method was actualy used during World War II for planning of the landing operations of allied forces. They realised that the wave parameters at a certain location depend on the duration of the wind, the fetch (distance over which a wavefield can develop, e.g., the size of a depression or the distance to the coast, measured in the direction where the wind comes from) and the local depth. They excluded the latter by considering wave evolution in deep water. Based on the energy balance of waves and using observational data, they were able to derive equations for the significant wave height and significant wave period as a function of time (in case of unlimited fetch) and as a function of the fetch (in case of unlimited duration). Thus, for both parameters two values were obtained and the lowest ones were used as predictors.

Later on, this method was modified by Bretschneider and others. These models are based on relationships of the following form:

$$\frac{gH_s}{U^2} = A_1 \tanh\left[B_1\left(\frac{gF}{U^2}\right)^{m_1}\right], \quad \frac{c}{U} = \frac{gT_s}{2\pi U} = A_2 \tanh\left[B_2\left(\frac{gF}{U^2}\right)^{m_2}\right],$$

where H_s is the significant wave height, T_s the significant wave period, F the fetch, U the wind speed at 10 m above the sea surface and $A_1, A_2, B_1, B_2, m_1, m_2$ are parameters determined from data. Bretschneider summarised his results in clear nomograms, of which an example is shown in Figure 6.6.

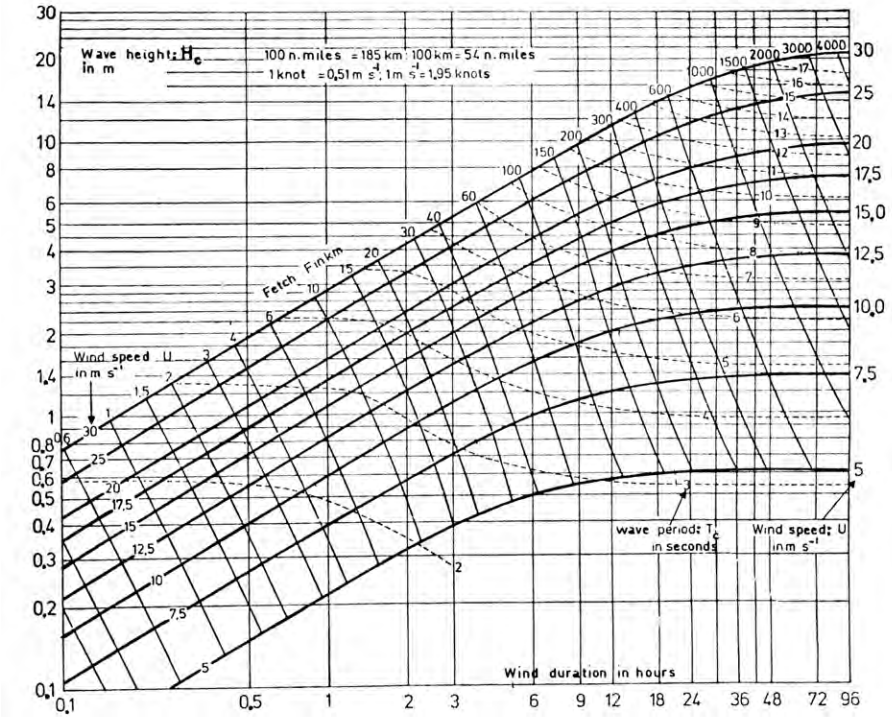

Figure 6.6: Nomogram which allows to determine significant wave height and period as a function of wind speed, duration and fetch.

To determine the significant wave height and period at a specific location for a given wind speed, duration and fetch, start in Figure 6.6 at the given wind speed, then move parallel to the 'fetch-axis' until the given values of either duration or fetch is reached and read the values of H_s and T_s at that point.

It turns out that a fully developed sea state in deep water (unlimited fetch) is characterised by

$$\frac{gH_{s,\infty}}{U^2} \simeq 0.243\,, \qquad \frac{gT_{s,\infty}}{U} \simeq 8.134\,,$$

which shows that $H_{s,\infty} \sim T_{s,\infty}^2$. More general expressions, including corrections for waves in finite depth, are given in *Komen et al.* [1994].

6.5.2 Spectral wave prediction models

Spectral wave prediction models are based on an equation describing the evolution of the frequency spectrum. In case that effects of currents on wave propagation are neglected, this equation reads

$$\frac{d}{dt} F(\sigma;\vec{x},t) = S(\sigma;\vec{x},t)\,, \tag{6.32a}$$

where S represents sources and sinks. Furthermore,

$$\frac{dF}{dt} = \frac{\partial F}{\partial t} + \vec{\nabla}\cdot(\vec{c}_g\,F)\,, \tag{6.32b}$$

which shows that the energy density of the wave field is advected with the group velocity, as was already explained in chapter 4. The function S is split into three parts:

$$S(\sigma;\vec{x},t) = S_{\text{in}} + S_{\text{nl}} + S_{\text{ds}}\,. \tag{6.32c}$$

Here, S_{in} describes the local input of energy due to the wind, S_{nl} is a term that describes the redistribution of energy within the spectrum due to nonlinear wave-wave interactions and S_{ds} represents dissipation of energy, which in deep water is mainly due to whitecapping.

In the literature (cf. *Khandekar* [1989]) three types of models are distinguished, called first-, second- and third-generation models. Those of the first generation ignore (or at most crudely parameterize) the nonlinear transfer function S_{nl}. Although used up to 1990, their drawback is that they can not describe the decrease in peak frequency with increasing fetch or duration (see Figure 1.13) and the observed overshoot in the spectral density of a frequency band as it tends to its equilibrium value on the long term (Figure 1.14).

Models of the second generation are based on evolution equations describing the evolution of the parameters in the JONSWAP spectrum, i.e., α and σ_p (in some

models also γ). These models account for nonlinear interactions in a parametric way, but they only yield reliable results in case of growing waves under fairly uniform wind conditions. This motivated the development of third-generation models which solve equation (6.32a) using expressions for the source/sink function which are based on physical principles. A major problem concerned the specification of the nonlinear transfer function S_{nl}. Already in 1962, Hasselman had derived an exact analytical expression for it, but when incorporating it in numerical models the latter became extremly time-consuming. A major break-through was in 1985, when Hasselman presented an efficient numerical algorithm that was able to compute the transfer function with a good accuracy and within a reasonable amount of time. This initiated the start of the WAM (WAve Modeller) group, lead by Hasselman, which aimed at developing a generic third-generation model: the WAM model. Details about the history and strcuture of this model are given in *Komen et al.* [1994]. The model is used on a routine basis for prediction of ocean wind waves. The results comprise wave spectra, but also secondary information such as significant wave height, significant wave period, dominant direction, etc. This information is used for ship routing and important for the offshore industry, etc..

Now, the different source/sink terms in the wave evolution equation (6.32a) are discussed. The energy input term S_{in} consists of two parts:

$$S_{\text{in}} \;=\; c_1(\sigma, U) \;+\; c_2(\sigma)\, F(\sigma)\,. \tag{6.33}$$

The first contribution on the right-hand side only depends on the frequency and wind speed. According to (6.32a) this term describes linear growth of waves in time, as is governed by the resonance mechanism of Phillips, which was mentioned in chapter 5. The second term on the right-hand side of (6.33) describes exponential growth of the energy density per frequency component. The underlying physical mechanism responsible for this term is the shear instability mechanism of Miles (see chapter 5). The final expressions given in secion 5.4 even reveal a full analytical expression for coefficient $c_2(\sigma)$. In practical simulations often a correction is applied to yield better forecasts.

The theory of nonlinear wave-wave interactions is quite extensive and complicated. To derive the expression for the term S_{nl} in (6.32a) it is necessary to analyse the spectral form of the energy balance of a weakly nonlinear wavefield. Here, only a few essences will be briefly sketched. Consider two waves with wave vectors $\vec{\kappa}_1, \vec{\kappa}_2$ and frequencies σ_1, σ_2. Assume that they are linear deep water gravity waves, hence they obey the dispersion relation $\sigma_i^2 = g\kappa_i$. Now, quadratic nonlinear terms in the equation of motion cause these two waves to interact and generate new wave components that have a wave vector $\vec{\kappa}_3 = \vec{\kappa}_1 \pm \vec{\kappa}_2$ and frequency $\sigma_3 = \sigma_1 \pm \sigma_2$, as is illustrated in Figure 6.7. For this wave to be resonantly excited (and obtain an appreciable amplitude) it should be free wave. However, it can be proven that σ_3 and κ_3 can not be chosen such that they obey the dispersion relation. In other words, quadratic wave interactions are nonresonant. It turns out that resonant forcing are due to the presence of cubic nonlinear terms in the equations of motion. They cause three free waves to interact and generate new free waves. Thus, resonant wave quartets are present, as sketched in Figure 6.8.

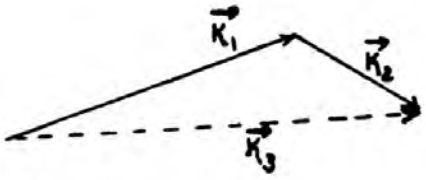

Figure 6.7: A triad wave interaction.

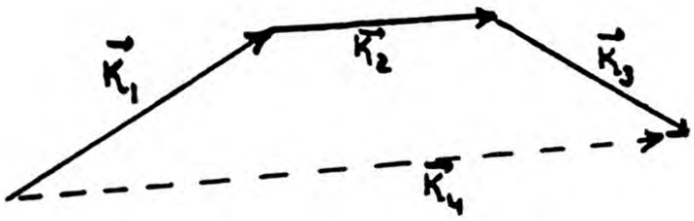

Figure 6.8: A resonant wave quartet.

These wave quartets obey the resonance conditions

$$\vec{\kappa}_4 = \vec{\kappa}_1 \pm \vec{\kappa}_2 \pm \vec{\kappa}_3\,, \qquad \sigma_4 = \sigma_1 \pm \sigma_2 \pm \sigma_3 \qquad \sigma_i^2 \;=\; g\,\kappa_i\,. \tag{6.34}$$

This description indicates that, for a specific frequency, part of the function S_{nl} describes the gain of energy density due to the transfer of energy to this wave by the interaction of three other waves. Schematically, this contribution is written as

$$S_{\text{nl},1}(\sigma) = \iiint F(\sigma_1)\,F(\sigma_2)\,F(\sigma_3)\;T_1(\sigma_1,\sigma_2,\sigma_3)\,d\sigma_1\,d\sigma_2\,d\sigma_3\,, \tag{6.35a}$$

i.e., the product of three energy densities, multiplied by a coupling coefficient T_1 and integrated over all possible wave interactions.

Any wave component that contains substantial energy density will also actively take part in nonlinear interactions with other waves. In this way energy is transferred from the wave to new waves. This is represented by a local energy loss term due to wave interactions of the form

$$S_{\text{nl},2}(\sigma) = F(\sigma) \iint F(\sigma_1)\,F(\sigma_2)\;T_2(\sigma,\sigma_1,\sigma_2)\,d\sigma_1\,d\sigma_2\,. \tag{6.35b}$$

The final result is that

$$S_{\text{nl}} \;=\; S_{\text{nl},1} \;+\; S_{\text{nl},2} \qquad \text{and} \qquad \int S_{\text{nl}}\,(\sigma)\;d\sigma \;=\; 0\,, \tag{6.35c}$$

where the last expression indicates that nonlinear wave-wave interactions only cause internal redistribution of energy. The algorithm developed by Hasselman, which was already mentioned, allows for an effective computation of these wave interactions in a numerical models. Often, reductions in the number of interactions is needed for reasons of efficiency, but still accurate results are obtained.

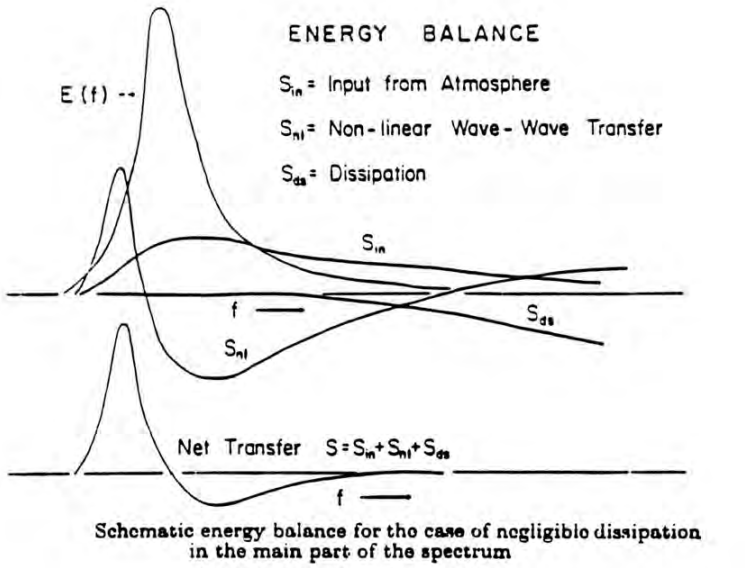

Figure 6.9: Source/sink functions in the energy balance as a function of wave frequency.

The formulation of the dissipation function S_{ds} is to a large extent based on empirical knowledge. This is due to the fact that the loss of energy by wave breaking is poorly understood. Since shorter waves are usually steeper than long waves, the first are most susceptible to breaking. Therefore, dissipation will mainly take part in the high-frequency regime of the spectrum. This can also be seen in Figure 6.9 which shows the three function $S_{\text{in}}, S_{\text{nl}}$ and S_{ds} as a function of frequency $f = \sigma/(2\pi)$. This figure also shows that nonlinear interactions cause a transfer of energy from the short waves to longer waves and thereby explain the observed decrease in the peak frequency with increasing fetch (or duration of the wind).

Third-generation models, like the WAM model, also yield information about the directional spreading of waves. This is done by calculating a frequency-direction spectrum of the form

$$F(\sigma, \theta) = F(\sigma)\, I(\theta)\,, \tag{6.36a}$$

with $I(\theta)$ the directional spectrum. Typical formulations for I are

$$I(\theta) = \begin{cases} \hat{I}_p \, \cos^p(\theta - \theta_d) & |\theta - \theta_d| < \frac{\pi}{2} \\ 0 & \text{for other values of } \theta\,, \end{cases} \tag{6.36b}$$

where $\hat{I}_p$ is such that $\int I(\theta)\, d\theta = 1$, p is a parameter and θ_d the dominant wave direction. Often $p = 2$, yielding $\hat{I}_p = 2/\pi$. A separate equation specifies the evolution of the dominant wave direction as a function of the initial angle and of the wind direction.

Part B

Long waves and tides

Chapter 7

Long waves: specific topics

In this chapter an overview of forthcoming topics is presented. First, consider Figure 7.1 that shows the registration of sea surface elevations at different locations in the world.

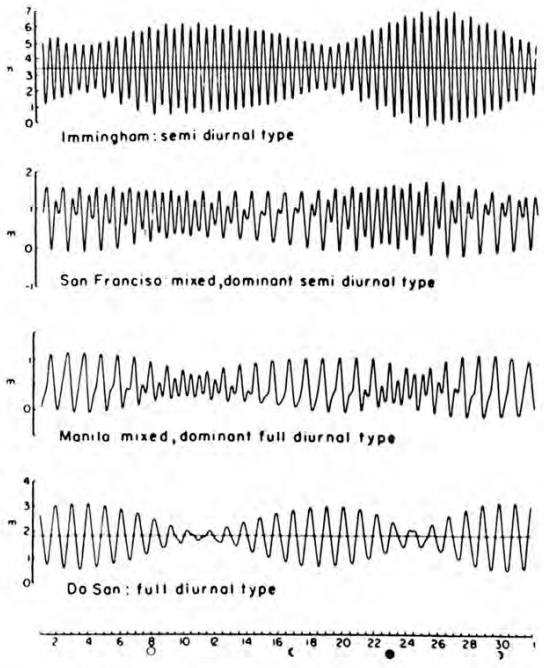

Sea-level variations at selected ports, for March 1936. (From German Tide Tables for the year 1940, Vol. II, Berlin 1939, as shown by Defant, 1958.)

Figure 7.1: Sea-level variations at selected ports, for March 1936. From *Defant* [1961].

- How can the manifestation of tides be explained?

  in particular the diurnal and semi-diurnal components, as well as the spring-neap cycle. The dominant tidal constituent in the North Sea is the semi-diurnal lunar (M_2) tide with a period $T = 12$ h 25 m. Addressing this problem requires a detailed analysis of tidal forces caused by the moon and sun.

Next, consider Figure 7.2B, which shows the co-amplitude lines of the surface tide in the North Sea.

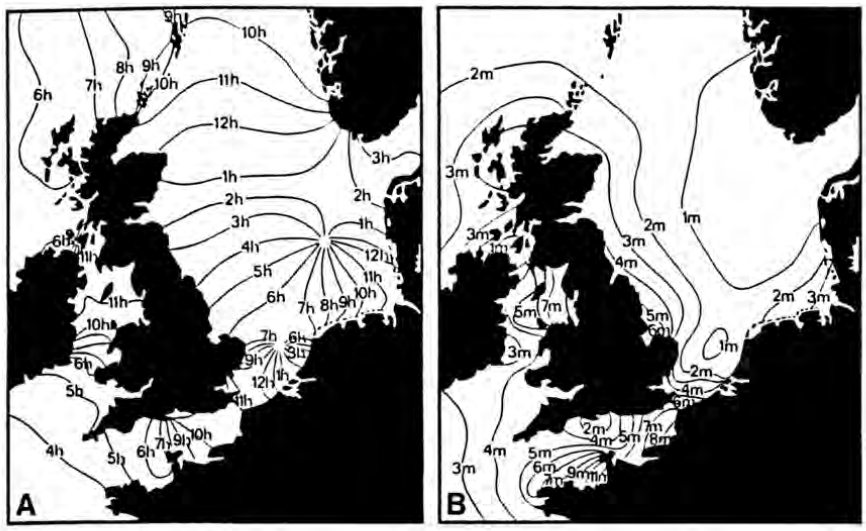

Tidal parameters of the North Sea and the British Isles. — A. Co-tidal lines; B. Co-range lines

Figure 7.2: Co-phase lines (A) and co-amplitude lines (B) of the semi-diurnal tide in the North Sea. From *Bowden* [1983].

- Why are the largest tidal amplitudes observed near the coast and why are the local variations in tidal amplitudes so large?

The tidal range in the Gulf of St Malo is more than 10 m. Here, a commercial power station is in use. The largest tidal range occurs in the Bay of Fundy (see Figure 7.3). Note also the strong variation of tidal characteristics in that area.

- How to understand the presence of amphidromic points (no tidal variations and why does the tide rotate cyclonically around such points?

This behaviour can be observed in both Figure 7.2A and in Figure 7.4.

The presence of amphidromic points is due to the fact that tidal forcing generates so-called Kelvin waves. The latter are gravity waves modified by Coriolis effects. They propagate along the coast, which (on the northern hemisphere) is to the right when looking in the direction of wave propagation. Their amplitudes decrease exponentially with increasing distance to the coast.

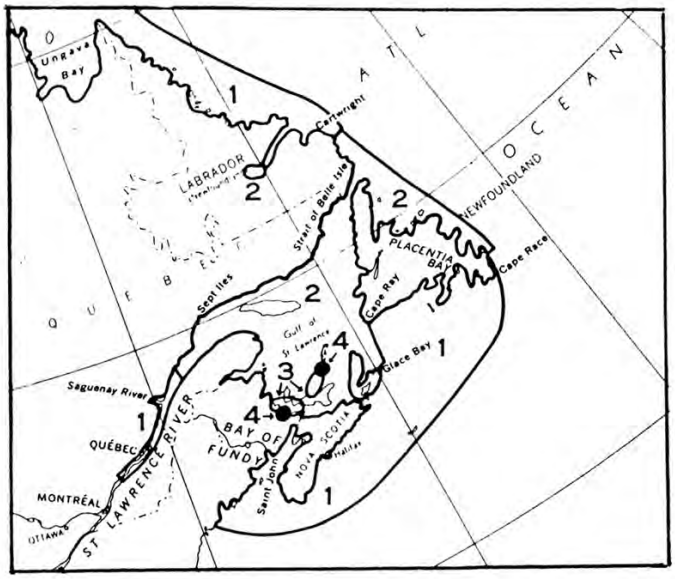

Figure 7.3: Location of the Bay of Fundy (east Canadian coast). From *LeBlond and Mysak* [1978]. The bold numbers indicate dominance of different tidal constituents (1=semi-diurnal, 2=mixed, 3=mainly semi-diurnal, 4=diurnal).

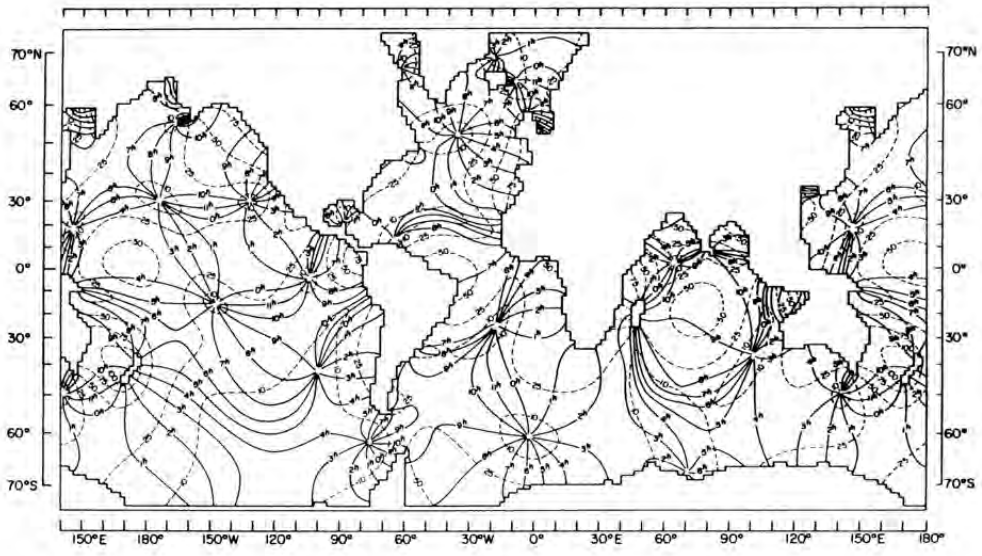

Figure 7.4: The M_2 tide as computed from a numerical model. The phase is shown by solid lines marked in Greenwich hours, and the range is shown by dashed lines, in centimetres. From *Gill* [1982]. In the last decade, numerical models have undergone major improvements because data obtained from satellites allowed for extensive validation.

Chapter 8

Equations of motion and boundary conditions

For studying the basic properties of long waves and tides it is possible to use simplified versions of the full equations of motion for the ocean. The latter have been derived in previous courses (Geophysical Fluid Dynamics), see also standard text books such as *Apel* [1987]; *Pedlosky* [1987]; *Cushman Roisin and Beckers* [2011], and are assumed to be known. Below, a brief summary of the major simplifications is given.

For modelling surface waves it is sufficient to analyse a homogeneous fluid, i.e. its density

$$\boxed{\rho = \text{constant.}} \tag{8.1}$$

This implies that baroclinic features, such as internal waves, will be filtered. Note that this is the same assumption as was used to describe short surface waves, see equation (2.1) in chapter 2.
The dynamics of such a fluid is governed by the continuity equation (conservation of mass) and the momentum equations (Newton's second law); thermodynamic effects do not play a role.

The resulting equations are further simplified by imposing the following assumptions:

I. The f-plane

The horizontal length scale (horizontal means: parallel to the earth's surface) of the phenomena under investigation are considered to be small with respect to the radius of the earth. This implies that the dynamics are hardly influenced by the curvature of the earth. It is then convenient to choose a local Cartesian coordinate system near a central latitude $\varphi = \varphi_0$. Here, x, y and z are coordinates along axes which point in the west-east-, south-north and vertical direction, respectively (see Figure 8.1). This is the so-called f-plane assumption, with $f = 2\Omega \sin \varphi_0$ the constant Coriolis parameter.

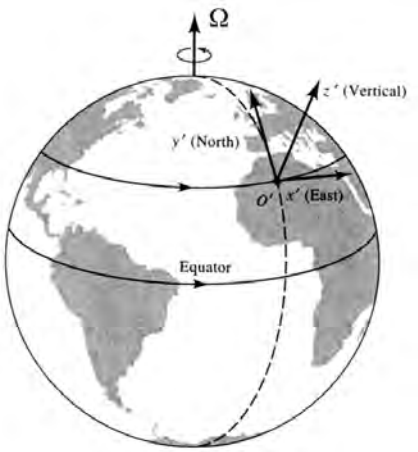

Figure 8.1: The f-plane on a rotating earth.

II. The shallow water limit

Since the horizontal length scales of the phenomena under investigation are much larger than their vertical length scales the vertical momentum balance reduces to hydrostatic equilibrium, i.e. a balance between pressure and gravity force.

III. Ideal fluid

Effects of friction will be neglected. It should be realized that in practice long waves are subject to friction, but in order to understand the basic properties of these waves it suffices to ignore friction.

IV. Linear dynamics

Also, nonlinear terms in the equations of motion will be neglected. This can be done if the typical velocity scale of water particles, U, is small compared to the characteristic wave speed of a long wave, i.e. $\sqrt{gH}$, where g is the acceleration due to gravity and H a characteristic depth. In other words, the Froude number

$$\boxed{F_r \equiv \frac{U}{\sqrt{gH}} \ll 1\,.} \tag{8.2}$$

Note that this condition is equivalent to that obtained in part A of these notes, see equation (3.3) in chapter 3. In case that F_r is not small the profile of the tidal wave will deform and ultimately breaking will occur (example: tidal bores in estuaries).

V. Depth-averaged formulation

Observations reveal that the flow field of long waves and tides has a vertical structure. Nevertheless, to understand the basic properties of long waves it suffices to consider a model that only describes the depth-averaged motion.

VI. Constant depth

The bottom is assumed to be horizontal, such that the undisturbed water depth is a constant.

This results in the linear depth-averaged shallow water equations for a homogeneous fluid on the f-plane:

$$\frac{\partial \zeta}{\partial t} + H\left[\frac{\partial u}{\partial x} + \frac{\partial v}{\partial y}\right] = 0\,, \tag{8.3a}$$

$$\frac{\partial u}{\partial t} - f\,v = -g\frac{\partial \zeta}{\partial x} - \frac{\partial \Phi}{\partial x}\,, \tag{8.3b}$$

$$\frac{\partial v}{\partial t} + f\,u = -g\frac{\partial \zeta}{\partial y} - \frac{\partial \Phi}{\partial y}\,. \tag{8.3c}$$

Here, u, v are the depth-averaged velocity components in the x and y direction, respectively and ζ is the elevation of the free surface. Furthermore, g is the acceleration due to gravity, the terms $-\partial\Phi/\partial x, -\partial\Phi/\partial y$ model as yet not specified forces per volume unit (e.g. tidal forces) with Φ the corresponding potential. A situation sketch (side-view) is shown in Figure 8.2.

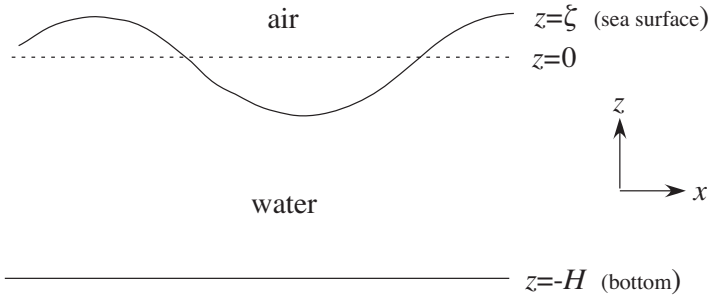

Figure 8.2: Situation sketch; side view.

Here, $z = 0$ is the location of the undisturbed water level, $z = \zeta$ is the interface between water and air (free surface) and H is the constant depth. More general formulations of this model (3D effects, friction, wind forcing, nonlinear effects, variable bottom) are studied in the course 'Physics of coastal systems'.

The depth averaged shallow water equations (also called 2DH equations) must be solved in a given domain (e.g., the one given in Figure 8.3) with boundary conditions.

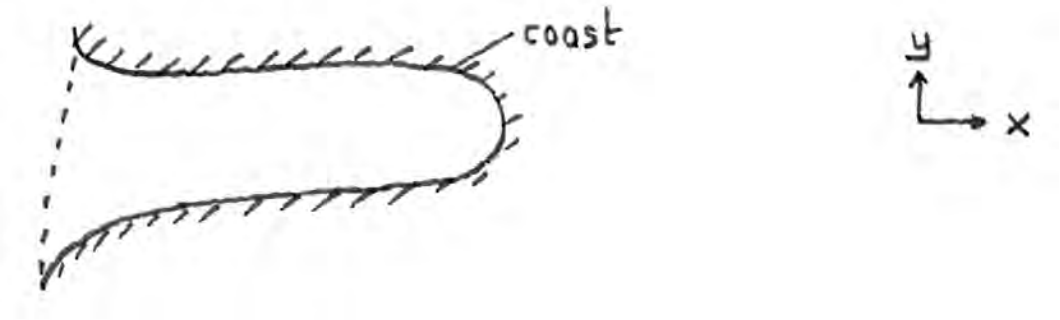

Figure 8.3: Example of a domain with open and closed boundaries.

The conditions at closed boundaries (e.g. coastlines) read $\vec{u} \cdot \vec{n} = 0$ ($\vec{n}$ is the normal vector at the boundary) and at open boundaries either the free surface or the normal velocity is prescribed.

In the next chapter the forcing terms $-\partial\Phi/\partial x$ and $-\partial\Phi/\partial y$ in the momentum equations will be specified.

Chapter 9

Theory of tides

9.1 Qualitative considerations

In this chapter, the forcing terms in the equations of motion that are related to tidal forces are specified. These forces originate from gravitational forces that are exerted by celestial bodies, in particular by the moon and the sun.

To define the tidal force, consider Figure 9.1, which shows the centre of mass M of the earth (mass m_a) and the centre of mass S of a celestial body (mass m_s). According to Newton's gravitation law, at any given point X the celestial body exerts a gravitational force that is directed from X to S, with a magnitude that is inversely proportional to the squared distance between X and S. The gravitational force in M thus causes the earth to accelerate towards S. The two bodies however do not collide, since both of them have a velocity component in the direction perpendicular to the line MS. The result is that earth and celestial body revolve as solid bodies about their common centre of mass (point C in Figure 9.1). According to Kepler's first law these orbits are ellipses.

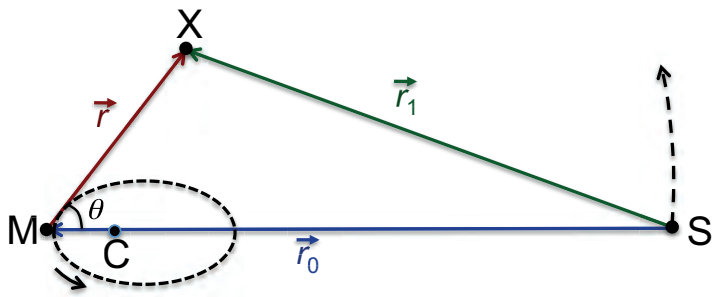

Figure 9.1: Situation sketch of two celestial bodies undergoing a rotation about their common centre of mass C. Symbols are explained in the text; θ is the zenith angle.

Note: for the moon $(m_s/m_a) = 1/81.53$, hence C is located close to M.
For the sun $(m_s/m_a) = 333420$, hence C is close to S.
The orbital periods follow from Kepler's third law. They are 27.3 days (a sidereal month) for the earth-moon and 1 year for the earth-sun.

Consequently, in a frame co-moving with M, at any point X a resultant force exists, being the difference between the local gravitational force and the gravitational force in M. This resultant force is called the tidal force.

An expression for the tidal force is obtained as follows. First, define (see Figure 9.1) the vectors $\vec{r}_0 = \overrightarrow{SM}, \vec{r}_1 = \overrightarrow{SX}$ and $\vec{r} = \overrightarrow{MX}$,
so $\vec{r}_1 = \vec{r}_0 + \vec{r}$ and in all relevant cases $r \ll r_0$.
Here e.g. r denotes the length of vector $\vec{r}$.
The gravitational forces (per mass unit) at points X and M read

$$\vec{F}_g(\mathrm{X}) = \frac{-\gamma m_s}{r_1^2}\,\frac{\vec{r}_1}{r_1}\,, \qquad\qquad \vec{F}_g(\mathrm{M}) = \frac{-\gamma m_s}{r_0^2}\,\frac{\vec{r}_0}{r_0}\,, \tag{9.1}$$

with $\gamma = 6.67 \times 10^{-11}$ Nm^{2}kg^{-2} the gravitation constant. Hence, the tidal force per unit of mass at location X is

$$\vec{K} = \vec{F}_g(\mathrm{X}) - \vec{F}_g(\mathrm{M}) \;=\; -\gamma m_s \left(\frac{\vec{r}_1}{r_1^3} - \frac{\vec{r}_0}{r_0^3}\right)\,. \tag{9.2}$$

A qualitative impression of both the length and direction of these forces at various locations at the surface of the earth is shown in Figure 9.2.

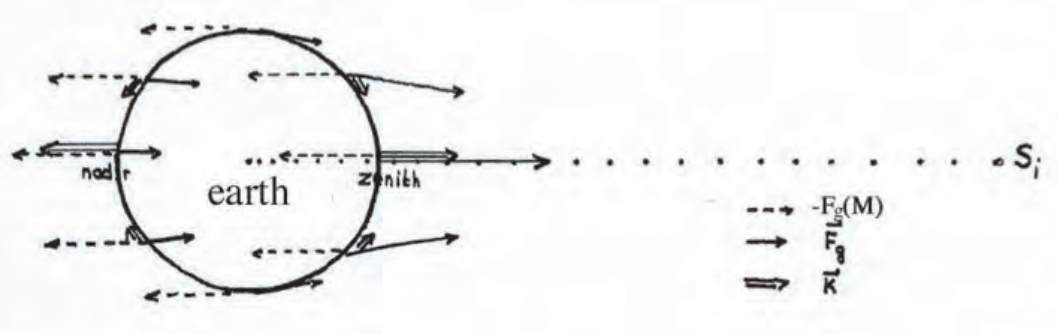

Figure 9.2: Gravitational force $\vec{F}_g(X)$, force $-\vec{F}_g(M)$ and tidal force $\vec{K}$ at different locations at the surface of the earth.

The largest tidal forces occur in the so-called zenith point and nadir point. For $r = R$, with $R \sim 6.4 \times 10^6$ m the radius of the earth, it follows

$$\left|\vec{K}\right|_{\text{max}} = \gamma m_s \left[\frac{1}{(r_0 - R)^2} \;-\; \frac{1}{r_0^2}\right] \;\simeq\; \frac{2\gamma m_s R}{r_0^3}\,, \tag{9.3}$$

where in the last step it has been used that $R \ll r_0$.
From this result it can be concluded that

- The ratio

$$\frac{K_{\text{max,sun}}}{K_{\text{max,moon}}} = \frac{m_{\text{sun}}}{m_{\text{moon}}}\left(\frac{r_{0,\text{moon}}}{r_{0,\text{sun}}}\right)^3 \simeq \frac{1.98 \times 10^{30}}{7.33 \times 10^{22}}\left(\frac{3.81 \times 10^8}{1.49 \times 10^{11}}\right)^3 \simeq 0.46\,,$$

  so tidal forces due to the sun are less than half as strong as those caused by the moon. This is a consequence of the $\sim r_0^{-3}$ dependence.

- In the zenith and nadir point the tidal force is directed perpendicular to the surface of the earth and it turns out that e.g.

$$\frac{K_{\text{max,moon}}}{g} \simeq 1.15 \times 10^{-7}\,.$$

So the vertical momentum balance is hardly affected by the presence of tidal forces. Only the horizontal component of the tidal force (called the traction) is dynamically important. Figure 9.2 shows that the latter drive the water towards the zenith and nadir point. This consideration leads to the manifestation of the equilibrium tide, consisting of two high-water areas and two low-water areas.

- In nature the equilibrium tide is not realised, because of
  - the rotation of the earth about its axis, in combination with inertial effects: the phase velocity of tidal waves in the ocean is smaller than the speed by which zenith and nadir points move over the surface of the earth;
  - the presence of continents, which in most areas do not allow for a freely propagating tidal wave around the earth (apart from the southern ocean);

Qualitatively, the following picture emerges. At first, assume that the celestial body is in the equatorial plane of the earth (see Figure 9.3).

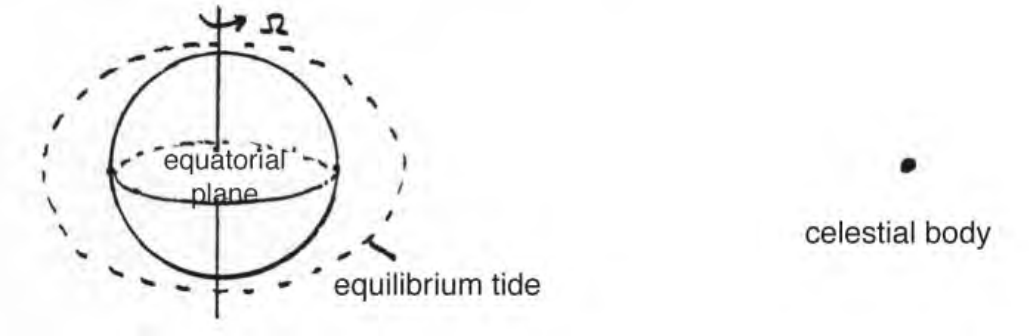

Figure 9.3: Equilibrium tide in case the celestial body is in the equatorial plane of the earth. Here Ω is the angular velocity of the earth about its axis.

Due to the rotation of the earth about its axis (with angular velocity $\Omega = 7.3 \times 10^{-5}$ s^{-1}), the zenith and nadir points move over the earth's surface. In case of tidal forcing by the sun, at each fixed location on the earth two high-waters and two low-waters pass each 24 hours. This causes the presence of the so-called S_2 tide, or semi-diurnal solar tide, with a period of $T_{S2} = T_\odot/2$, with $T_\odot/2$ a solar day. Likewise, the forcing due to the moon results in the presence of the semi-diurnal lunar tide, or M_2 tide, with a period of $T_\lozenge/2$=12 h 25 m and $T_\lozenge$ a lunar day. This period is slightly longer than that of the S_2 tide, because after one revolution of the earth about its axis the orientation of the moon with respect to a fixed point at the earth's surface is different because the moon rotates about the earth.

More details and further explanation are given in the appendix at the end of this chapter.

The M_2 tide and S_2 tide are also the principal cause of the spring-neap tidal cycle (see Figure 9.4).

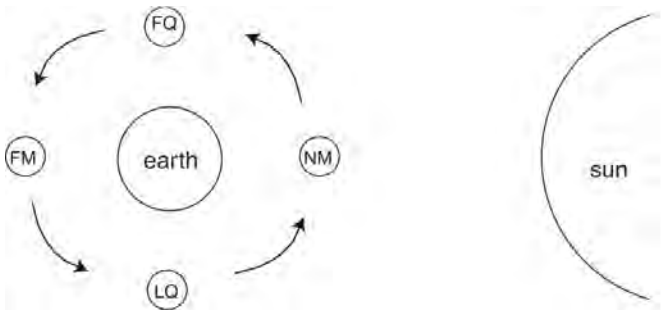

Figure 9.4: Generation of spring tides and neap tides.

If the sun and moon are in line, i.e. at full moon (FM) and new moon (NM), the M_2 tide and S_2 tide reinforce eachother and result in spring tide. During the first and last quarter (FQ, LQ) the tidal components are out of phase, resulting in neap tide. The period between successive spring tides is 14 days, 18 h 22 m, i.e., half a lunar period. Note that the lunar period is longer than the sidereal month of 27.3 days, as it also involves the effect of the earth rotating about the sun, see the appendix at the end of this chapter. In nature spring tide occurs some time (about 1 day) after full moon and new moon which is due to inertial effects.

Besides the M_2 and S_2 tide there are many (hundreds of) other tidal consituents. A number of them were already identified in 1778/79 by Laplace; in 1931 a further refinement was given by Doodson. An overview of the history of tidal theory can be found in *Cartwright* [1998]. Most of them are related to two important aspects, which are discussed below.

I. The eclipse (the plane of the earth's orbit around the sun) and the plane of the moon's orbit around the earth do not coincide with the equatorial plane. The declination angle between the plane of the lunar orbit and equatorial plane is 28^o and that of the eclipse and equatorial plane is 23.5^o. This implies that, at a fixed point on the earth's surface, the highest position of the moon (sun) with respect to the surface varies sinusoidally with a period of 27.3 days (1 year). The consequence is that long-periodic tidal consituents are generated (with periods of half a sidereal month and half a solar year), as well as diurnal components. Figure 9.5 shows that in case the line between the earth's centre and the celestial body is not in the equatorial plane, a fixed point at earth experiences an alternation of 'high' high-water and 'low' high-water. The result is thus a daily inequality of the tide, of which the amplitude varies periodically, because the angle δ in Figure 9.5 is time-dependent. Also other declination tides are generated (for more details see the appendix).

II. The lunar orbit around the earth (and the earth's orbit around the sun) are ellipses. Consequently, the distance between the earth's centre and the celestial

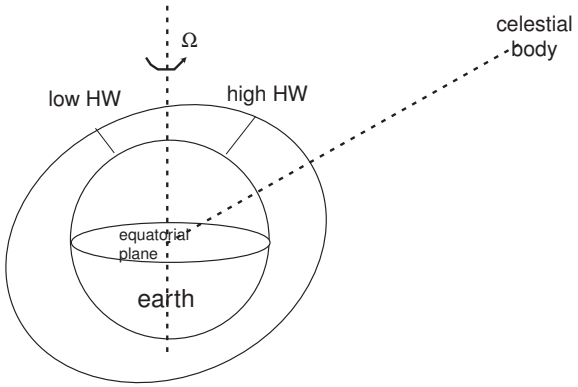

Figure 9.5: Diurnal inequality of tides due to declination effects.

bodies varies in time. Lunar tidal forces are about 20% larger than average if the distance earth-moon is at its minimum (perigee). Likewise, when the distance reaches its maximum (apogee) the lunar tidal force is reduced by 20%. For the sun this effect is quite weak: the variations are less than 1%. This effect leads to the generation of elliptical tides, details are discussed in the appendix.

9.2 Derivation of the tidal potential

The qualitative considerations of the previous section will now be quantified by deriving a mathematical expression of the tidal potential, to be incorporated in the equations of motion. The procedure closely follows that described in *Platzman* [1982].

Since gravitational and centrifugal forces are both potential forces, it is clear that the tidal force can be written as the gradient of a potential:

$$\vec{K} \;=\; -\vec{\nabla}\Phi \tag{9.4}$$

and with the use of equation (9.2) it follows

$$d\Phi \;=\; \frac{\gamma m_s}{r_1^3}\,\vec{r}_1 \,\cdot d\vec{r} \;-\; \frac{\gamma m_s}{r_0^3}\,\vec{r}_0 \cdot d\vec{r}\,.$$

From Figure 9.1 it can be inferred that

$$\Phi \;=\; \int_{r_0}^{r_1} \frac{\gamma m_s}{{r_1'}^2}\, dr_1' \;+\; \int_0^r \frac{\gamma m_s}{r_0^2}\,\cos\theta\, dr\,,$$

where the integration limits have been chosen such that $\Phi(r=0)=0$.
Development yields

$$\boxed{\Phi \;=\; -\gamma m_s \left[\frac{1}{r_1} \;-\; \frac{1}{r_0} \;-\; \frac{r\cos\theta}{r_0^2}\right].} \tag{9.5}$$

The distance r_1 can be expressed in the variables r_0, r and θ: from the definition of vector $\vec{r}_1$ and Figure 9.1 it follows

$$\frac{1}{r_1} \;=\; \frac{1}{r_0}\left[1 \,-\, 2\frac{r}{r_0}\cos\theta \,+\, \left(\frac{r}{r_0}\right)^2\right]^{-1/2} \tag{9.6}$$

Now, the ratio $(r/r_0) < 1$, so the right-hand side can be expanded with the use of the binomial formula. The result is

$$\begin{aligned}\left[1 \,-\, 2\frac{r}{r_0}\cos\theta \,+\, \left(\frac{r}{r_0}\right)^2\right]^{-1/2} \;&=\; 1 \,+\, \frac{1}{2}(2\cos\theta - \frac{r}{r_0})\,\frac{r}{r_0} \,+\, \ldots \\ &+\, \frac{1\cdot 3\cdot 5\cdot \ldots (2n-1)}{2^n\, n!}\left(\frac{r}{r_0}\right)^n \left(2\cos\theta - \frac{r}{r_0}\right)^n \,+\, \ldots\end{aligned}$$

After collection of terms with equal powers of $(r/r_0)^n$ it appears that

$$\left[1 \,-\, 2\frac{r}{r_0}\cos\theta \,+\, \left(\frac{r}{r_0}\right)^2\right]^{-1/2} \;=\; \sum_{n=0}^{\infty} P_n(\cos\theta)\,\left(\frac{r}{r_0}\right)^n , \tag{9.7}$$

where

$$P_n(x) \;=\; \frac{1}{2^n}\sum_{m=0}^{[n/2]}(-1)^m \binom{n}{m}\binom{2n-2m}{n}\, x^{n-2m}$$

are Legendre polynomials of degree n and $[n/2]$ denotes the nearest lowest integer of $n/2$. So,

$$\begin{aligned} P_0(\cos\theta) \;&=\; 1\,, & P_2(\cos\theta) \;&=\; \tfrac{1}{2}(3\cos^2\theta - 1)\,, \\ P_1(\cos\theta) \;&=\; \cos\theta\,, & P_3(\cos\theta) \;&=\; \tfrac{1}{2}(5\cos^3\theta - 3\cos\theta)\,, \end{aligned}$$

etc. Substitution of (9.6)-(9.7) in expression (9.5) yields

$$\Phi(r,\theta) \;=\; -\frac{\gamma m_s}{r_0}\sum_{n=2}^{\infty} P_n(\cos\theta)\,\left(\frac{r}{r_0}\right)^n \;\equiv\; \sum_{n=2}^{\infty}\Phi_n(r,\theta)\,. \tag{9.8}$$

Note that the polynomials P_0 and P_1 do not appear in this result.

Now, realise that $(r/r_0) \ll 1$: in case of the moon and sun this ratio is ~ 0.01 and $\sim 10^{-5}$, respectively. Hence, for practical applications the series expansion for the tidal potential can be truncated after the first term. The final result is

$$\begin{aligned}\Phi(r,\theta) \;&=\; \Phi_2(r,\theta)\left[1 + \mathcal{O}\left(\frac{r}{r_0}\right)\right], \\ \Phi_2(r,\theta) \;&=\; -\frac{\gamma m_s r^2}{r_0^3}\,\frac{3}{4}\left[\cos 2\theta \,+\, \frac{1}{3}\right].\end{aligned} \tag{9.9}$$

The potential $\Phi_2(r,\theta)$ consists of two parts.

- A constant term (independent of zenith angle θ), which contributes to a permanent deformation of the geoid; this term is not relevant from a dynamical point of view.

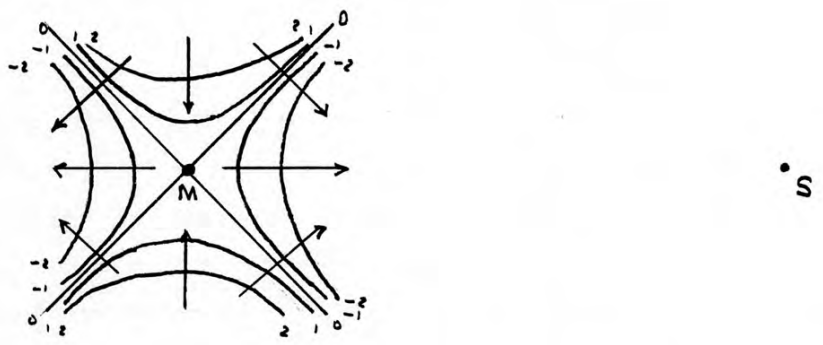

Figure 9.6: Contour lines of the contribution to tidal potential $\Phi_2(r, \theta)$ that is proportional to $\cos 2\theta$. Values are scaled by $\gamma m_s / r_0$ and the arrows indicate the corresponding forces.

- A contribution that is proportional to $\cos 2\theta$.
  In Figure 9.6 equipotential lines are sketched of this contribution (scaled by $\gamma m_s / r_0$); the arrows indicate the corresponding forces.

Compare this result with that shown in Figure 9.2. Again, the presence of two high-water and low-water areas can be seen.
Higher-order contributions in the tidal potential cause other contributions, e.g., Φ_3 generates diurnal and three-day tides (with very small amplitudes).
For practical use, the tidal potential must be expressed in terms of coordinates defined on a rotating earth, i.e., longitude λ and latitude φ. Consider to that end Figure 9.7.

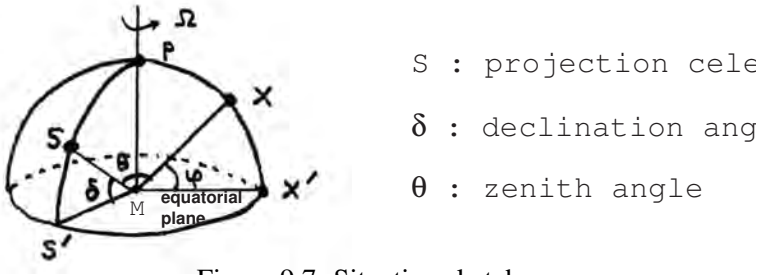

Figure 9.7: Situation sketch.

When projected onto the equatorial plane, the situation is as is sketched in Figure 9.8.

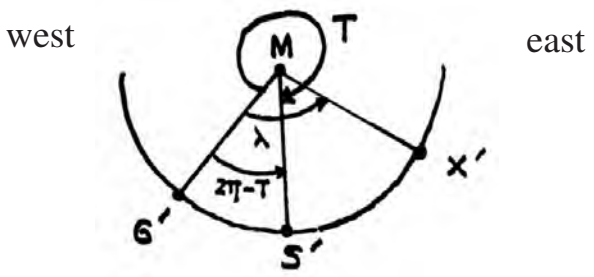

Figure 9.8: Situation sketch in the equatorial plane.

Here

S'	: projection of S onto equatorial plane ,
X'	: projection of X onto equatorial plane ,
MG'	: Greenwich meridian ,
T	: hour angle (position celestial body) (from east to west) .

So the longitude of point S is $2\pi - T$ and its latitude is δ. Due to the earth's rotation $dT/dt = 2\pi/$(solar day), which is 15^o/(mean solar hour), plus the time change of the mean longitude (increases by 2π/solar year).

The zenith angle can now be expressed in terms of λ, φ, δ and T by applying the cosine-rule to the vectors $\overrightarrow{MX}$ and $\overrightarrow{MS}$. The result is that

$$\cos\theta \;=\; \sin\varphi\,\sin\delta \;+\; \cos\varphi\,\cos\delta\,\cos(T+\lambda)\,. \tag{9.10}$$

Substitution of this result in (9.8) and finally setting $r = R$ (mean earth radius) yields

$$\Phi_2 \;=\; \Phi_2^{(0)} \;+\; \Phi_2^{(1)} \;+\; \Phi_2^{(2)}\,, \tag{9.11a}$$

where

$$\Phi_2^{(0)} \;=\; -\frac{3}{4}\,\frac{\gamma m_s R^2}{r_0^3}\,\frac{1}{3}\left[\left(1-3\sin^2\varphi\right)\left(1-3\sin^2\delta\right)\right]\,, \tag{9.11b}$$

$$\Phi_2^{(1)} \;=\; -\frac{3}{4}\,\frac{\gamma m_s R^2}{r_0^3}\,\sin 2\varphi\,\sin 2\delta\,\cos(T+\lambda)\,, \tag{9.11c}$$

$$\Phi_2^{(2)} \;=\; -\frac{3}{4}\,\frac{\gamma m_s R^2}{r_0^3}\,\cos^2\varphi\,\cos^2\delta\,\cos[2(T+\lambda)]\,. \tag{9.11d}$$

The dimensional prefactor in all expressions is known as the Doodson factor.

Note that $\Phi_2^{(0)}$ is independent of longitude, $\Phi_2^{(1)}$ is periodic in $(T+\lambda)$ and $\Phi_2^{(2)}$ is periodic in $2(T+\lambda)$. They describe tides of the first, second and third kind, respectively, a nomenclature that was introduced by Laplace (1799).

The potential $\Phi_2^{(0)}$ describes long-periodic tides due to temporal variations in the angle δ (declination effects) and variations in the distance r_0 (elliptical effects). A contour plot of $\Phi_2^{(0)}$ on the earth's surface (in case of $\delta = 0$) is shown in Figure 9.9.

The values of the potential are negative for latitudes φ between $\pm 35.3^o$ (dashed area in Figure 9.9) and positive outside that area. This is a zonally harmonic function. The corresponding forces are directed from poles to the equator.

The potential $\Phi_2^{(1)}$, which is periodic in the hour angle T, has quite a different structure. In case that the celestial body is the sun (moon) this potential is periodic in time with a period of 24 h (24 h 25 m). The amplitudes of the corresponding diurnal tides vary with the declination angle and vanish if $\delta = 0$ (celestial body in

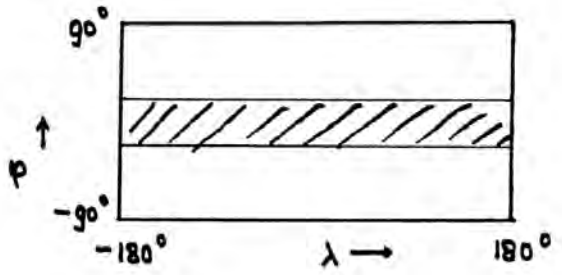

Figure 9.9: Contour lines of the tidal potential $\Phi_2^{(0)}$, defined in (9.11b), for $\delta = 0$. Dashed areas indicate negative values of the potential.

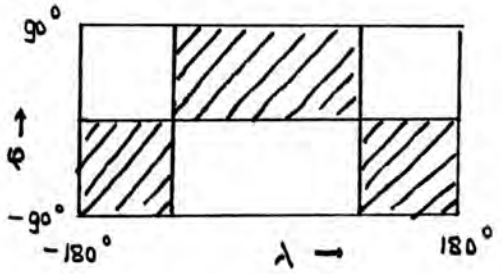

Figure 9.10: Contour lines of the tidal potential $\Phi_2^{(1)}$, defined in (9.11c), for $\delta > 0$. Dashed and white areas indicate negative and positive values of the potential, respectively.

the equatorial plane).
The potential is a terresal function; a contour plot for $T = 0$ and fixed $\delta > 0$ is sketched in Figure 9.10.

Finally, the second-order potential $\Phi_2^{(2)}$ describes the most important tidal components on earth, i.e., the semi-diurnal tides. The corresponding tidal forces have their largest amplitudes if $\delta = 0$. A contour plot of $\Phi_2^{(2)}$ is sketched in Figure 9.11.

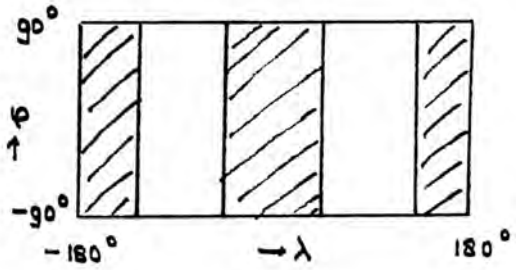

Figure 9.11: Contour lines of the tidal potential $\Phi_2^{(2)}$, defined in (9.11d), for $\delta > 0$. Dashed and white areas indicate negative and positive values of the potential, respectively.

9.3 Tidal forces in the equations of motion; equilibrium tide

The information obtained in the previous section can now be used to introduce tidal forces in the equations of motion of chapter 8. This force is given in (9.4), whilst the tidal potential is defined in (9.8)-(9.11).

In practice the concept of equilibrium tide is used instead of the tidal potential. This is the water level, measured with respect to an equipotential surface of the gravity force, that would be attained if the earth was entirely covered by water and the ocean would instantaneously respond to tidal forces. A relation between the equilibrium tide and tidal potential is derived as follows.
Consider first the situation in the absence of tides. In that case the equipotential surfaces of gravity are given by $r = r_*(\lambda, \varphi)$, such that

$$\Phi_g(r_*, \lambda, \varphi) \;=\; \text{constant}\,,$$

with Φ_g the gravity potential.
Next, define $r = r_* + \zeta_e$ as the imaginary water level that would result from the presence of tidal forces. The corresponding surface is described by

$$\Phi_g(r_* + \zeta_e, \lambda, \varphi) \;+\; \Phi(r_* + \zeta_e, \lambda, \varphi) \;=\; \text{constant}\,.$$

The fact that $\zeta_e \ll r$ allows the first term to be expanded in a Taylor series. The result is

$$\zeta_e \left(\frac{\partial \Phi_g}{\partial r}\right)_{r=r_*} \;+\; \Phi(r_* + \zeta_e, \varphi, \lambda) \;=\; \text{constant}\,, \tag{9.12}$$

where the first term of the Taylor series is incorporated in (a new value of) the constant. Since

$$\left(\frac{\partial \Phi_g}{\partial r}\right)_{r=r_*} \;=\; g \tag{9.13}$$

and the constant in (9.12) is chosen such that $\zeta_e = 0$ if $\Phi = 0$. This yields

$$\boxed{\zeta_e \;=\; -\frac{\Phi}{g}\,.} \tag{9.14}$$

If in this expression the tidal potentials of the moon and sun are substituted it turns out that the amplitudes of the corresponding equilibrium tides are 36.4 cm (moon) and 16.8 cm (sun).

Appendix: celestial mechanics and tides

Some a priori definitions:

$T_\odot$: solar day = 24 h,	frequency $\omega_\odot = 2\pi/T_\odot$,
$T_{d,s}$: sidereal day= 0.9973 solar day,	frequency $\Omega = 2\pi/T_{d,s}$,
T_2 : solar year= 365.242 solar days,	frequency $\omega_2 = 2\pi/T_2$,
T_m : lunar period= 29.5306 solar days .	

- After 1 solar day a fixed point at the earth's surface has the same orientation with respect to the sun.
- After 1 sidereal day a fixed point at the earth has the same orientation with respect to a fixed star. So a sidereal day is $T_2/(1+T_2)$ solar days, because in one year the earth makes a complete revolution about the sun.
- After 1 lunar period the earth-moon system has the same orientation with respect to the sun.

First, the length $T_{m,s} \equiv T_1$ of the sidereal month will be determined. This period of the revolution of the earth-moon around their common centre of mass will be shorter than the lunar period, since it does not involve the rotation of the earth-moon system about the sun.
Figure 9.12 shows that after one lunar period T_m the moon has rotated over an angle $(2\pi + \alpha)$ with angular velocity $\omega_1 = 2\pi/T_1$ (additional 2π due to the rotation of the moon about the earth).

So

$$2\pi + \alpha = (2\pi T_m)/T_1 \,.$$

In the same period the earth has rotated over an angle α with angular velocity $\omega_2 = 2\pi/T_2$,
so

$$\alpha = (2\pi T_m)/T_2 \,.$$

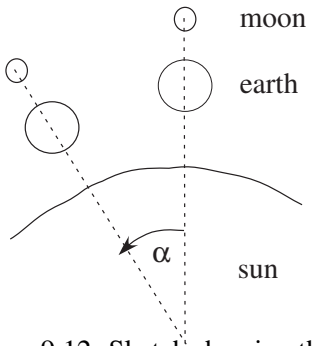

Figure 9.12: Sketch showing the rotation of the moon and earth about the sun.

From these two relations it follows

$$\frac{1}{T_m} + \frac{1}{T_2} = \frac{1}{T_1} \qquad \Rightarrow T_1 \equiv T_{m,s} = 27.3216 \text{ solar days} \,.$$

Now, an expression can be derived for the 'lunar day' $T_{\text{☾}}$. After a time $T_{\text{☾}}$ a fixed point at the earth has again the same orientation with respect to the moon (see Figure 9.13).

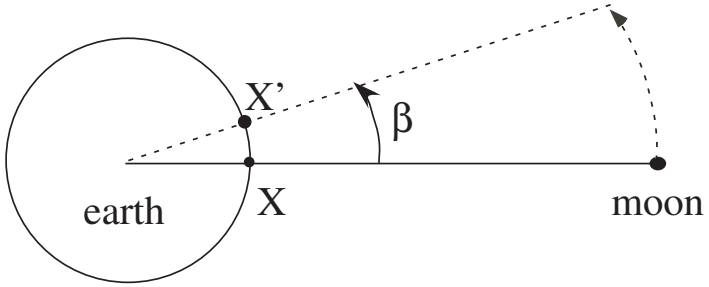

Figure 9.13: Sketch illustrating the movement of the moon for an observer at the rotating earth.

After one lunar day a fixed point at the earth has rotated about the earth's centre over an angle $(2\pi + \beta)$ with angular velocity $\Omega = 2\pi/T_{d,s}$ (additional 2π because of the rotation of the earth about its axis). So

$$2\pi \,+\, \beta \,=\, \frac{2\pi}{T_{d,s}}\, T_{\lozenge}\,.$$

In the same time the moon has rotated over an angle β with angular velocity ω_1, so

$$\beta \,=\, \frac{2\pi}{T_1}\, T_{\lozenge}\,.$$

Combination of the last two expressions yields

$$T_{\lozenge} \,=\, \frac{T_{d,s}}{1 - (T_{d,s}/T_1)}\,, \quad \text{or} \quad T_{\lozenge} \,=\, \text{24h 50m 28s}\,.$$

In this chapter it has been shown that the main lunar and solar tidal constituents are the M_2 tide (frequency $2\omega_{\lozenge}$) and the S_2 tide (frequency $2\omega_{\odot}$, respectively. Below, other tidal constituents are listed and their origin is briefly explained.

I. Declination effects cause

- long-periodic tides, viz. the

Mf tide (lunar):	frequency $2\omega_1$,	period $T/2 \simeq 13.6$ days ,
Ssa tide (solar):	frequency $2\omega_2$,	period $T_2/2 \simeq 182.6$ days .

- diurnal tides. Locally, the diurnal forcing will show modulation behaviour because the declination angle varies with time. The diurnal tidal force component caused by the moon is proportional to

$$\cos(\omega_{\lozenge}\, t)\cos(\omega_1\, t) = \frac{1}{2}\cos[(\omega_{\lozenge} - \omega_1)t] + \frac{1}{2}\cos[(\omega_{\lozenge} + \omega_1)t]\,,$$

which results in the manifestation of the

O_1 tide (moon),	frequency $\omega_{\lozenge} - \omega_1$,	period 25.823 h ,
K_1^M tide (moon),	frequency $\omega_{\lozenge} + \omega_1 \equiv \Omega$,	period 23.93 h ,
P_1 tide (sun),	frequency $\omega_{\odot} - \omega_2$,	period 24.07 h ,
K_1^S tide (sun),	frequency $\omega_{\odot} + \omega_2 \equiv \Omega$,	period 23.93 h .

- additional semi-diurnal constituents:

K_2^M tide,	frequency $2(\omega_{\text{☽}} + \omega_1) = 2\Omega$,	period 11.97 h ,
K_2^S tide,	frequency $2(\omega_{\odot} + \omega_2) = 2\Omega$,	period 11.97 h .

In practice, the K_1^M and K_1^S tide are indistinguishable and combined into one K_1 tide. Likewise, the K_2^M and K_2^S constituents are combined into one K_2 tide.

II. Due to the ellipsoidal orbits of celestial bodies elliptic tides are generated. Considering the orbit of the moon around the earth, it turns out that this ellipse itself rotates about the earth in a period of 8.85 year (frequency ω_3), as is illustrated in Figure 9.14.

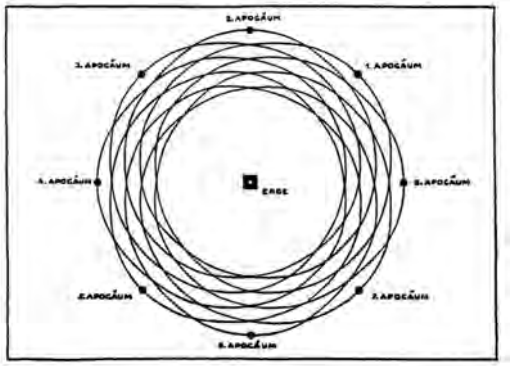

Figure 9.14: Sketch illustrating the orbit of the moon around the earth. Here, the full apogee cycle is completed in 8 sidereal months, in reality it takes about 118 sidereal months.

The frequency of the apogee cycle is $(\omega_1 - \omega_3)$, the period is 27.56 days. In case of the moon the additional tidal components are

Mm tide,	frequency $\omega_1 - \omega_3$,	period 27.56 days ,
N_2 tide,	frequency $2\omega_{\text{☽}} - (\omega_1 - \omega_3)$,	period 12.66 h ,
L_2 tide,	frequency $2\omega_{\text{☽}} + (\omega_1 - \omega_3)$,	period 12.19 h ,
Q_1^S tide,	frequency $\omega_{\text{☽}} - \omega_1 - (\omega_1 - \omega_3)$,	period 26.87 h ,
$2N_2$ tide,	frequency $2\omega_{\text{☽}} - \omega_1$,	period 12.90 h ,

and in case of the sun

Sa tide,	frequency ω_2,	period 365.25 days ,
T_2 tide,	frequency $2\omega_{\odot} - \omega_2$,	period 12.01 h ,
π_1 tide,	frequency $\omega_{\text{☽}} - 2\omega_2$,	period 24.13 h .

III. There are many other tidal constituents, in particular

- The 18.6 nodal year cycle: in this period the intersection points of the lunar orbital plane and the equatorial plane rotate about the earth's centre. This cycle is recognizable in both sea level variations and in marine deposits.

- The following tidal constituents are also significant along the Dutch coast:

μ_2 tide,	frequency $2\omega_{\text{☽}} + (\omega_1 - \omega_2)$,	period 12.87 hours ,
ν_2 tide,	frequency $2\omega_{\text{☽}} + (\omega_1 - 2\omega_2 + \omega_3)$,	period 12.62 hours .

  The variational μ_2 tide is caused by the fact that the angular velocity of the moon about the earth is slightly larger during full and new moon than during the first and last quarter.
  The ν_2 (evection) tide is excited because the sidereal month is not a constant (about 27.3 days), but it shows minor variations due to the influence of the sun on the revolution of the earth-moon system about their common centre of mass.

- Other important constituents are

M_4 tide,	frequency $2\omega_{\text{☽}}$,	period 6h 13m ,
MS_4 tide,	frequency $(\omega_{\text{☽}} + \omega_{\odot})$,	period 6h 6m ,
M_6 tide,	frequency $3\omega_{\text{☽}}$,	period 4h 8m .

  The important difference with all previous constituents is that these components are not excited by external tidal forces, but rather they are forced internally in the sea by nonlinear terms in the equations of motion. For example, the M_4 tide is due to self-interaction of the M_2 tide, the MS_4 is due to nonlinear interaction between the M_2 and S_2 tide, etc. The underlying mechanism is discussed in the course 'Physics of coastal systems'.

Further details are given in 'Getijtafels Nederland', http://www.getij.nl, *LeBlond and Mysak* [1978] and *Platzman* [1982].

Chapter 10

Free modi in a channel: Kelvin waves and Poincaré waves

10.1 Model formulation and general solutions

In order to understand the response of the ocean to tidal forcing, it is important to first identify and understand the free waves (i.e., no forcing and no dissipation) of the system. The reason is that these waves provide for the adjustment to equilibrium (see course Geophysical Fluid Dynamics) and also, when the forcing has a component with the same length and timescale of a free modi, resonance may occur. Here, the free modi of the linear 2DH shallow water equations will be investigated. The domain is an open channel with width B and a flat, horizontal bottom (see Figure 10.1). This problem is also discussed in *Gill* [1982]; *Pedlosky* [1987].

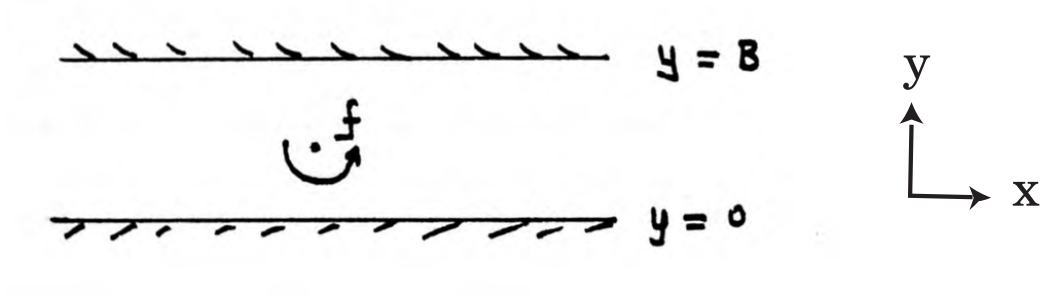

Figure 10.1: Situation sketch.

The equations of motion follow from equation (8.3a) and read

$$\frac{\partial u}{\partial t} - f\,v = -g\,\frac{\partial \zeta}{\partial x}\,, \qquad \frac{\partial v}{\partial t} + f\,u = -g\,\frac{\partial \zeta}{\partial y}\,, \tag{10.1}$$

$$\frac{\partial \zeta}{\partial t} + H\left[\frac{\partial u}{\partial x} + \frac{\partial v}{\partial y}\right] = 0\,. \tag{10.2}$$

with boundary conditions

$$v = 0 \qquad \text{at} \qquad y = 0\,,\ y = B\,. \tag{10.3}$$

From this, one equation can be derived for the free surface. The procedure is to start from the momentum equations and derive two equations that describe the evolution of the divergence ($(\partial u/\partial x + \partial v/\partial y)$ and of the relative vorticity

$$\omega \;=\; \frac{\partial v}{\partial x} \;-\; \frac{\partial u}{\partial y}\,. \tag{10.4}$$

Substitution of the continuity equation in these expressions yields

$$\frac{\partial^2 \zeta}{\partial t^2} \;+\; fH\,\omega \;-\; gH\nabla^2\zeta \;=\; 0\,, \qquad\qquad \frac{\partial \omega}{\partial t} \;-\; \frac{f}{H}\,\frac{\partial \zeta}{\partial t} \;=\; 0\,. \tag{10.5}$$

The solution of the vorticity equation is

$$\omega \;=\; \frac{f}{H}\,\zeta\,, \tag{10.6}$$

where the integration constant has been chosen such that the relative vorticity vanishes in the absence of any motion. Note that if a fluid column is stretched (positive elevation of the free surface) cyclonic vorticity is generated (i.e., fluid columns on the northern hemisphere rotate anticlockwise) because of conservation of potential vorticity.

Substitution of (10.6) in the first equation of (10.5) yields

$$\frac{\partial^2 \zeta}{\partial t^2} \;-\; gH\nabla^2\zeta \;+\; f^2\,\zeta \;=\; 0\,, \tag{10.7}$$

which is known as the Klein-Gordon equation.

Next, the boundary conditions (10.3) will be expressed in terms of the free surface. The procedure is to derive first the so-called polarisation equations for the velocity field, which relate both u and v directly to ζ. They follow from taking linear combinations of one momentum equation with the time derivative of the other momentum equation. The results are

$$\begin{aligned} \frac{\partial^2 u}{\partial t^2} \;+\; f^2\,u \;&=\; -g\left\{\frac{\partial^2 \zeta}{\partial x \partial t} \;+\; f\frac{\partial \zeta}{\partial y}\right\}\,, \\ \frac{\partial^2 v}{\partial t^2} \;+\; f^2\,v \;&=\; -g\left\{\frac{\partial^2 \zeta}{\partial y \partial t} \;-\; f\frac{\partial \zeta}{\partial x}\right\} \end{aligned} \tag{10.8}$$

and thus the boundary conditions (10.3) can be recast as

$$\boxed{\frac{\partial^2 \zeta}{\partial y \partial t} \;-\; f\frac{\partial \zeta}{\partial x} \;=\; 0 \qquad \text{at} \quad y = 0\,,\; y = B\,.} \tag{10.9}$$

Before finding solutions of system (10.7)-(10.9) it is worthwhile to consider the energy balance of the system. An energy equation is obtained from multiplying the momentum equations (10.1) with $\rho H u$ and $\rho H v$, respectively, adding the results and finally substituting the continuity equation. This yields

$$\frac{\partial E}{\partial t} \;+\; \vec{\nabla}\cdot\vec{F} \;=\; 0 \tag{10.10a}$$

with

$$E \;=\; E_k \,+\, E_p\,; \qquad\qquad \vec{F} \;=\; \rho g H \zeta \vec{u}\,, \tag{10.10b}$$

$$E_k \;=\; \frac{1}{2}\rho H(u^2+v^2)\,; \qquad E_p \;=\; \frac{1}{2}\rho g \zeta^2\,. \tag{10.10c}$$

This describes the energy balance of a column of sea water: the time evolution of the energy density E (energy per surface area) is determined by the divergence of the energy flux vector $\vec{F}$. This flux is due to work done by pressure forces. Furthermore, the energy density consists of a kinetic part (E_k) and a potential part (E_p). Equation (10.10) is a conservation law: in the absence of forcing and dissipation the total energy in the domain is conserved. Note the equivalence between this result and the energy balance (4.19a) for short waves, derived in chapter 4.

System (10.7)-(10.9) allows for solution of the form

$$\begin{aligned} \zeta \;&=\; \Re\left\{\hat{\zeta}(y)\; e^{i(kx-\sigma t)}\right\}\,, \\ u \;&=\; \Re\left\{\hat{u}(y)\; e^{i(kx-\sigma t)}\right\}\,, \qquad\qquad v \;=\; \Re\left\{\hat{v}(y)\; e^{i(kx-\sigma t)}\right\}\,. \end{aligned} \tag{10.11}$$

These are free waves, with frequency $\sigma > 0$ and wavenumber k (positive/negative k represent waves travelling in the positive/negative x-direction) and an as yet arbitrary structure in the cross-channel direction. Substitution of these solutions in the equations of motion results in the following equation for the amplitude of the free surface:

$$\frac{d^2\hat{\zeta}}{dy^2} \,+\, \alpha^2\,\hat{\zeta} \;=\; 0\,, \qquad\qquad \alpha^2 \;=\; \frac{\sigma^2-f^2}{gH} \,-\, k^2\,, \tag{10.12a}$$

with boundary conditions

$$\frac{d\hat{\zeta}}{dy} \,+\, \frac{kf}{\sigma}\,\hat{\zeta} \;=\; 0 \qquad\qquad \text{at} \quad y=0\,,\; y=B \tag{10.12b}$$

and

$$\hat{u} \;=\; \frac{g}{\sigma^2-f^2}\left(k\sigma\hat{\zeta} + f\frac{d\hat{\zeta}}{dy}\right)\,, \quad \hat{v} \;=\; \frac{-ig}{\sigma^2-f^2}\left(kf\hat{\zeta} + \sigma\frac{d\hat{\zeta}}{dy}\right)\,. \tag{10.13}$$

In fact, system (10.12) defines an eigenvalue problem. The general solution of the differential equation is

$$\hat{\zeta} \;=\; A\cos\alpha y \,+\, \hat{B}\sin\alpha y \tag{10.14a}$$

and development of the boundary conditions then result in

$$\begin{pmatrix} \frac{fk}{\sigma} & \alpha \\ \frac{fk}{\sigma}\cos\alpha B - \alpha\sin\alpha B & \alpha\cos\alpha B + \frac{fk}{\sigma}\sin\alpha B \end{pmatrix} \cdot \begin{pmatrix} A \\ \hat{B} \end{pmatrix} \;=\; 0\,. \tag{10.14b}$$

This system has only non-trivial solutions if the determinant of the coefficient matrix vanishes, compare with how the dispersion relation (3.6) for free short waves

was derived in chapter 3. In this case it follows, using the definition of parameter α, that

$$\boxed{(\sigma^2 - f^2)\left(\frac{\sigma^2}{gH} - k^2\right)\sin\alpha B = 0\,.} \tag{10.15}$$

There are three roots of this equation, which will be systematically analysed in the next sections.

10.2 Poincaré waves

Consider the root

$$\sin\alpha B = 0\,, \qquad \text{or} \qquad \alpha B = n\pi\,, \quad n = 1, 2, \ldots \tag{10.16}$$

of (10.15). Note that, according to (10.14a), the choice $n = 0$ (hence $\alpha = 0$) immediately results in $\hat{\zeta} = \text{constant} = 0$, where in the last step boundary condition (10.12b) has been applied. Also, taking negative integer values for n yields no new information: in that case the same solution is obtained if the integration constant $A \to -A$.

Using definition (10.12a) of parameter α it follows

$$\boxed{\sigma^2 = f^2 + c_0^2\left(k^2 + \frac{n^2\pi^2}{B^2}\right)\,, \qquad c_0 = \sqrt{gH}\,.} \tag{10.17}$$

This is the dispersion relation for discrete Poincaré waves; for fixed wavenumber k there is a discrete set of frequencies σ_n. The solutions are shown in Figure 10.2. In case that the channel width $B \to \infty$ the variable $n\pi/B$ can be replaced by the continuous wavenumber l; the solutions are known as Sverdrup waves.

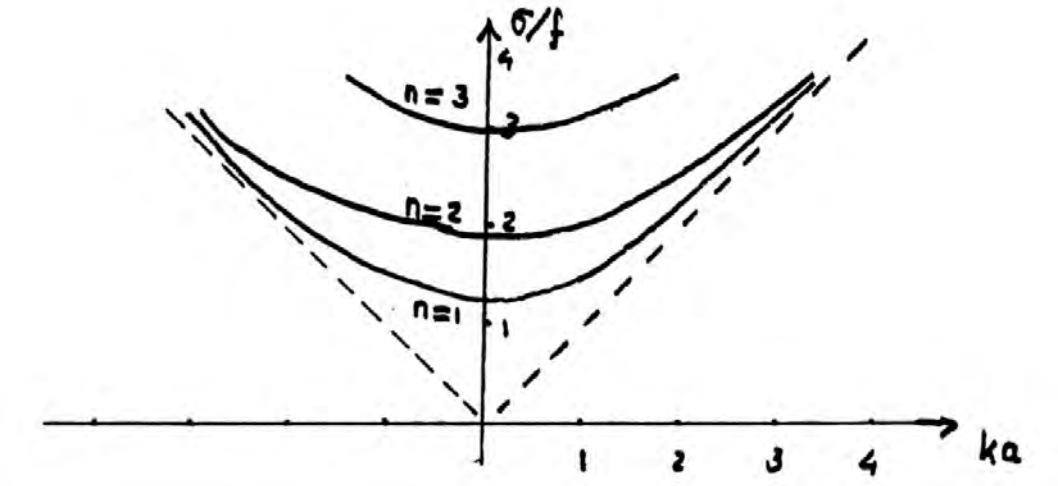

Figure 10.2: Dispersion curves for discrete Poincaré modi.

In Figure 10.2

$$\boxed{a = \frac{\sqrt{gH}}{f} \qquad \left(= \frac{c_0}{f}\right)} \tag{10.18}$$

is the Rossby deformation radius. It is the length scale on which dynamic effects of earth rotation are of the same order as those due to gravity. To understand this, the general solutions (10.11) are expanded for the specific case of Poincaré waves. With the use of equations (10.14a) and (10.17) it follows for the free surface

$$\zeta_n = Z_n \left[\cos\left(\frac{n\pi y}{B}\right) - \frac{fkB}{n\pi\sigma} \sin\left(\frac{n\pi y}{B}\right)\right] \cos(kx - \sigma t - \varphi_n) \tag{10.19a}$$

(Z_n and φ_n being an arbitrary amplitude and phase, respectively) and for the velocity components

$$u_n = \frac{Z_n}{H}\left[\frac{gHk}{\sigma}\cos\left(\frac{n\pi y}{B}\right) - \frac{fB}{n\pi}\sin\left(\frac{n\pi y}{B}\right)\right]\cos(kx - \sigma t - \varphi_n)\,, \tag{10.19b}$$

$$v_n = \frac{Z_n}{H}\left[\frac{B}{n\pi\sigma}\left(f^2 + \frac{gHn^2\pi^2}{B^2}\right)\sin\left(\frac{n\pi y}{B}\right)\right]\sin(kx - \sigma t - \varphi_n)\,. \tag{10.19c}$$

Figure 10.3 shows a sketch of the solution for $n = 1$ and specific choices for the channel width and frequency.

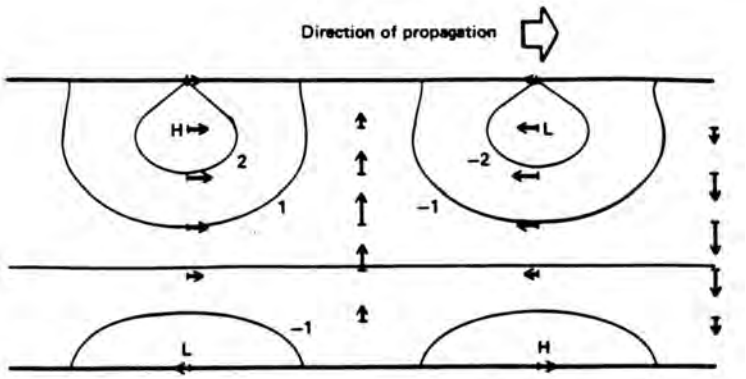

Figure 10.3: Progressive Poincaré wave ($n = 1$ mode) in a channel of width $B = \pi a$ and frequency $\omega = 2kc_0$. Contours are of surface elevation and arrows indicate currents. The signs are those for the northern hemisphere, so the greatest elevations are found on the left side of the channel (facing in the direction of propagation) where particles move anticyclonically. The nodal line is about 65% of the way across the channel. From *Gill* [1982].

Note that for $ka \ll 1$ and $(n\pi a/B) \ll 1$ (i.e., wavelength and channel width much larger than the Rossby deformation radius) the dispersion relation (10.17) can be approximated by $\sigma^2 \simeq f^2$. In this limit earth rotation effects clearly determine the dynamics: the wave frequency equals the inertial frequency f. Such inertial waves are commonly observed in the ocean, for example after a major change in weather conditions.

For $ka \gg 1$ and $(n\pi a/B) \gg 1$ (length scales are small compared to the Rossby deformation radius) it follows $\sigma_n^2 \simeq c_0^2\kappa^2$, with $\kappa^2 = k^2 + (n^2\pi^2/B^2)$ the squared total wavenumber. In this limit the wave dynamics is fully controlled by gravity, earth rotation does not play a role. In fact, the solutions become long gravity waves.

From dispersion relation (10.17) and Figure 10.2 it follows that Poincaré waves have a minimum frequency which is given by

$$\boxed{\sigma_{P,min} = \left(f^2 + c_0^2 \frac{\pi^2}{B^2}\right)^{1/2}} \quad . \tag{10.20}$$

Since the major tidal frequencies have values close to the inertial frequency, it turns out that progressive Poincaré waves can not exist in basins which are too narrow. An example of such a basin is the North Sea ($B \sim 500$ km, $H \sim 70$ m, $f \sim 10^{-4}$ s^{-1}). Neverthless, Poincaré waves are important for tidal propagation in seas and oceans having widths of the order of the Rossby deformation radius or larger, see chapter 11.

The phase velocity and group velocity are, respectively, given by

$$\begin{aligned} c = \frac{\sigma}{k} \quad &\rightarrow \quad c = c_0 \left[1 + \frac{1}{k^2a^2}\left(1 + \frac{n^2\pi^2a^2}{B^2}\right)\right]^{1/2} , \\ c_g = \frac{\partial\sigma}{\partial k} \quad &\rightarrow \quad c_g = c_0 \frac{ka}{\left[1 + k^2a^2 + \frac{n^2\pi^2}{B^2}a^2\right]^{1/2}} \quad . \end{aligned} \tag{10.21}$$

In Figure 10.4 the variables c/c_0 and c_g/c_0 are sketched as a function of ka for $n\pi a/B = 1$.

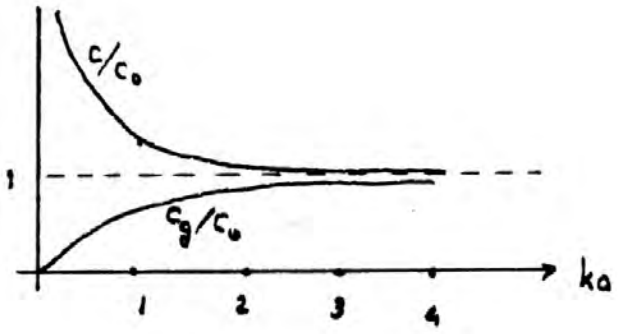

Figure 10.4: Dependence of dimensionless phase velocity c/c_0 and dimensionless group velocity c_g/c_0 of Poincaré waves on ka.

Note that the group velocity is always smaller than the phase velocity. Hence the wave envelope (and also the energy density) propagate slower than individual wave crests. For $ka \ll 1$ (inertia-dominated waves) the phase velocity becomes infinite, whilst the group velocity vanishes. In the gravity regime $ka \gg 1$ it turns out that $c \sim c_g \sim c_0$.

Finally, the energy balance of Poincaré waves is considered. For this, the solutions (10.19) are substituted in (10.10) and subsequently averaged over the width of

the channel and over the wave phase. With $< \cdot >$ indicating the avarage operator, the results are

$$\begin{aligned} < E_p > &= \frac{1}{8}\rho g Z_n^2 \left[1 + \frac{c_0^2 k^2}{\sigma^2} \frac{B^2}{n^2\pi^2 a^2} \right] , \\ < E_k > &= \frac{1}{8}\rho g Z_n^2 \left[1 + \frac{B^2}{n^2\pi^2 a^2} + \frac{f^2}{\sigma^2} \left(1 + \frac{B^2}{n^2\pi^2 a^2} \right) \right] , \\ < F_x > &= < E > \, c_g \, . \end{aligned} \tag{10.22}$$

From this it follows:

- $< E_k >$ larger than or equal to $< E_p >$: Poincaré waves generally have more kinetic than potential energy;
- if $ka \ll 1$ the total energy almost only consists of kinetic energy;
- if $ka \gg 1$ there is equipartition of energy: $< E_k > \simeq < E_p >$;
- the energy density flux is the product of the energy density and the group velocity.

10.3 Kelvin waves

Next, the second root of equation (10.15) is analysed, i.e.

$$\boxed{\sigma^2 \, = \, gHk^2 \qquad (= \, c_0^2 \, k^2) \, .} \tag{10.23}$$

This dispersion relation is identical to that of long gravity waves, but it comprises a more general feature, viz. the Kelvin wave. The dispersion relation is indicated in Figure 10.2 by the dotted lines.

For this root equation (10.12a) yields that parameter $\alpha^2 \, = \, -f^2/(gH)$, or $\alpha \, = \, i/a$. Here, a is the Rossby deformation radius; the 'minus' root needs not to be considered for reasons similar as those given in the previous section. Development of (10.11)-(10.12) then yields $\hat{B} = \pm iA$, where the positive (negative) root applies to $\sigma/k \, > \, 0 \; (< \, 0)$, i.e., for waves travelling in the positive (negative) x-direction. The solutions for the free surface then become

$$\zeta \, = \, Z_r \, e^{-y/a} \, \cos(|k|x - \sigma t + \varphi_r) \qquad (\sigma/k \, > 0) \, , \tag{10.24a}$$

or

$$\zeta \, = \, Z_l \, e^{-(B-y)/a} \, \cos(|k|x + \sigma t + \varphi_l) \quad (\sigma/k \, < 0) \, , \tag{10.24b}$$

with Z_r, Z_l arbitrary constants and φ_r, φ_l arbitrary phases. So the waves have amplitudes that decay exponentially with increasing distance to the coast. The e-folding length scale is a, the Rossby deformation radius.

The velocity components are

$$u = -\frac{g}{f}\frac{\partial \zeta}{\partial y}\,, \qquad\qquad v = 0\,. \tag{10.24c}$$

Thus, there is no velocity in the cross-channel direction and the along-channel component is determined by geostrophic balance. The behaviour of the two Kelvin waves is sketched in Figure 10.5.

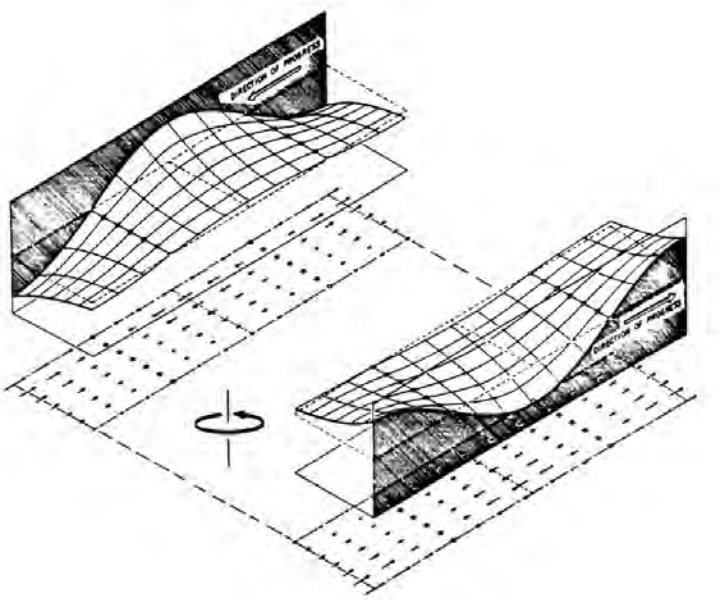

Figure 10.5: Northern hemisphere Kelvin waves on opposite side of a channel that is wide compared with the Rossby deformation radius. In each vertical plane parallel to the coast, the currents (shown by arrows) are entirely within the plane and are exactly the same as those for a long gravity wave in a nonrotating channel. However, the surface elevation varies exponentially with distance from the coast in order to give a geostrophic balance. This means that Kelvin waves move with the coast on their right in the northern hemisphere and on their left in the southern hemisphere. Adopted from *Gill* [1982].

The dispersion relation (10.23) indicates that Kelvin waves can have any frequency. In other words, they can be excited in a channel by tidal forcing. This fact explains why many observed characteristics of tidal waves (e.g., largest tidal range at the coast) can be understood from the dynamics of Kelvin waves.

If $B \ll a$ (narrow channel), then $e^{\pm B/a} \sim 1$ and the Kelvin wave behaves as a long gravity wave without any cross-channel structure. Such a situation applies for example to estuaries and tidal channels. In case of the North Sea, $B \sim 500$ km, $a \sim 300$ km, hence it can not be considered as a narrow channel.

From the dispersion relation (10.23) it immediately follows that

$$c = c_g = \pm c_0 \quad (= \sqrt{gH})\,, \tag{10.25}$$

so the Kelvin wave is dispersionless. The kinetic energy, potential energy and energy flux are, respectively, given by

$$\begin{aligned} <E_p> &= <E_k> = \frac{1}{4}\rho g Z^2 \left[1 - e^{-2B/a}\right] \frac{a}{2B}\,, \\ <F_x> &= <E>\, c_g\,. \end{aligned} \tag{10.26}$$

10.4 The third root

Finally, a remark about the third root of (10.15). This yields

$$\sigma = f\,, \tag{10.27}$$

which is the dispersion relation of an inertial wave. It turns out that the corresponding solution is fully equivalent to a Kelvin wave having the inertial frequency. In other words, the third root contains no new information and the spectrum of free waves in a rotating channel consists of Poincaré modi and Kelvin waves.

Chapter 11

Free modes in a semi-enclosed basin: the Taylor problem

The theory developed in the two previous chapters can be used to study tidal propagation in the southern ocean. However, many oceans and seas (Atlantic Ocean, North Sea) are bounded at *three* sides by coasts. It is thus important to study the possible free waves in semi-enclosed basins. This issue is known as the Taylor problem, after G.I. Taylor, who first presented solutions of this problem in 1920. Here, the problem will be investigated for a rectangular basin with a constant depth (see Figure 11.1).

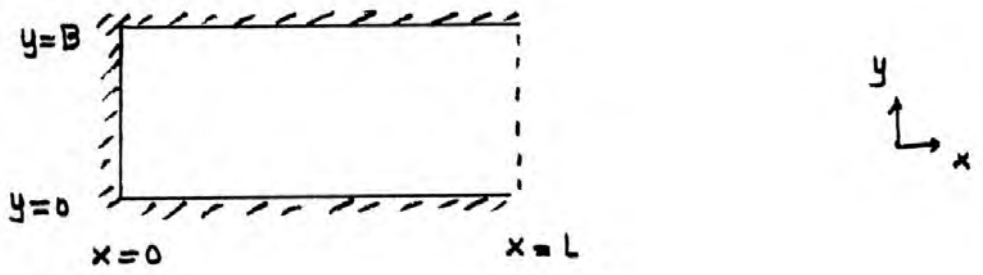

Figure 11.1: The semi-enclosed basin studied in this chapter.

The dynamics is still governed by eqs. (10.1)-(10.3), but with the additional boundary conditions

$$u = 0 \qquad \text{at} \quad x = 0\,, \qquad \text{at} \quad x = L: \ \text{not yet specified}\,. \tag{11.1}$$

At this point it is important to realise that linear free waves in (semi-)enclosed basins can be constructed from free waves that exist in an open channel. The reason is that the latter comprise a complete set.

In this specific case the free waves are Kelvin waves and Poincaré waves. Now assume that the frequency σ of the wave under consideration is smaller than the minimum frequency $\sigma_{P,min}$ of Poincaré waves, as given in (10.20). This situation is representative for the North Sea. Other cases are discussed in *LeBlond and Mysak* [1978]. If $\sigma < \sigma_{P,min}$ then in most part of the basin the free wave will consist of

a superposition of the incoming and reflected Kelvin wave. Thus, with the use of eqs. (10.11) and (10.24):

$$\begin{aligned} \zeta &= \Re\left\{ Z\, e^{-y/a}\, e^{i(kx-\sigma t)} \;+\; Z\, e^{-(B-y)/a}\, e^{-i(kx+\sigma t)} \right\} , \\ u &= \Re\left\{ \frac{Z}{H}\, c_0\, e^{-y/a}\, e^{i(kx-\sigma t)} \;-\; \frac{Z}{H}\, c_0 e^{-(B-y)/a}\, e^{-i(kx+\sigma t)} \right\} , \\ v &= 0\,. \end{aligned} \tag{11.2}$$

reflected(to right) incoming (to left)

Note that the incoming and reflected wave have identical amplitudes and phases, because full reflection takes place. These solutions can also be recast as

$$\zeta = \alpha(x,y)\, \cos\left[\sigma t - \beta(x,y)\right] , \tag{11.3}$$

$$u = \gamma(x,y)\, \cos\left[\sigma t - \delta(x,y)\right] , \tag{11.4}$$

with $\alpha(x,y), \gamma(x,y)$ amplitudes and $\beta(x,y), \delta(x,y)$ phases. This follows by application of standard goniometric relationships. In Figure 11.2 contour plots of the amplitude $\alpha(x,y)$ (dashed lines) and phase $\beta(x,y)$ (solid lines) are sketched. These are qualitative results, the details depend on the ratio B/a.

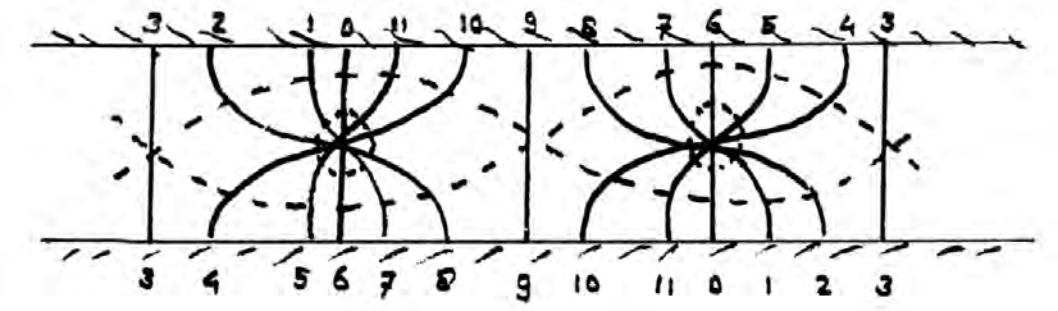

Figure 11.2: Co-amplitude lines (dashed) and co-phase lines (solid) of the free surface, resulting from the superposition of two Kelvin waves with equal amplitudes and travelling in opposite directions.

The conclusions are:

- The tidal wave rotates cyclonically (anticlockwise on the northern hemisphere) around amphidromic points (nodal points), where $\alpha(x,y) = 0$. The distance between successive points is half the wavelength of a progressive Kelvin waves.
- In the present case (full reflection, no friction) the amphidromic points are located on the mid-axis of the channel.
- In between successive amphidromic points the so-called stagnation points are located where $u = v = 0$. The co-amplitude and co-phase lines of the velocity field have similar shapes as those of the free surface.

- There is no location x=constant where amplitude $\gamma(x, y) = 0$ for all values of y. Hence, the solution (11.2) can not obey the boundary condition at the coast where the Kelvin wave is reflected. In this area other waves must play a role as well.

These new waves appear to be trapped Poincaré waves, which have an exponential structure in x, rather than an oscillatory structure. These waves can now exist because of the presence of the closed coast at $x = 0$. Expressions of their free surface and velocity field can be derived from eqs. (10.17), (10.19a) and (10.19b) by replacing wavenumber k by is_n. Here, s_n is a real-valued quantity and σ is the imposed frequency, which is identical to that of the Kelvin waves in (11.2). This yields

$$\zeta_n = \Re\left\{ Z_n \left[\cos\left(\frac{n\pi y}{B}\right) - \frac{iB}{n\pi}\frac{f s_n}{\sigma} \sin\left(\frac{n\pi y}{B}\right)\right] e^{-s_n x}\, e^{-i\sigma t}\right\}, \tag{11.5a}$$

$$u_n = \Re\left\{ \frac{Z_n}{H}\frac{B}{\sigma n\pi}\left[\frac{igHs_n n\pi}{B} \cos\left(\frac{n\pi y}{B}\right) - \sigma f \sin\left(\frac{n\pi y}{B}\right)\right] e^{-s_n x}\, e^{-i\sigma t}\right\}, \tag{11.5b}$$

$$v_n = \Re\left\{ \frac{iZ_n}{H}\frac{B}{\sigma n\pi}\left(f^2 + \frac{gHn^2\pi^2}{B^2}\right) \sin\left(\frac{n\pi y}{B}\right) e^{-s_n x}\, e^{-i\sigma t}\right\}. \tag{11.5c}$$

and the dispersion relation

$$\sigma^2 = f^2 - gHs_n^2 + gH\frac{n^2\pi^2}{B^2}. \tag{11.6}$$

The latter determines the quantities s_n which determine how fast the amplitudes of the different modi decay with increasing distance x from the coast. Hence, s_n^{-1} are the efolding length scales of the modi. From (11.6) it follows $s_1 < s_2 < \ldots$. This implies that in this example s_1^{-1} is the spatial scale on which trapped Poincaré modi emerge. For most basins it appears that this scale is much smaller than the length of the basin, so trapped Poincaré modi will only be observed closed to the boundaries. Here the situation near the coast $x = 0$ will be further investigated. This means that the final solution in the region near the coast $x = 0$ is not affected by Poincaré modi that are excited near $x = L$.

The qualitative picture is now that near the coast $x = 0$ the solution consists of an incoming Kelvin wave, a partially reflected outgoing Kelvin wave (reflection coefficient R) and trapped Poincaré waves. The reason to introduce a reflection coefficient is that the properties of the reflected Kelvin wave will be influenced by the excitation of Poincaré waves. The behaviour of the particle orbits in the basin will thus be as sketched in Figure 11.3.
At distances x larger than s_1^{-1} the velocity field is determined by the two Kelvin waves only; here the cross-channel velocity component is negligible. The presence of trapped Poincaré modi near the coast $x = 0$ causes the local velocity field to become polarized, but at the coast the velocity field only has a cross-channel component, such that the condition of no normal flow at the coast is obeyed. This structure of the velocity field is indeed observed in basins like the North Sea.

To determine the final solution the boundary condition $u = 0$ at $x = 0$ must be elaborated. It imposes that the x-component of the velocity of the incoming Kelvin wave ($u_{K,l}$), that of the partially reflected Kelvin wave ($u_{K,r}$) and those of all the

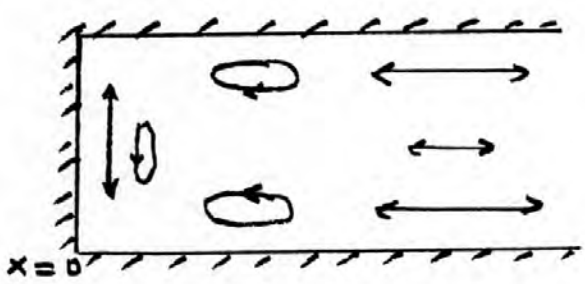

Figure 11.3: Sketch of the expected velocity field near the coast $x = 0$.

trapped Poincaré waves ($u_{P,n}$) must vanish at this location. After substitution of expressions (11.2) and (11.5) and evaluation at $x = 0$ the final result is

$$-Z\left[e^{-(B-y)/a} - Re^{-y/a}\right] + \sum_{n=1}^{\infty} Z_n \left[\frac{ic_0 s_n}{\sigma}\cos\left(\frac{n\pi y}{B}\right) - \frac{fB}{n\pi c_0}\sin\left(\frac{n\pi y}{B}\right)\right] = 0.$$

In this expression the amplitude Z of the incoming Kelvin wave is chosen to be real (this is always possible by a suitable phase shift) and R is the (complex) reflection coefficient. The unknowns are Z_n/Z and R.

The equation given above can be solved using a collocation technique. The assumption is that the equation is obeyed at a finite number of collocation points $(y/B) = (j-1)/N (j = 1, 2, \ldots, N+1)$. Development then yields $(N+1)$ linear algebraic equations for $(N+1)$ unknowns, being R and $Z_n/Z (n = 1, 2, \ldots, N)$. Thus, only N trapped Poincaré waves are taken into account. In the limit $N \to \infty$ convergence of the solution is guaranteed by the fact that the Kelvin waves and Poincaré waves form a complete set.

In Figure 11.4 the original solution of Taylor is shown for a basin with dimensions that resemble that of the North Sea. The agreement with Figure 7.2 is remarkable. Other solutions (e.g. $\sigma > \sigma_{P,min}$, hence also progressive Poincaré waves, partially absorbing coasts, influence of friction, two open boundaries) are discussed in *LeBlond and Mysak* [1978]; *Bowden* [1983]; *Parker* [1991].

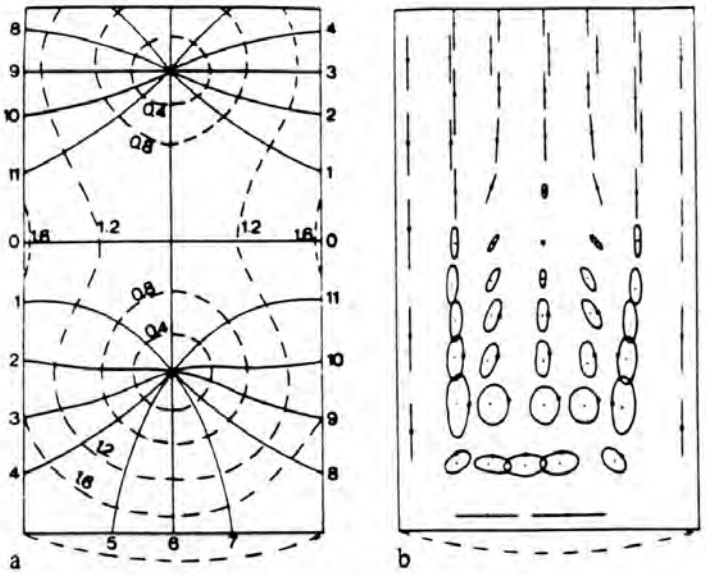

Figure 11.4: The amphidromic pattern (a) and particle trajectories (b) near the closed end of a channel for a reflected Kelvin wave. Curves of equal amplitude are given by the broken lines; curves of constant phase by the solid lines. (From *Gill* [1982], adopted from the original 1920 paper of G.I. Taylor.

Chapter 12

Co-oscillation and tidal resonance: a simple model

The response of basins to direct tidal forcing is generally small, because their width is small compared to the wavelength of the equilibrium tide (being half the local earth circumference). Despite this fact, large differences between low and high water occur in many seas and bays, e.g. in the North Sea. The explanation for this behaviour is that the tidal wave that is generated in the ocean propagates into a shelf sea. In this process the wave experiences a strong reduction in depth, hence mass conservation causes a strong increase of its amplitude. Moreover, as is illustrated in Figure 12.1, resonance can occur within the basin because the incoming wave interacts with the wave that is excited by reflection at the coast.

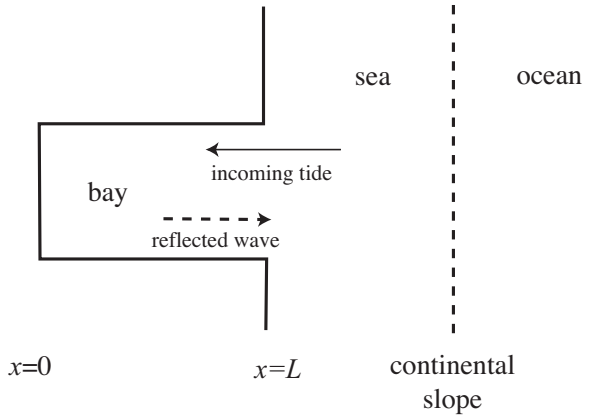

Figure 12.1: The tidal basin studied in this chapter.

The latter mechanism can be studied by prescribing the water level at the boundary. Hence, the forcing occurs through boundary conditions, rather than through forces in the momentum equations. Consequently, tides in the basin co-oscillate with those in the adjacent ocean, hence their name co-oscillating tides.

In this chapter only a simple, illustrative model will be discussed. Consider a semi-enclosed basin with a constant width B, constant depth H and length L. The dynamics are assumed to be governed by the cross-sectionally averaged shallow water

equations in which Coriolis and tidal forces are ignored. This boils down to equations (8.3) of chapter 8, in which $v = 0$, $f = 0$. The boundary conditions are that at the closed coast (here at $x = 0$) the along-channel velocity component vanishes, whilst at the open boundary the free surface is prescribed. The latter consists of one tidal constituent with radian frequency σ and amplitude $\hat{Z}$. So the model is

$$\begin{array}{lll} \dfrac{\partial u}{\partial t} = -g\dfrac{\partial \zeta}{\partial x} & , & \dfrac{\partial \zeta}{\partial t} + H\dfrac{\partial u}{\partial x} = 0\,, \\ \text{with} \quad u = 0 \quad (x = 0) & \text{and} & \zeta = \hat{Z}\,\cos(\sigma t) \quad (x = L)\,. \end{array} \tag{12.1}$$

From this a single equation for the free surface elevations can be derived, with corresponding boundary conditions:

$$\begin{array}{ll} \dfrac{\partial^2 \zeta}{\partial t^2} - gH\dfrac{\partial^2 \zeta}{\partial x^2} = 0\,, & c_0^2 = gH\,, \\ \dfrac{\partial \zeta}{\partial x} = 0 \quad (x = 0)\,, & \zeta = \hat{Z}\,\cos(\sigma t) \quad (x = L)\,. \end{array} \tag{12.2}$$

The nontransient solution is a forced wave:

$$\zeta = Z(x)\,\cos(\sigma t)\,. \tag{12.3}$$

Substitution in (12.2) yields

$$\begin{array}{ll} \dfrac{d^2 Z}{dx^2} + \dfrac{\sigma^2}{gH}\,Z = 0\,, & \\ \dfrac{dZ}{dx} = 0 \quad (x = 0)\,, & Z = \hat{Z} \quad (x = L)\,. \end{array} \tag{12.4}$$

The general solution of the equation above is

$$Z = A\,\cos(kx) + D\,\sin(kx)\,, \qquad k = \frac{2\pi}{\lambda} = \frac{\sigma}{c_0}\,.$$

Note that k is the wavenumber of the tide and λ is the corresponding wavelength.

The boundary conditions yield

$$D = 0\,, \qquad A = \frac{\hat{Z}}{\cos(kL)}\,,$$

so that the solution of the original system (12.1) reads

$$\boxed{\begin{array}{lll} \zeta & = & \dfrac{\hat{Z}}{\cos(kL)}\,\cos(kx)\,\cos(\sigma t)\,, \\ u & = & \dfrac{g}{c_0}\dfrac{\hat{Z}}{\cos(kL)}\,\sin(kx)\,\sin(\sigma t)\,, \end{array}} \tag{12.5}$$

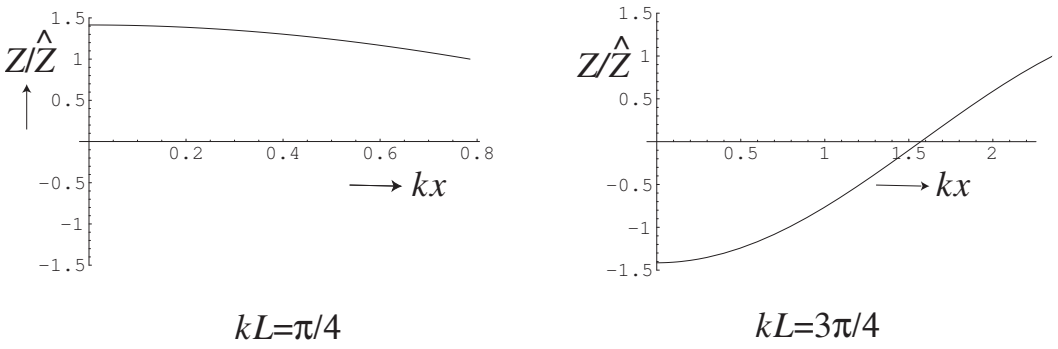

Figure 12.2: Amplitude of the vertical tide as a function of kx for different values of parameter kL.

In Figure 12.2 the amplitude of the sea surface variations is sketched as a function of the along-channel coordinate x for different values of kL. The latter parameter is, apart from a factor of 2π, the ratio of the channel length and the wavelength of the tide. The number of amphidromic points depends on this parameter, as can be understood from the results of the previous chapter.
It is important to realise that parameter kL also determines the amplitude of the sea surface variations. In fact, if $\cos(kL) = 0$, in other words, if

$$\boxed{\frac{\sigma L}{\sqrt{gH}} = \left(\frac{2n-1}{2}\right)\pi\,, \qquad n = 1, 2, \ldots\,,} \tag{12.6}$$

then resonance occurs. The physical interpretation is that in these cases the system is forced at one of its eigenmodi.

Condition (12.6) can also be recast as

$$\frac{L}{\lambda} = \frac{2n-1}{4}\,, \qquad n = 1, 2, \ldots\,.$$

This shows that resonance occurs in case the length of the basin L is a quarter (or three-quarter, five-quarter, etc.) of the tidal wavelength.

Another alternative expression of condition (12.6) is

$$\frac{2L}{c_0} = \left(\frac{2n-1}{2}\right)T\,, \qquad\qquad T = \frac{2\pi}{\sigma}\,.$$

This shows that resonance occurs if the time needed for the tidal wave to travel up and down the basin equals (half + a multiple) of the tidal period. This means that the incoming and outgoing wave are 180^o out of phase at the open boundary, such that local extinction occurs.

The most spectacular example of tidal resonance is observed in the Bay of Fundy (NE Canada) (see also Figure 7.3). This bay has a length $L = 350$ km, a depth $H = 100$ m and the tidal period $T = 12$ h 25 m. The wavelength of the tide is then $\lambda = 1413$ km, so the bay is close to quarter-wave resonance.

A second example is the North Sea: its characteristics are $L = 900$ km, $H = 70$ m, $T = 12$ h 25 m, so $\lambda = 1200$ km. This shows that the system is close to three-quarter resonance. Of course, this conclusion is based on a simple model that ignores Coriolis effects, which are known to modify the dynamics in this case (see previous chapter). On the other hand, the tidal wavelength is that of the Kelvin wave, which is not affected by Coriolis forces.

A few final remarks, related to limitations of the present model and which will be discussed in more depth in the course 'Physics of coastal systems':

- An additional eigenfrequency is obtained in case that the basin is connected with the sea by means of a narrow strait. This geometry is illustrative for that of e.g. Wadden Sea basins. The new eigenmode is called the Helmholtz mode.

- The model discussed so far ignores the influence of the tidal dynamics inside the basin on that in the adjacent sea, since the sea level variations at the open boundary are fixed. In particular near resonance this assumption is not valid, because the basin radiates energy into the sea. The mechanism of radiation damping, discussed in e.g. *Mei* [1989], causes the amplitude of the tidal wave to be finite, even in exact resonance.
- Another important mechanism that is ignored in the model discussed here is dissipation due to bottom friction. This also causes the amplitude of the tidal wave to be finite in all cases. For shallow basins, like those in the Wadden Sea, friction plays a very important role. However, analysing a system with friction is not trivial, because the bottom shear stress depends quadratically (hence: nonlinearly) on the velocity field.
- Most basins have a width and depth that decrease in the landward direction. Moreover, tidal flats are present that fall dry during low water. These so-called hypsometric characteristics have a significant effect on the dynamics of the tide.

Recommended literature

Introductory books:

- ***Groen and Dorrestein* [1976]**
- ***Van Dyke* [1982]**
- ***Open Univ. Course Team* [2001]**

General textbooks that discuss ocean waves:

- ***LeBlond and Mysak* [1978]**
- ***Gill* [1982]**
- ***Pedlosky* [1987]**
- ***Pedlosky* [2003]**
- ***Apel* [1987]**

Specific textbooks on water waves/wind waves:

- *Kinsman* [1965]
- *Phillips* [1977]
- ***Crapper* [1984]**
- ***Sørensen* [1993]**
- ***Mei* [1989] or *Mei et al.* [2005a]**
- *Komen et al.* [1994]
- *Dingemans* [1997]
- ***WMO* [1998]**
- *Janssen* [2005]
- ***Holthuijsen* [2007]**
- *Massel* [2013]

Advanced books on water waves/wind waves:

- *Ross* [1996]
- *Johnson* [1997]
- *Ochi* [1998]
- *Young* [1999]
- *Lavrenov* [2003]
- *Mei et al.* [2005b]
- *Levin and Nosov* [2009]
- *Osborne* [2010]
- *Babanin* [2011]

Specific textbooks on long waves and tides:

- *Dronkers* [1964]
- *Hendershott* [1981]
- *Boon* [2004]
- ***McCully* [2006]**
- ***Pugh and Woodworth* [2014]**

Advanced textbooks on long waves and tides:

- *Godin* [1977]
- *Marchuk and Kagan* [1989]
- *Gosh* [1998]
- *Parker* [1991]
- *Cartwright* [1998]
- *Charlier and Finkl* [2009]
- *Hardisty* [2009]

Bibliography

Apel, J. R., *Principles of ocean physics*, Academic Press, London, 1987.

Babanin, A., *Breaking and dissipation of ocean surface waves*, 480 pp., Cambridge University Press, Cambridge, 2011.

Boon, J. D., *Secrets of the tide: tide and tidal current analysis and applications, storm surges and sea level trends*, 212 pp., Ellis Horwood, Chichester, 2004.

Bowden, K. F., *Physical oceanography of coastal waters*, Ellis Horwood, Chichester, 1983.

Cartwright, D. E., *Tides, a scientific history*, Cambridge Univ. Press, Cambridge, 1998.

Charlier, R. H., and C. W. Finkl, *Tide and tidal power*, 262 pp., Springer Verlag, Berlin, 2009.

Crapper, G. D., *An introduction to water waves*, Ellis Horwood Ltd., Chichester, 1984.

Cushman Roisin, B., and J. M. Beckers, *Introduction to geophysical fluid dynamics, 2th edition*, Elsevier, Amsterdam, 2011.

Debnath, L., *Nonlinear water waves*, Academic Press, Boston, 1994.

Defant, A., *Physical Oceanography*, Pergamon Press, Oxford, 1961.

Dingemans, M. W., *Water wave propagation over uneven bottoms; part 1 & 2, linear (nonlinear) wave propagation*, World Scientific, Singapore, 1997.

Dronkers, J. J., *Tidal computations*, North Holland, Amsterdam, 1964.

Gill, A. E., *Atmosphere ocean dynamics*, Academic Press, New York, 1982.

Godin, G. G., *The analysis of tides*, University Press, Liverpool, 1977.

Gosh, S. N., *Tidal hydraulic engineering*, Balkema, Rotterdam, 1998.

Groen, P., and R. Dorrestein, *Zeegolven (in Dutch)*, Staatsuitgeverij, Den Haag, 1976.

Hardisty, J., *The analysis of tidal stream power*, 342 pp., John Wiley & Sons, Ltd, Chichester, 2009.

Hasselman, K., et al., Measurements of wind-wave growth and swell decay during the Joint North Sea Wave Project (JONSWAP), *Dtsch. Hydrogr. Z. Suppl. A*, *8 (12)*, 289–300, 1973.

Hendershott, M. C., Long waves and ocean tides, in *Evolution of physical oceanography*, edited by B. A. Warren and C. Wunsch, pp. 292–341, MIT Press, Cambridge (MA), 1981.

Holthuijsen, L. H., *Waves in oceanic and coastal waters*, Cambridge Univ. Press, 2007.

Janssen, P., *The interaction of ocean waves and wind*, Cambridge Univ. Press, Cambridge, 2005.

Johnson, R. S., *A modern introduction to the mathematical theory of water waves*, Cambridge Univ. Press, Cambridge, 1997.

Khandekar, M. L., *Operational analysis and prediction of ocean wind waves*, Springer Verlag, New York, 1989.

Kinsman, B., *Wind waves, their generation and propagation on the ocean surface*, Prentice Hall, 1965.

Komen, G. J., L. Cavaleri, M. Donelan, K. Hasselman, S. Hasselman, and P. A. E. M. Janssen, *Dynamics and modelling of ocean waves*, Cambridge Univ. Press, Cambridge, 1994.

Lavrenov, I. V., *Wind-waves in oceans*, Springer Verlag, Berlin, 2003.

LeBlond, P. H., and L. Mysak, *Waves in the ocean*, Elsevier, Amsterdam, 1978.

Levin, B., and M. Nosov, *Physics of tsunamis*, 327 pp., Springer Verlag, Berlin, 2009.

Marchuk, G. I., and B. A. Kagan, *Dynamics of ocean tides*, Kluwer Acad. Press, Dordrecht, 1989.

Massel, S. R., *Ocean surface waves, their physics and prediction, second edition*, World Scientific, Singapore, 2013.

McCully, J. G., *Beyond the moon, a conversational common sense guide to understanding the tides*, World Scientific, Singapore, 2006.

Mei, C. C., *The applied dynamics of ocean surface waves*, 740 pp., World Scientific, Singapore, 1989.

Mei, C. C., M. Stiassnie, and D. K.-P. Ye, *Theory and applications of ocean surface waves, part 1: Linear aspects*, World Scientific, Singapore, 2005a.

Mei, C. C., M. Stiassnie, and D. K.-P. Ye, *Theory and applications of ocean surface waves, part 2: Nonlinear aspects*, World Scientific, Singapore, 2005b.

Neumann, G., and W. J. Pierson jr., *Principles of physical oceanography*, Prentice-Hall Inc., Englewood Cliffs (NJ), 1966.

Ochi, M. K., *Ocean waves, the stochastic approach*, Cambridge Univ. Press, Cambridge, 1998.

Open Univ. Course Team, *Waves, tides and shallow water processes*, Pergamon Press, Oxford, 2001.

Osborne, A., *Nonlinear ocean waves and the inverse scattering transform*, 944 pp., Academic Press, 2010.

Parker, B. B. (Ed.), *Tidal hydrodynamics*, John Wiley & Sons, New York, 1991.

Pedlosky, J., *Geophysical fluid dynamics*, Springer Verlag, New York, 1987.

Pedlosky, J., *Waves in the ocean and atmosphere*, Springer Verlag, New York, 2003.

Phillips, O. M., *The dynamics of the upper ocean*, Cambridge Univ. Press, Cambridge, 1977.

Platzman, G. W., Ocean tides and related waves, in *Mathematical methods in the geophysical sciences, part 2: inverse problems, dynamo theory and tides*, edited by W. H. Reid, pp. 239–292, Amer. Math. Soc., 1982.

Pugh, D. T., *Changing sea levels: effects of tides, weather and climate*, Cambridge Univ. Press, Cambridge, 2004.

Pugh, D. T., and P. L. Woodworth, *Sea-level science; understanding tides, surges, tsunamis and mean sea-level changes*, Cambridge University Press, Cambridge, 2014.

Ross, D., *Power from the waves*, Oxford Univ. Press, Oxford, 1996.

Sørensen, R. M., *Basic wave mechanics*, John Wiley & Sons, 1993.

Van Dyke, M., *An album of fluid motion*, Parabolic Press, Stanford (CA), 1982.

Whitham, G. B., *Linear and nonlinear waves*, John Wiley & Sons, New York, 1974.

WMO, Guide to wave analysis and forecasting, *Tech. rep.*, World Meteorological Organization, WMO publ. nr. 702, Geneva (Switzerland), 1998.

Young, I. R., *Wind generated ocean waves*, Elsevier, 1999.